A PRACTICAL SIMULATION METHODOLOGY TO IMPROVE FATIGUE LIFE PREDICTION OF ENGINE OIL COOLER UNDERGOING PRESSURE CYCLE TESTING

A PRACTICAL SIMULATION METHODOLOGY TO IMPROVE FATIGUE LIFE PREDICTION OF ENGINE OIL COOLER UNDERGOING PRESSURE CYCLE TESTING

By

THOMAS KAM-CHEUNG CHAN, B.Sc. (Eng.)

A Thesis

Submitted to the School of Graduate Studies

in Partial Fulfillment of the Requirements

for the Degree

Master of Applied Science

McMaster University

MASTER OF APPLIED SCIENCE (2013) McMaster University
(Mechanical Engineering) Hamilton, Ontario

TITLE:	A Practical Simulation Methodology to Improve Fatigue Life Prediction of Engine Oil Cooler Undergoing Pressure Cycle Testing
AUTHOR:	Thomas Kam-Cheung Chan, B.Sc. (Eng.) (University of Hong Kong)
SUPERVISOR:	Professor Mukesh K. Jain
NUMBER OF PAGES:	xiii, 106

ABSTRACT

Computer simulation is widely used to predict the fatigue life of engine oil coolers that fail under pressure cycles. The objective of this study is to develop a practical simulation methodology to accurately predict the fatigue life of an engine oil cooler undergoing pressure cycle testing. The study focuses on two key areas of the simulation process. First, it investigates the effect of using linear and nonlinear FEA to provide stress or strain results for subsequent fatigue analysis. Second, due to lack of fatigue material properties for the aluminum coreplate material, approximate material models derived from tensile properties are used in fatigue life calculation. The study has attempted to find out the material model that gives the best correlation in life prediction. The life prediction correlation based on the Seeger, the Modified Universal Slopes and the Modified Mitchell models, together with the Modified Universal Slopes-Al model, are evaluated.

It is concluded that the Modified Universal Slopes-Al model, which is a re-assessment of the Modified Universal Slopes model based on the fatigue data of 16 wrought aluminum alloys, gives the best life prediction for simulations using either linear or nonlinear approaches. Life prediction using nonlinear finite element results together with this approximate material model is recommended to be the best approach. On the other hand, a simple and quick linear analysis, followed by fatigue life calculation using this material model still gives life estimates with an acceptable level of confidence.

In the last part of the study, the life prediction performance using different strain-life criteria, together with either Morrow or Smith-Watson-Topper (SWT) mean stress correction, are evaluated. It is found that SWT mean stress correction method is worse than that of Morrow in EOC fatigue life prediction in both linear and nonlinear approaches. Using the principal strain criterion with SWT mean stress correction gives conservative life prediction in both approaches. On the other hand, there are no

significant differences in life prediction correlations using the principal strain, the Brown-Miller combined strain and the maximum shear strain strain-life criteria, with Morrow mean stress correction. As such, the Brown-Miller combined strain criterion with Morrow mean stress correction is the recommended strain-life model used in fatigue life calculation.

ACKNOWLEDGEMENT

I thank God for His abundant blessing in my life so that I can have the strength and wisdom to complete my research study.

I wish to express my sincere gratitude to my supervisor, Professor Mukesh Jain, for his time, support, encouragement, guidance and ideas provided throughout this research. Without his help, the successful completion of this thesis and the quality of work achieved would not be possible. His contributions and help are greatly appreciated.

I wish to thank Dana Corporation for providing the resources needed in the research work. I would like to thank my work supervisor, Dr. Michael Bardeleben, for his support throughout the whole study. I wish to express my gratitude to my colleagues in Dana Corporation including Ben Lowry, Greg Kolesar and all others who have been involved in this project, providing support in building prototypes and performing testing.

I would like to express my gratitude to Pouya Sharifi and Dr. Robert Klassen of University of Western Ontario, for their expertise and help in conducting micro-indentation testing and subsequent data analysis. Their eagerness to help me, an unknown fellow researcher to them, is greatly appreciated.

Finally, I thank my wife, Edith, for her support and encouragement offered to me throughout my study, and for her caring of the whole family.

TABLE OF CONTENTS

LIST OF FIGURES

LIST OF TABLES

1. INTRODUCTION

In an automobile, engine oil lubricates and cleans moving metallic surfaces of the engine. As metallic surfaces rub on each other, heat is dissipated due to friction. When engine oil heats up, it loses its ability to lubricate and the surfaces requiring lubrication begin to wear. Continued exposure to elevated temperature can result in premature engine wear and eventual failure. Engine oil coolers (EOCs) are commonly found in high performance engines, heavy duty commercial vehicles, and vehicles with increased trailer towing capacity. They are used to cool engine oil and to maintain the optimal operating temperature of it. With more stringent fuel economy standards imposed on new vehicles, EOC has become a common component on most automobiles.

In the engine oil circuit of a vehicle, the EOC is constantly exposed to pressure pulsations from the oil pump. It is susceptible to fatigue failure due to pressure cycles that results in leaking of oil or coolant that runs through the cooler. Thus, it is of utmost importance to ensure that the EOC is designed to have good durability performance against fatigue failure due to pressure cycles. As such, every newly developed EOC design is subjected to stringent pressure cycle (PC) testing requirements. They include an initial design validation test, vehicle road test and final pre-production approval test. In the early stage of product development, cooler prototypes have to undergo PC lab testing to validate the design. Building prototypes and conducting PC validation testing are very expensive and time consuming. With the advancement of computer aided engineering technology, design validation in the early stage of product development can be carried out using computer simulation, in lieu of lab testing. This virtual design technology reduces the amount of prototype testing required and helps cut the lead time to product launch. The whole simulation process uses computer software packages to perform computer aided design (CAD) of the EOC, to carry out stress analysis using finite element (FE) method, and to do fatigue life prediction calculation based on finite element analysis (FEA) results. The success of using this virtual design technology to validate the durability

performance of cooler designs during new product launch depends critically upon the accuracy of fatigue life prediction.

EOCs undergoing pressure cycle testing usually fail at the base of the first coreplate, which is located next to the baseplate. Coreplates are made of 3000 series aluminum alloy brazing sheet, which is not a structural aluminum alloy commonly used in automotive and aerospace industry. Thus, there are no published fatigue data available in the handbooks or references. Moreover, different cooler designs may use different types of brazing sheet in order to meet specific application needs such as corrosion resistance requirements. Also, fatigue testing of thin gauge sheet material poses a challenge in itself. Furthermore, the PC testing may be conducted at a different temperature for different cooler designs. As such, to perform an extensive fatigue testing to meet all these needs is very expensive. All these factors collectively cause the unavailability of fatigue material test data for life prediction calculation. As an alternative, a practical simulation methodology for life prediction needs to use an approximate fatigue material model with parameters derived from a simpler mechanical test such as monotonic uniaxial tensile test.

The objective of the present study is to develop a practical simulation methodology to accurately predict the fatigue life of an EOC undergoing PC testing. The simulation work involves two parts. First, an FEA is performed to obtain the stress and strain data on the loaded cooler. Second, the FEA result data are used as inputs for a fatigue life calculation that utilizes a strain-life fatigue material model. Fatigue life calculation can be performed using linear or nonlinear FE results. In the past, most of the fatigue predictions in simulation were conducted using linear results, especially in cases in which structures are subjected to a large number of load cycles with varying strain amplitudes. Typically, an FE model with the size of 1 to 2 million elements is required to properly capture the EOC geometry. Even with the advancement in computer hardware capability in recent years, using nonlinear results in fatigue calculation, from an FEA with

numerous load steps is still computationally prohibitive. However, as the PC test of the EOC in the current study uses a simple pressure cycle profile, it is viable to perform nonlinear FEA to get stress and strain data for the subsequent fatigue analysis.

The current study focuses on the two areas of the simulation process. First, it investigates the performance of using linear and nonlinear FEA results on fatigue life prediction. Second, due to lack of fatigue material properties for the aluminum brazing sheet used in the coreplates, there is a need to estimate the material data from approximate material models in life prediction. Several approximate material models with fatigue parameters derived from tensile testing properties are used and their life prediction performances are evaluated.

In order to evaluate the performance of different FE simulation approaches, lab based PC tests are conducted to collect data for life prediction correlation purposes. A production cooler design is chosen as the subject of investigation. This is a compact heat exchanger with stacked plate design. In a PC test, the cooler is bolted-down to the fixture by applying a specified torque to the bolts. Pressure cycles are then applied to the oil channels of the cooler. A series of PC tests with different pressure amplitudes are performed to collect life data covering low, intermediate and high cycle fatigue failures.

The FE modeling includes simple linear analysis and multiple-step nonlinear analysis that includes the initial bolt-down step. In the bolt-down step of a PC lab test, the baseplate is pressed against the O-rings that sit on the fixture groove. As a result, there is substantial bending of the baseplate that causes the development of high stresses in the lower part of the cooler. Two different approaches are studied. In the first approach, the linear stress results are used as inputs for a fatigue calculation. This is a commonly used method that is simple as only one FEA with an arbitrary pressure loading is needed to be performed. In the subsequent fatigue calculation, the linear stress results are scaled according to the specified pressure cycle profiles. The calculation also includes mean stress effect and

plasticity correction. The second approach uses nonlinear multiple-step FEA. The steps include the initial bolt-down and the subsequent application of pressure cycles. In this approach, different nonlinear FE simulations are conducted for different pressure cycle tests. The nonlinear stress and strain datasets are used as inputs for a fatigue life calculation.

The coreplate of the cooler under investigation is made of 3534 aluminum brazing sheet whose fatigue properties such as strain-life and cyclic stress-strain curves are not available in literature. Therefore, an approximate material model with fatigue material parameters derived from a simple monotonic tensile test is used. There is considerable research done in this field and more than ten approximate models have been proposed in the past. Based on an extensive literature search, three existing models that appear to have good performance for aluminum alloys have been chosen and their performances in life prediction are evaluated. Finally one of the approximate material models from the literature is re-assessed with material parameters derived from published data exclusively on aluminum alloys. This re-assessed model has shown to give the best life prediction correlation with lab testing data for the whole fatigue life range covering low, intermediate and high cycle failures of the EOC.

2. ENGINE OIL COOLER UNDER INVESTIGATION

A production EOC design (Figure 1), which is a product of Dana Corporation, is chosen as the subject of the study. This is a compact heat exchanger with alternate oil and coolant flow channels formed from stacked coreplates (Figure 2). The EOC is made of aluminum alloys and the assembly drawing is shown in Appendix A1.

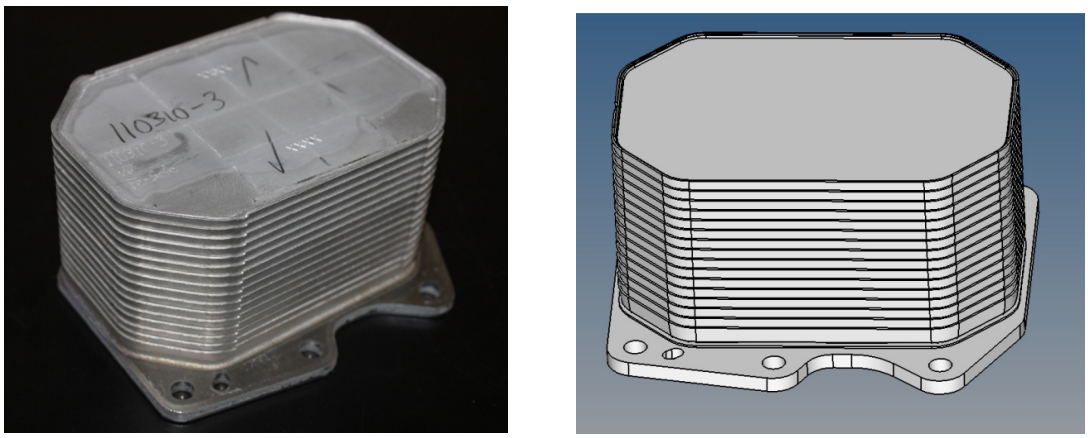

(a) (b)

Figure 1. (a) The cooler prototype and (b) the CAD model of the cooler assembly.

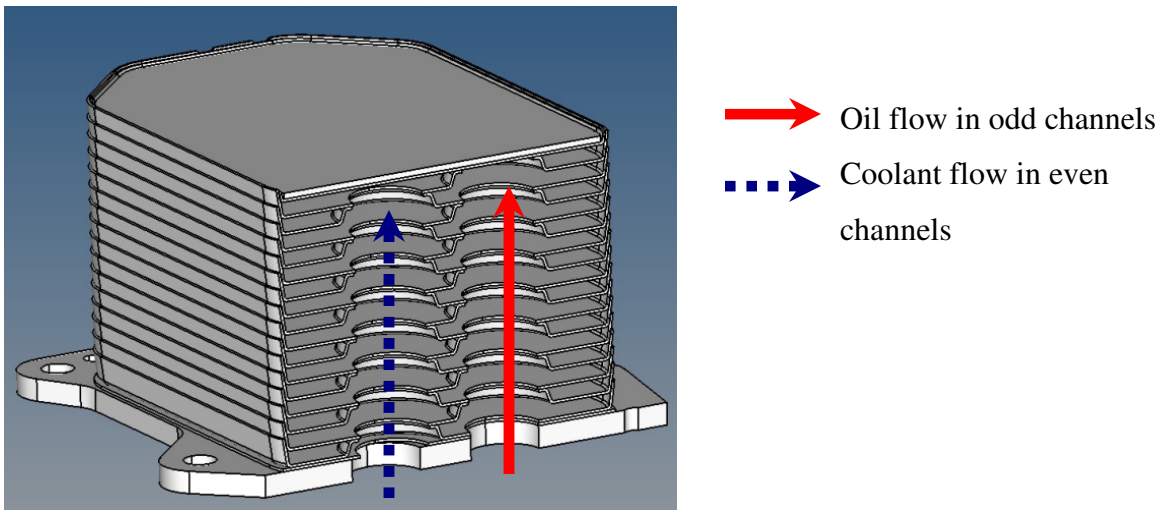

Figure 2. Cut-out view of the EOC showing oil and coolant channels (turbulators not shown).

Both oil and coolant channels have so-called turbulators. The turbulator is comprised of a pattern of corrugated convolutions (Figure 3), used to introduce turbulence to the fluid flow in both oil and coolant channels. The turbulators are used to enhance the heat transfer performance of the cooler and to provide structural reinforcement against bursting when the channels are subjected to internal pressure loading.

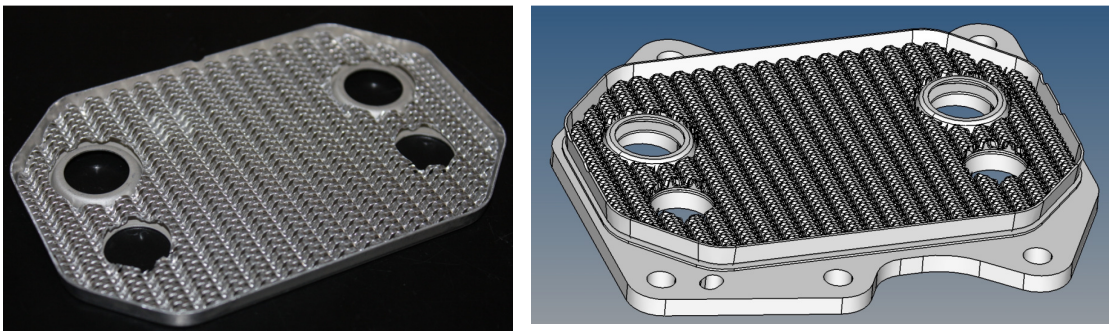

Figure 3. A turbulator put inside a coreplate.

During production, the assembly comprising of a baseplate at the bottom, a shim plate, 16 coreplates and 16 turbulators, a lid plate and a top plate at the top, is held by a fixture and undergoes a brazing process in a belt furnace. After cooling, the oil cooler becomes a brazed structure with every component bonded together. The parts and the materials for the cooler assembly are shown in Figure 4.

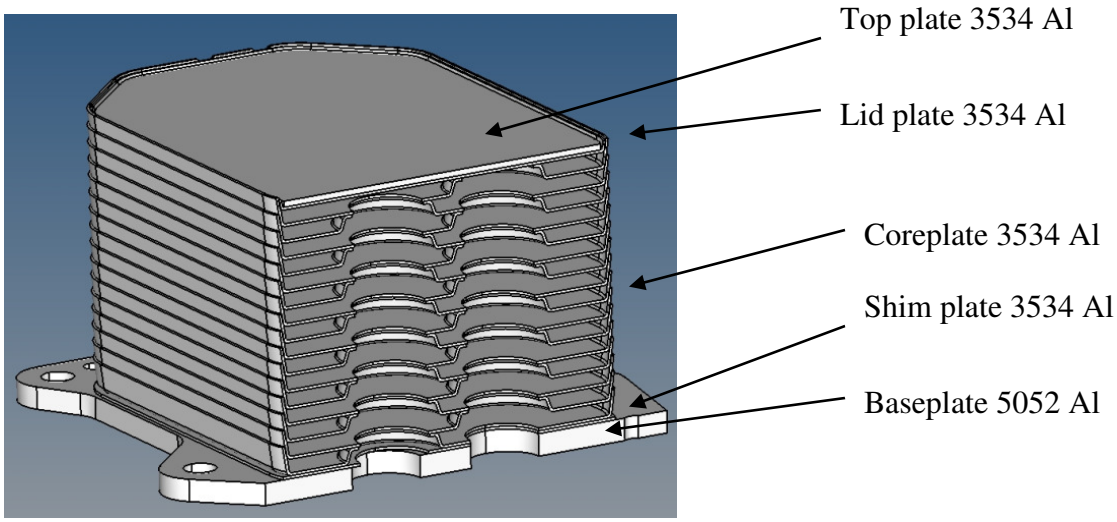

Figure 4. The various components and materials for the cooler assembly (turbulators made of 3104 Al are not shown).

3. EXPERIMENTAL PRESSURE CYCLE TESTING

3.1. TESTING SET-UP

In an experimental pressure cycle test, the cooler is mounted on a fixture at five bolt-holes and an internal oil pressure loading is applied to the oil side of it. The coolant side of the cooler is exposed to air. Two O-rings, one oblong and one circular in shape, are used to seal the oil inlet and outlet areas of the cooler (Figure 5). The drawing for the PC test fixture is shown in Appendix A2.

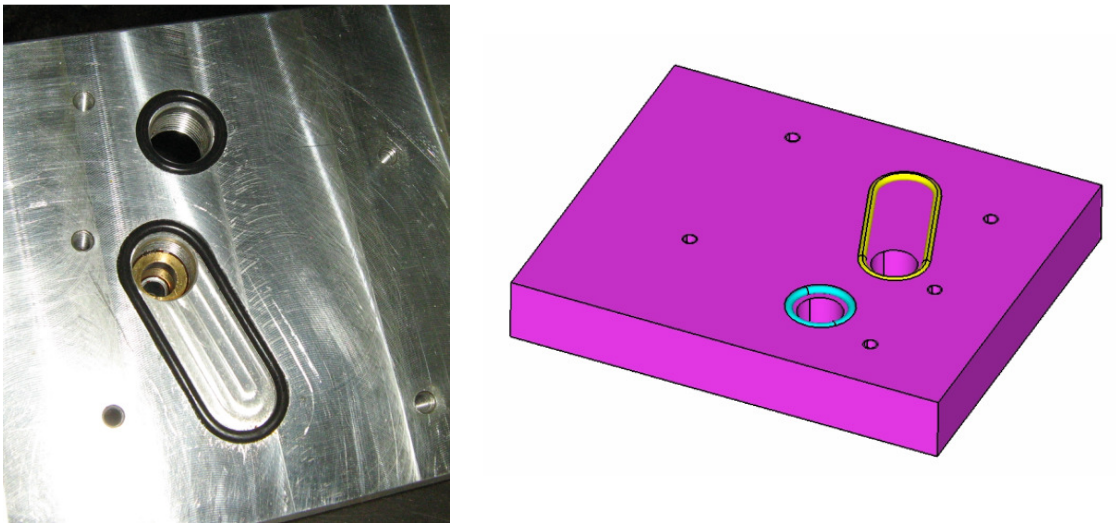

(a) (b)

Figure 5. (a) Fixture with O-rings and (b) the CAD model.

At the beginning of the test, the EOC is bolted down to the fixture by applying a specified torque of 10 Nm to the M6 bolts used for mounting. Figure 6 depicts the section view of the assembly in one of the mounting locations. At the beginning, there is an initial gap of 0.535 mm between the baseplate and the fixture before the O-rings are compressed. This will be explained in details in a later section.

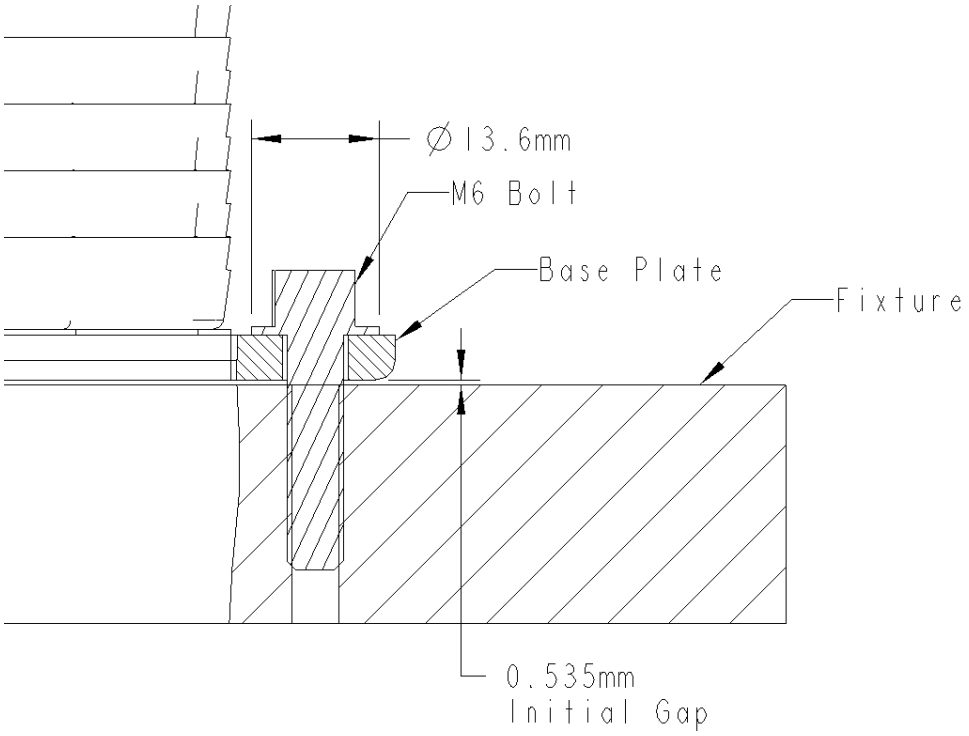

Figure 6. Diagram showing the section view in the bolt-hole area.

In the present study, the PC testing is done at room temperature. In order to collect a full range of fatigue life data of the EOC undergoing PC testing, from low cycle to high cycle, multiple tests with different maximum pressure magnitude are conducted at room temperature. Figure 7 depicts the set up for the testing.

(a)

(b)

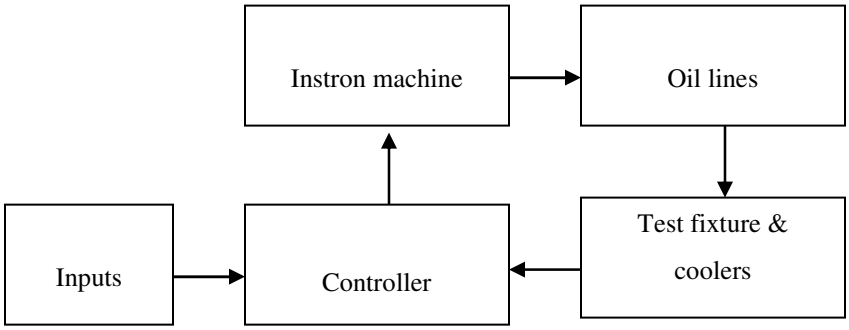

(c)

Figure 7. Experimental setup: (a) Instron 8501 servo-hydraulic machine, (b) a set of 3 coolers mounted on test fixture and (c) a schematic diagram of the oil circuit of the PC test setup.

PC tests are run by applying sinusoidal loads of constant amplitude, in load control mode, using an Instron 8501 servo-hydraulic testing machine. In each test, a set of three coolers is mounted to the fixture by applying a tightening torque of 10 Nm to the bolts. The oil inlet and outlet of the fixture are connected to the oil circuit of the system. The coolers are subjected to pressure cycles at 2 Hz (time period 0.5 s), with a profile similar to that shown in Figure 8. The test is run continuously until a leak has occurred, which is detected by a 10% drop in the preset maximum pressure value. Once a leak is detected, the leaked cooler is removed and the test is resumed. This procedure is continued until all three coolers have failed. Alternatively, the test will be suspended if the preset maximum number of cycles (3.5 million) is reached.

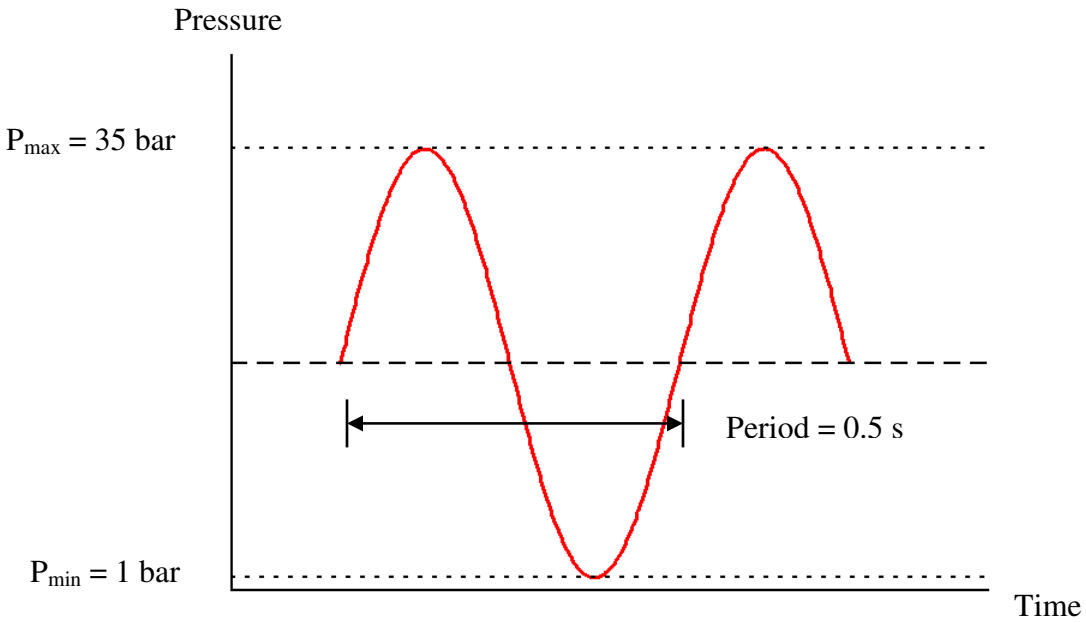

Figure 8. A typical pressure cycle profile. The 1-35 bar PC test profile is used as an example.

3.2. TEST RESULTS

A total of ten tests with different pressure cycle profiles are performed. In the longest life test using a pressure profile of 1-13 bar (1 bar = 10^5 Pa), the coolers pass the test when 3.5 million cycles are achieved without failure. In the shortest life test using a pressure profile of 1-35 bar, the coolers fail at about 7000 cycles. Tests with different maximum pressure magnitudes are performed and the results expressed as pressure range versus life are shown in Figure 9.

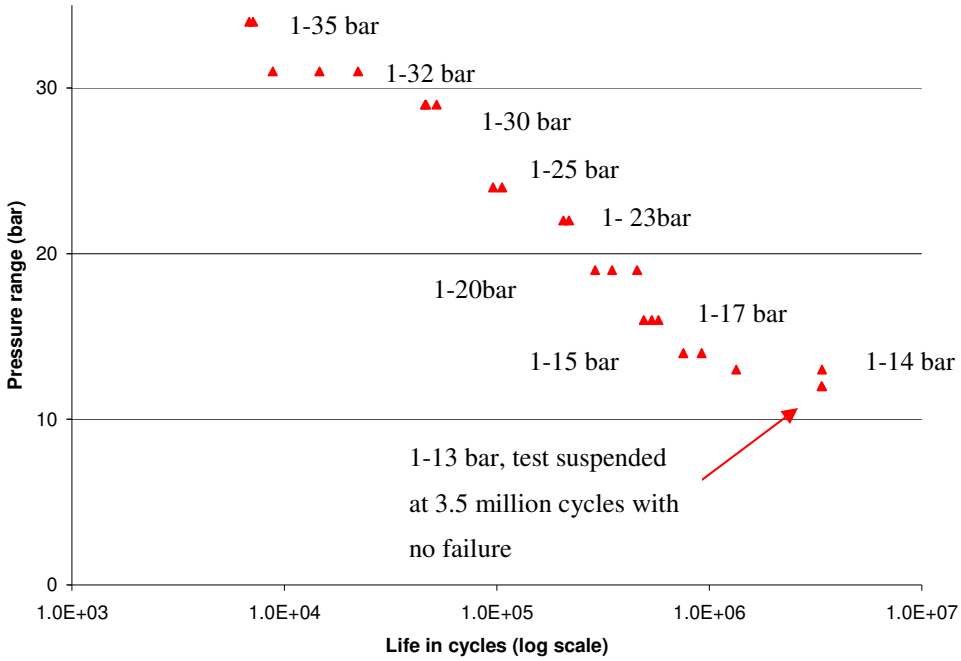

Figure 9. Pressure cycle test results: pressure range vs. life.

The typical failure location of the cooler in these tests is found at the base of the first coreplate, with oil leakage observed in the area near the mounting hole (Figure 10). Sectioning of the cooler in the failure location reveals that a crack has initiated on the outside surface of the coreplate, in the area above the braze fillet, and propagates across the wall of the plate (Figure 11).

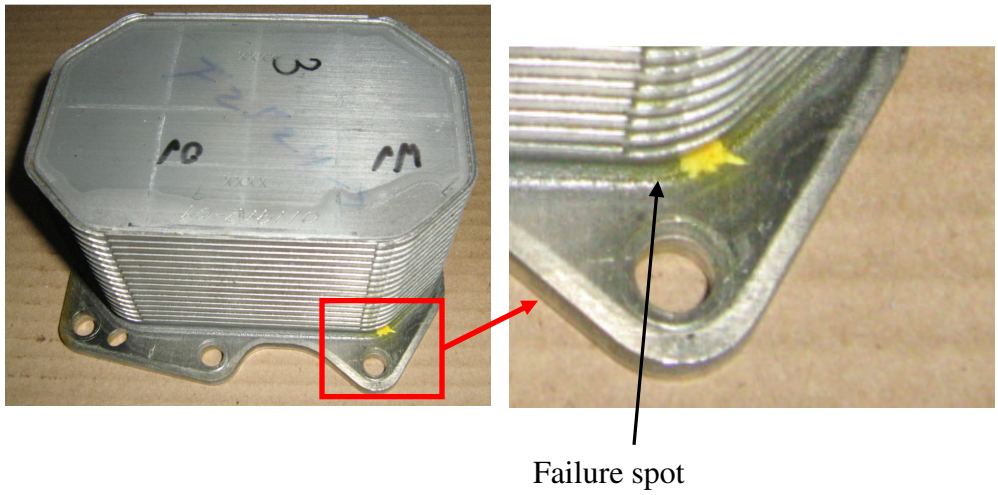

Figure 10. Oil leakage location near the spot marked with yellow ink.

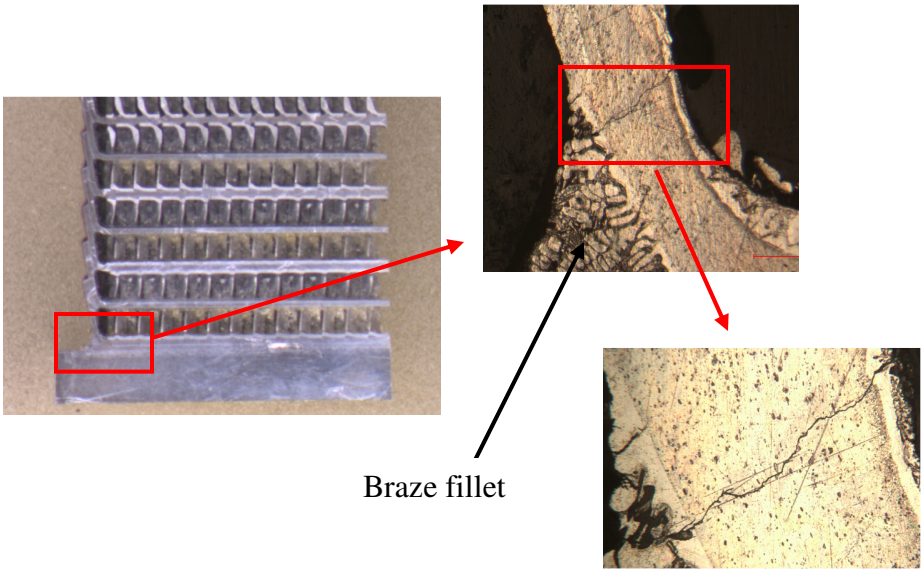

Figure 11. Crack developed at the base of the first coreplate and propagates across its wall.

4. LINEAR FINITE ELEMENT ANALYSIS

4.1. LINEAR FE MODEL

All finite element analyses are performed using SIMULIA Abaqus/Standard 6.11 software [1]. The FE model of the cooler assembly for linear analysis is shown in Figure 12. Totally, there are 1.8 million elements in the FE model. All components except for the turbulators are meshed predominantly with 8-node solid elements. The turbulators are meshed with shell elements (Figure 13). In order to get accurate stress results in the critical area where failure is observed in experimental testing, fine mesh with good quality elements are used in this area (Figure 12b).

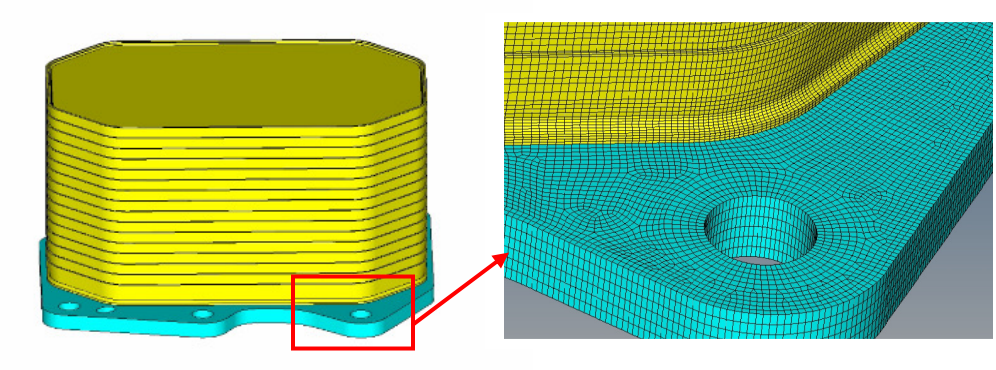

(a) (b)

Figure 12. FE model of the cooler assembly with good element mesh in the critical area.

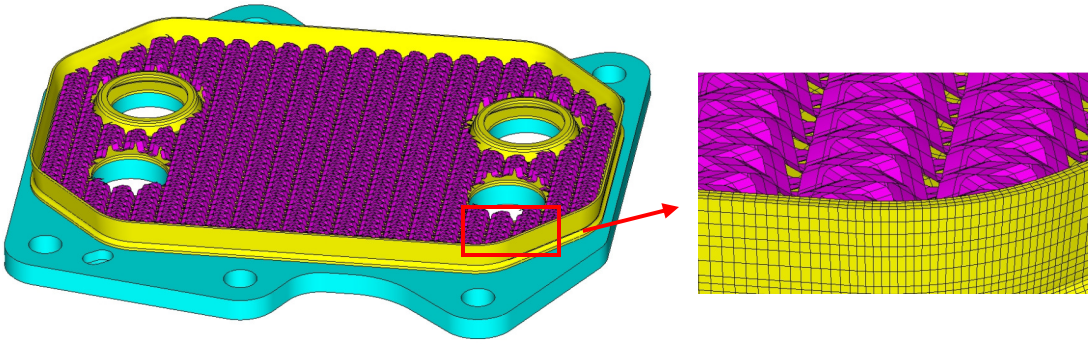

Figure 13. Turbulator is meshed with thin shell elements.

4.2. MODELING OF BRAZE FILLET

In modeling the EOC, it is important to include the braze fillet geometry that exists between the first coreplate and shim plate (Figure 14).

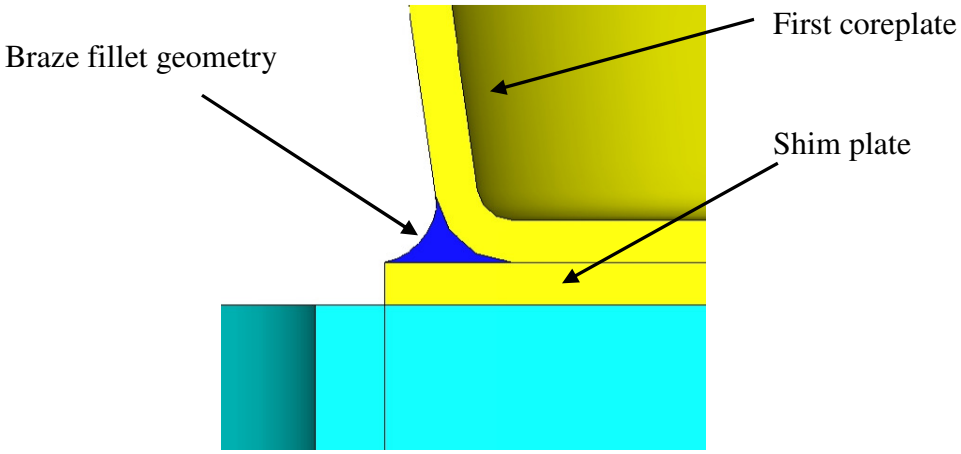

Figure 14. Braze fillet geometry in the FE model.

Without the braze fillet, the maximum stress in the critical area will be developed at the junction (or corner) between the first coreplate and shim plate, when the cooler is pressurized. Figure 15 depicts a typical stress plot to illustrate the phenomenon. This result will lead to a wrong prediction of the location of the critical high stress area as the corner feature does not exist in reality. Furthermore, the accuracy of the stresses recorded at the corner cannot be improved by mesh refinement due to the occurrence of stress singularity.

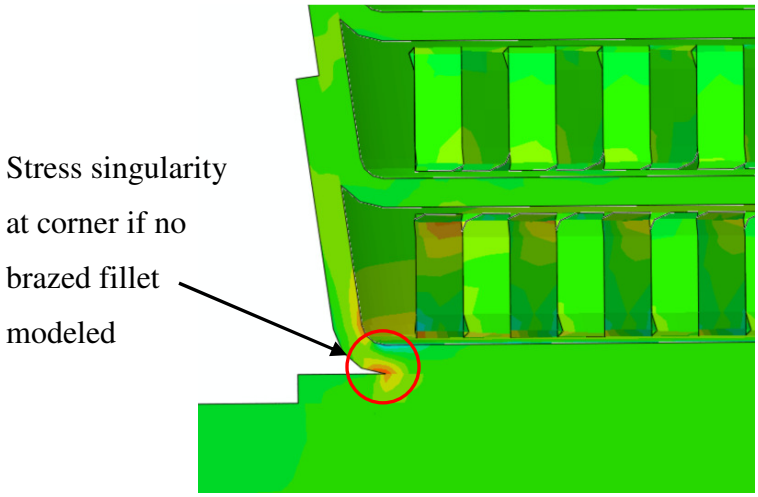

Figure 15. A typical stress plot showing the maximum stress developed at the corner between the first coreplate and shim plate when the EOC is pressurized.

In the FE model, the sectional geometry profile of the braze fillet is simplified as a circular arc whose radius is determined from measurement. Sections in different areas along the braze joint between the first coreplate and shim plate are prepared and the fillet radius is measured using metallographic imaging.

Figure 16 depicts the image of a typical section with fillet radius measurement of 955.8 μm is shown at the upper left corner. As a result, the average fillet radius is about 1 mm. This value is taken as the fillet radius in modeling.

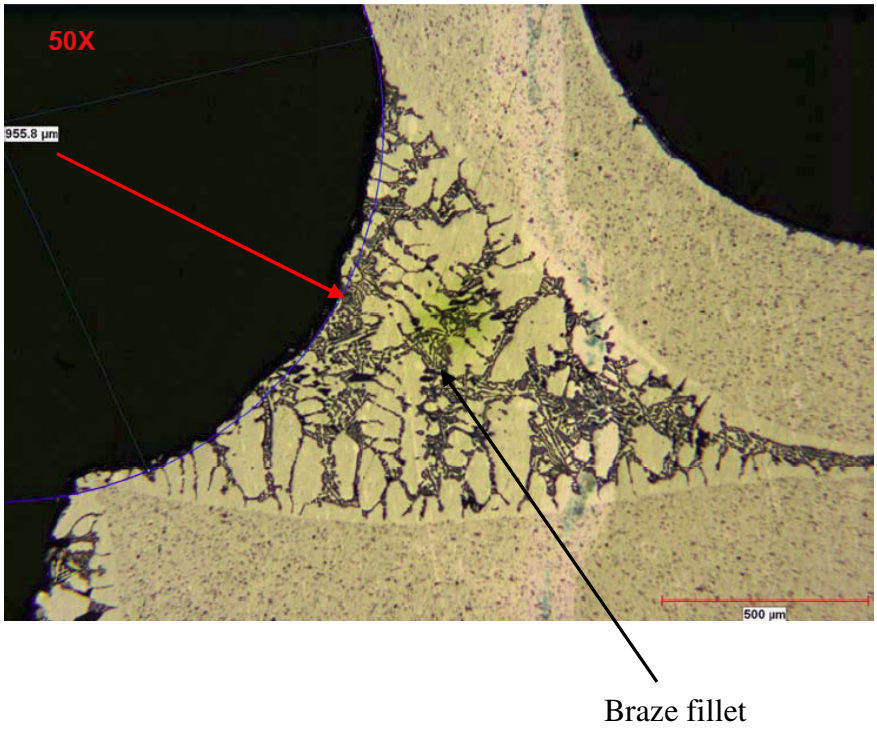

Figure 16. A metallographic image of the braze fillet with radius measurement of 0.9558mm.

In the FE model, A380 cast aluminum is used as the material for the braze fillet. An attempt has been made to investigate the possibility of using micro-indentation method to characterize the properties of the braze fillet material. Micro-indentation has been conducted on a braze fillet sample. The details of the micro-indentation testing are summarized in Appendix 3. Unfortunately, the testing cannot provide the required full range stress-strain data for FEA. However, the test results have shown that the stress-strain relationship of the braze fillet material is very close to that of A380 cast aluminum in the strain range tested.

4.3. BOUNDARY CONDITIONS

In the linear analysis, a simplified mounting configuration is used. The baseplate is fully clamped in the bolt-hole areas of the baseplate (Figure 17). The nodes lying within the bolt head area (13.6 mm in diameter) are fully restrained. No interactions between the baseplate and the O-rings or test fixture surface are included in the linear analysis.

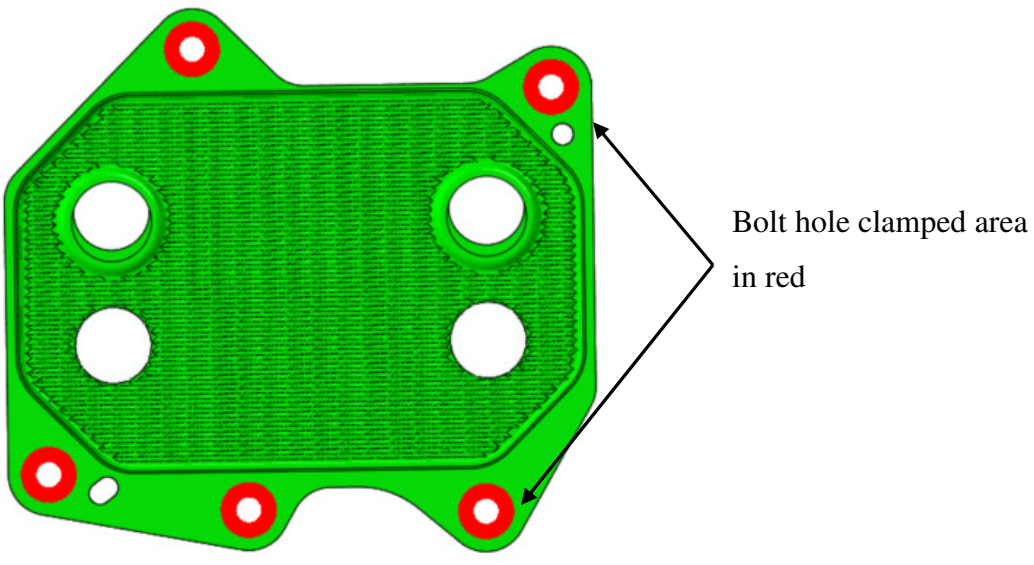

Figure 17. Five bolt holes at the periphery of the baseplate are utilized for clamping the EOC to the test fixture.

A pressure load of 20 bar is applied to the surfaces exposed to oil, which include the surfaces in the oil channels and the sealed area around the oil holes on the bottom surface of the baseplate (Figure 18).

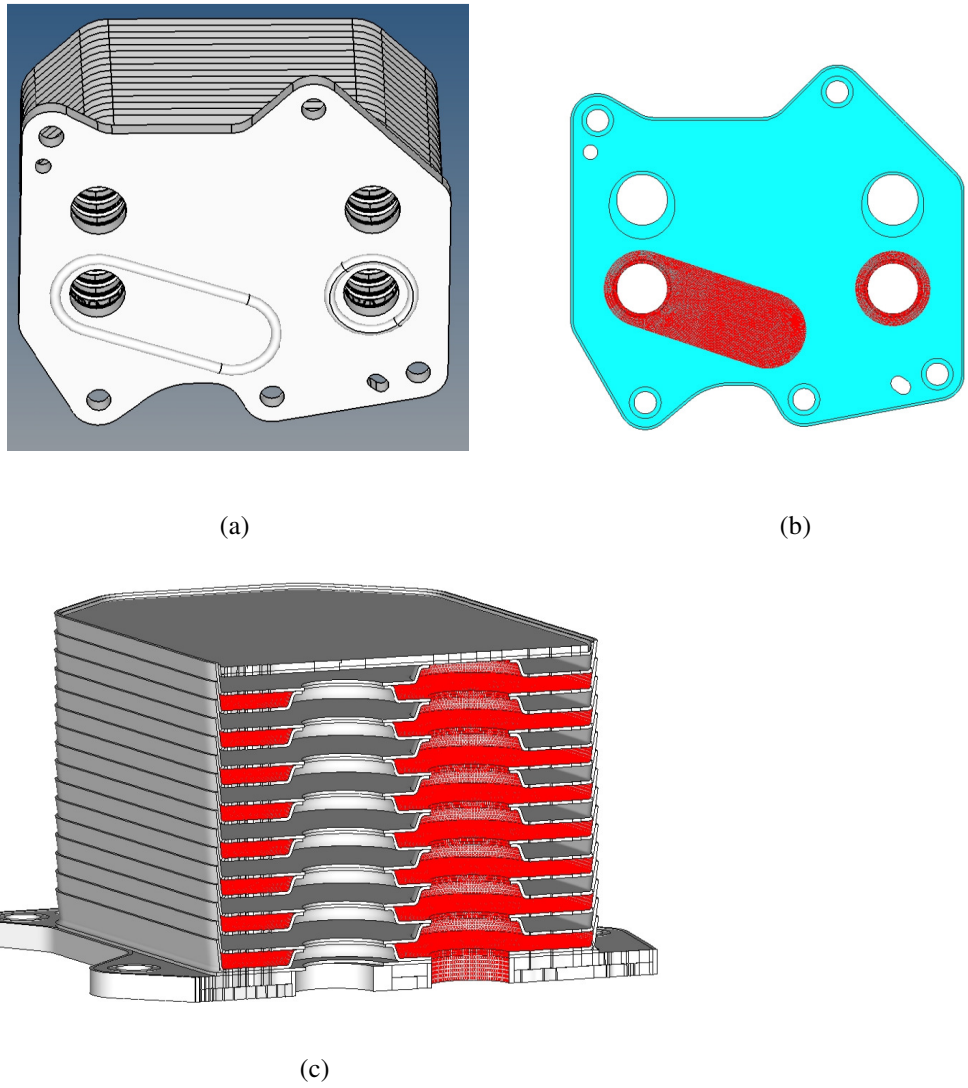

(a) (b)

(c)

Figure 18. Pressure loading area in red: (a) bottom view showing location of O-rings, (b) pressure areas on bottom face of baseplate and (c) internal surfaces exposed to oil pressure.

4.4. MATERIAL PROPERTIES

The tensile properties of the aluminum alloys at room temperature are based on data obtained from standard ASTM tensile testing. Tensile testing on post-braze sheet specimens of 3534 and 5052 Al are performed by Innoval [2]. Tensile test data on post-braze sheet specimens of 3104 Al are provided by supplier Novelis [3]. For A380 cast Al, testing with rod specimens is performed by Dana Corporation [4]. The engineering stress-strain curves for the alloys are depicted in Figure 19.

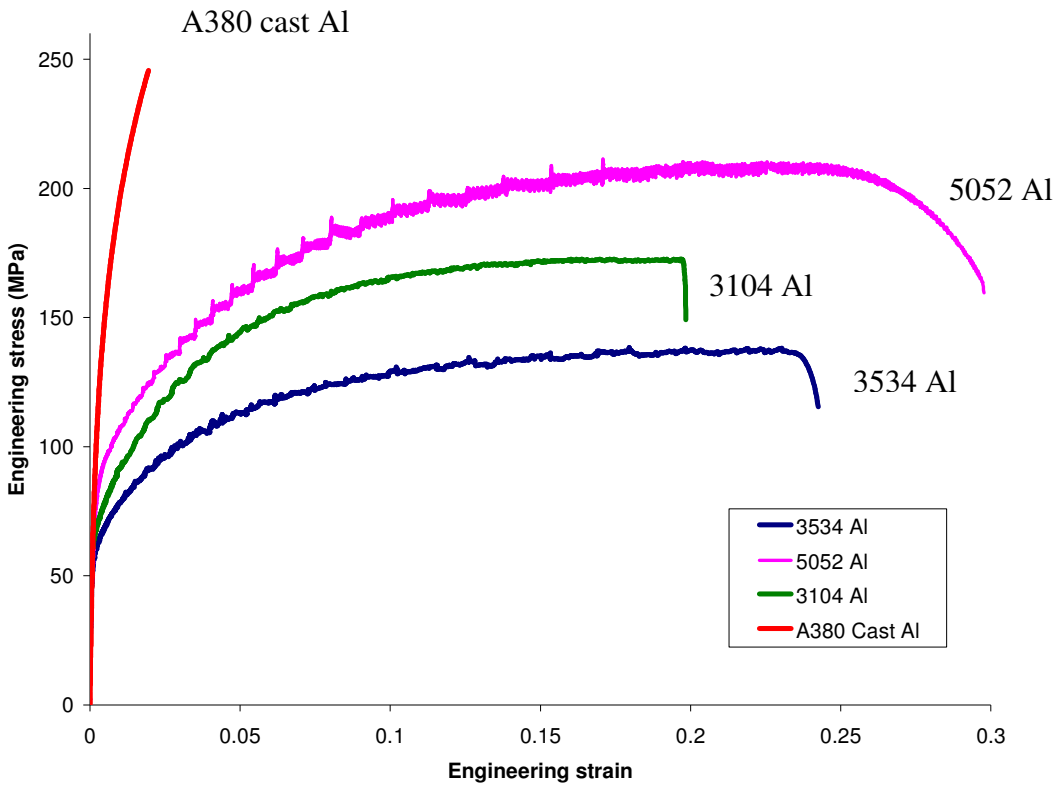

Figure 19. Tensile stress-strain curves for A380 cast aluminum and 3534, 5052 and 3104 aluminum alloys. The curve for A380 cast aluminum is extracted from reference [4].

The material properties used in the linear analysis are summarized in Table 1.

Part	Material	Elastic modulus (GPa)	Poisson's ratio	Yield strength (MPa)	UTS (MPa)
Coreplate, top plate, lid plate, shim plate	3534 Al	69	0.33	63	138
Turbulator	3104 Al	69		72	172
Baseplate	5052 Al	70		89	211
Braze fillet	A380 cast Al	74		134	245

Table 1. Material properties for various aluminum alloys used in the EOC.

4.5. RESULTS OF LINEAR ANALYSIS

Figure 20 depicts the deflection plot on the lower part of the EOC. When the cooler is subject to oil pressure loading, the upward force caused by pressure acting on the oblong sealed area of the baseplate causes large deflection occurring in this area of the baseplate. As a result, high stresses are developed at the base of the first coreplate, in the area located above the braze fillet (Figure 21). The maximum Mises stress recorded in this area is 124 MPa, which is higher than the yield strength of the material (63 MPa). Note that the linear analysis does not account for any post-yield material behaviour. Any stresses higher than yield strength is over-estimated and a nonlinear analysis is required to get accurate stress results. The analysis indicates that extensive yielding has occurred in this critical area. A plot of the maximum principal stress (σ_1) in Figure 22 indicates that these high stresses are tensile in nature, and the direction is perpendicular to the braze line. All these results are consistent with those associated with the failures

observed in experimental testing, both in the location of the crack and the direction of crack propagation.

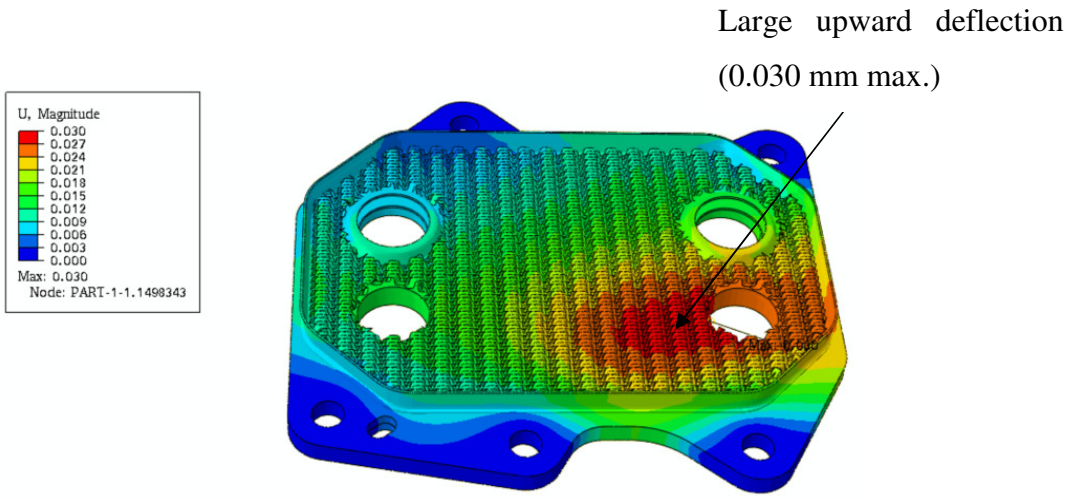

Figure 20. Deflection plot (mm) on the lower part of the cooler.

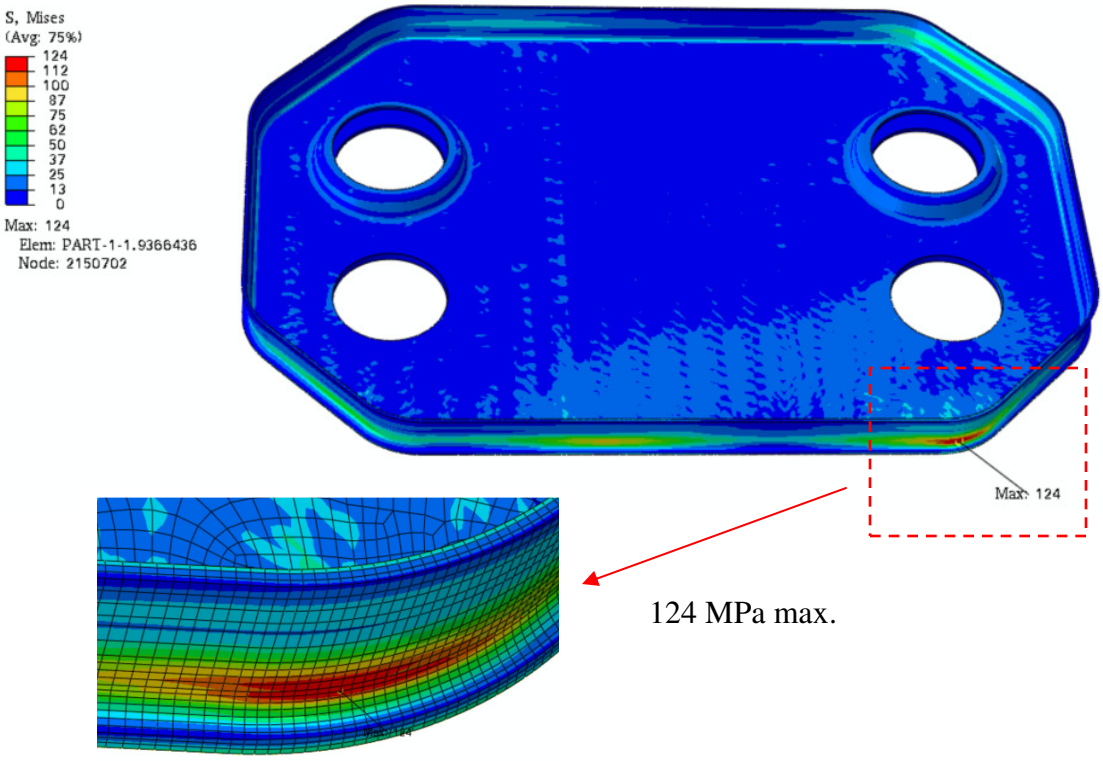

Figure 21. Mises stress plot (in MPa) on the first coreplate.

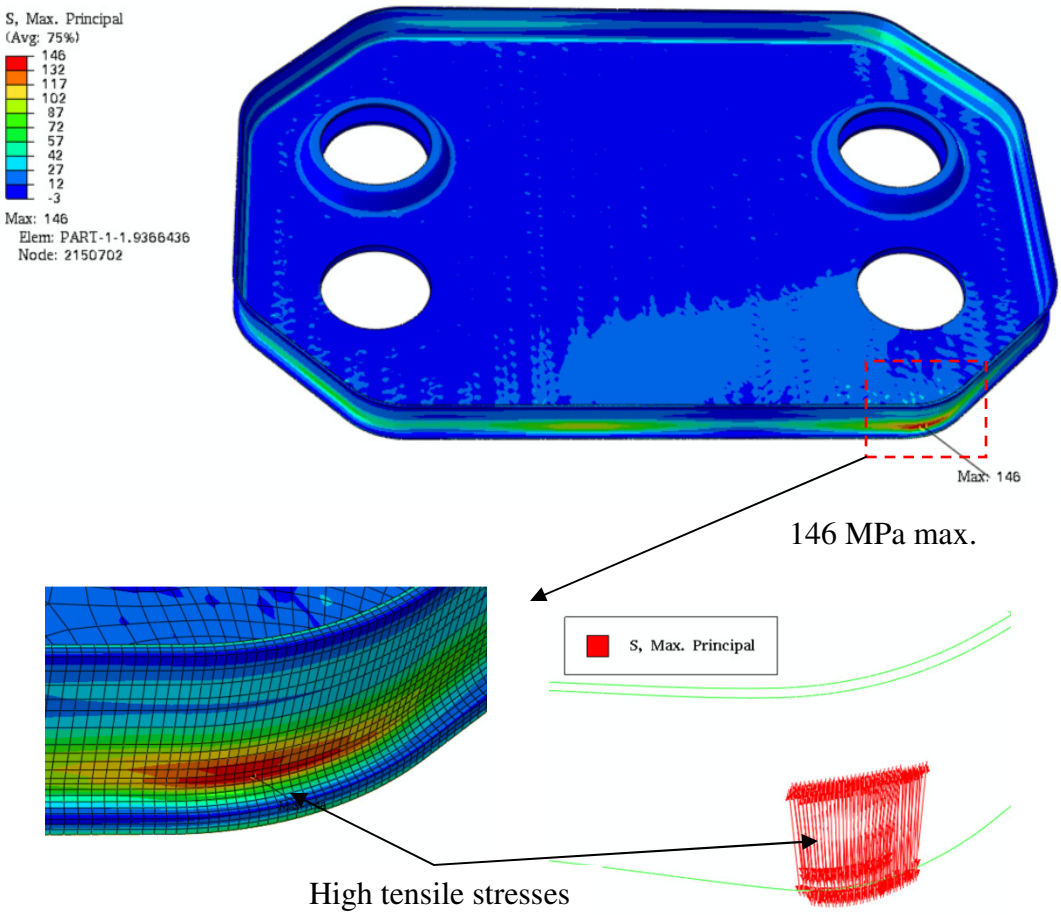

Figure 22. Maximum principal stress (in MPa) contour and vector plots in the critical area.

5. NONLINEAR FINITE ELEMENT ANALYSIS

5.1. NONLINEAR FE MODEL

The nonlinear model is constructed by modifying the linear model. A linear analysis calculation only requires elastic properties of the materials including the modulus of elasticity and Poisson's ratio. For nonlinear analysis, the stress-strain data of the materials are used as inputs to account for post-yield material behaviours. The nonlinear calculations are based on isotropic J2 plasticity with Mises yield criterion. The flow stress-plastic strain curves depicted in Figure 23 are derived from the tensile test data of the aluminum alloys.

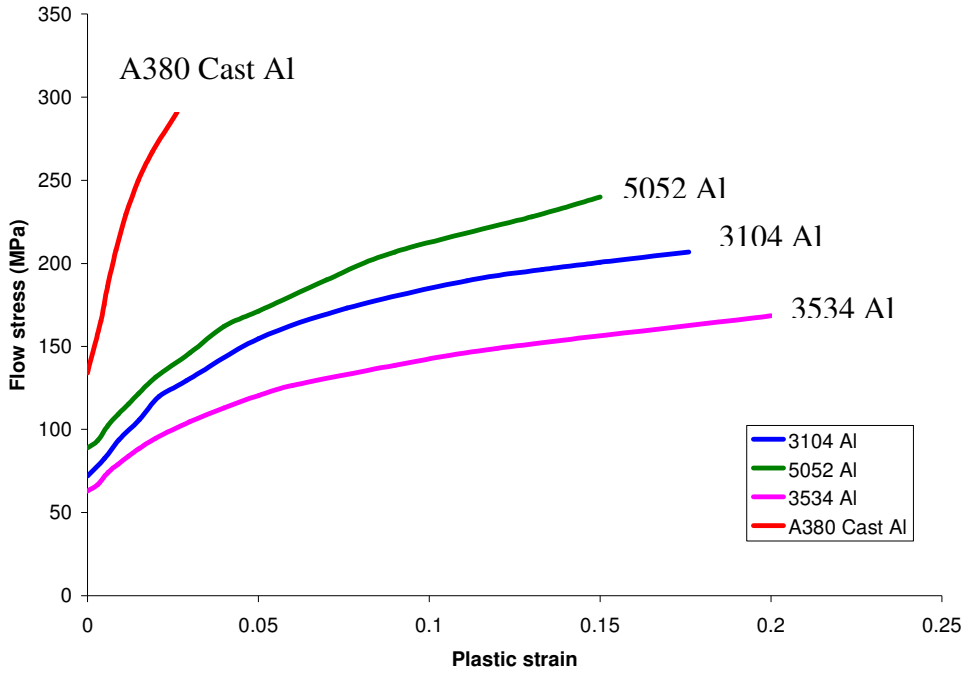

Figure 23. Flow stress – plastic strain curve for the aluminum alloys.

The nonlinear analysis is a contact analysis that accounts for the interactions between the baseplate and the fixture or the O-rings. It is a multiple-step analysis that includes the following steps:

1) bolt-down of cooler to fixture by pre-tensioning of bolts;
2) application of oil pressure, ramping up from zero to upper limit defined by PC profile;
3) ramping down of pressure to the lower limit, 1 bar;
4) ramping up of pressure to the upper limit again;
5) ramping down of pressure to the lower limit, 1 bar, again.

As the stress and strain state of the cooler varies nonlinearly with applied pressure, models with different pressure profiles are run to simulate different pressure cycle tests. Figure 24 shows the pressure variation for different load steps of a nonlinear FE model with a pressure cycle profile of 1-35 bar.

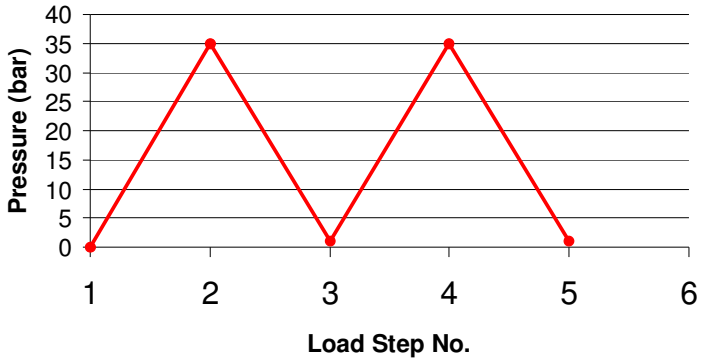

Figure 24. A typical pressure variation profile used in the nonlinear analysis (1-35 bar pressure cycle case).

At the start of an experimental PC test, the cooler is clamped to the fixture with bolts. Five M6 bolts are used and the specified tightening torque is 10 Nm. In modeling, the bolts are meshed with beam elements. In the first bolt-down step, these beam elements are pretensioned with a force of 8333 N, which is calculated according to the following bolt equation [5]:

$$\text{Tightening torque} = 0.2 \times \text{Nominal bolt diameter} \times \text{Bolt preload} \quad (1)$$

The pretensioning of the beam elements forces the cooler pressing against the fixture surface and compressing the O-rings. As the test fixture is made of 6061-T6 aluminum block of 1 inch thickness, the fixture surface is assumed to be rigid and modeled as a rigid surface (Figure 25).

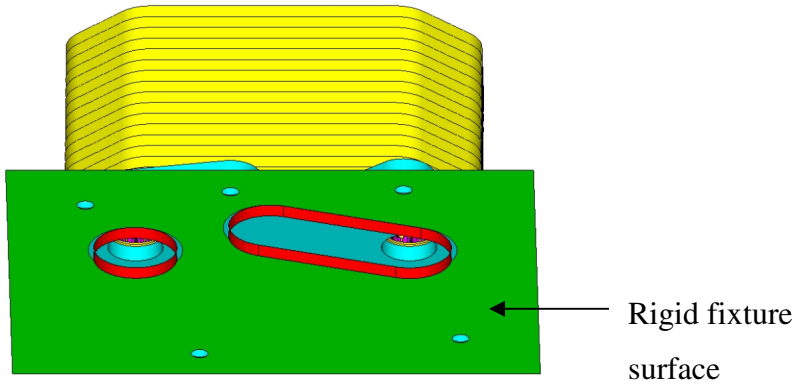

Figure 25 Nonlinear FE model with rigid fixture surface.

The O-rings are made of FKM rubber (Viton fluoroelastomer) with durometer hardness A75. Since the cooler FE model is very large, it is not practical to run a nonlinear multiple-step contact analysis with the O-rings meshed in detail geometry with three dimensional solid elements. Instead, the O-rings are meshed with three dimensional (3D) line gasket elements (Figure 26) with their properties extracted from a separate two dimensional (2D) O-ring compression analysis.

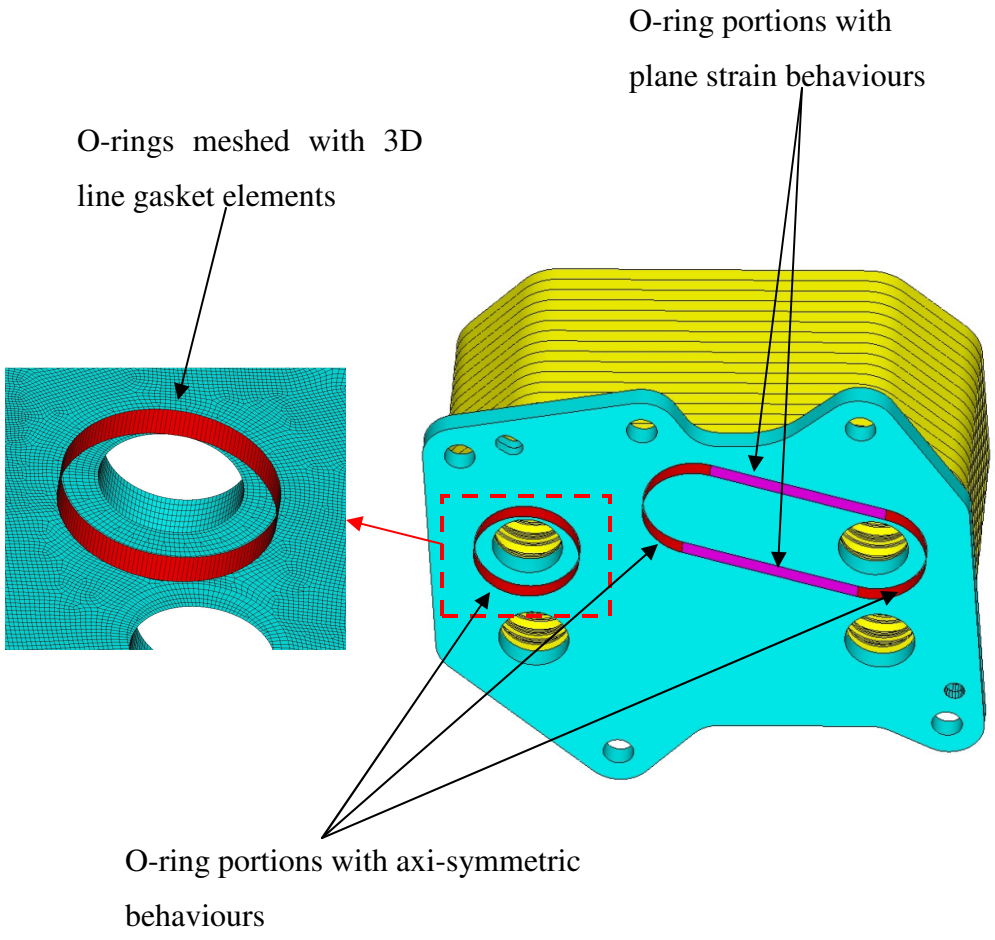

Figure 26. O-rings modeled with 3D line gasket elements.

5.2. TWO DIMENSIONAL ANALYSIS OF O-RING COMPRESSION

The circular and oblong O-rings have the same circular cross-section of 3.175 mm in diameter. According to their 3D geometry, the O-ring portions exhibit either axisymmetric or plane strain behaviours (Figure 26). A 2D analysis is conducted to investigate the behaviours of the O-rings when under compression. A hyperelastic material model is used to capture the rubber-like behaviours of the O-rings. Appendix A3 documents the details of the hyperelastic material model used. Two models are run, one with axi-symmetric elements and the other with plane strain elements, to study the behaviours of different portions of the O-rings. In the initial unstrained state of the O-ring, there is a standoff of 0.535 mm between the baseplate and the fixture surface (Figure 27). The 2D compression simulation is performed by moving the baseplate towards the fixture surface, thereby compressing the O-ring. The analysis accounts for the contact interaction between the O-ring and the baseplate and fixture surfaces. It does not include the interaction between the baseplate and the fixture surface.

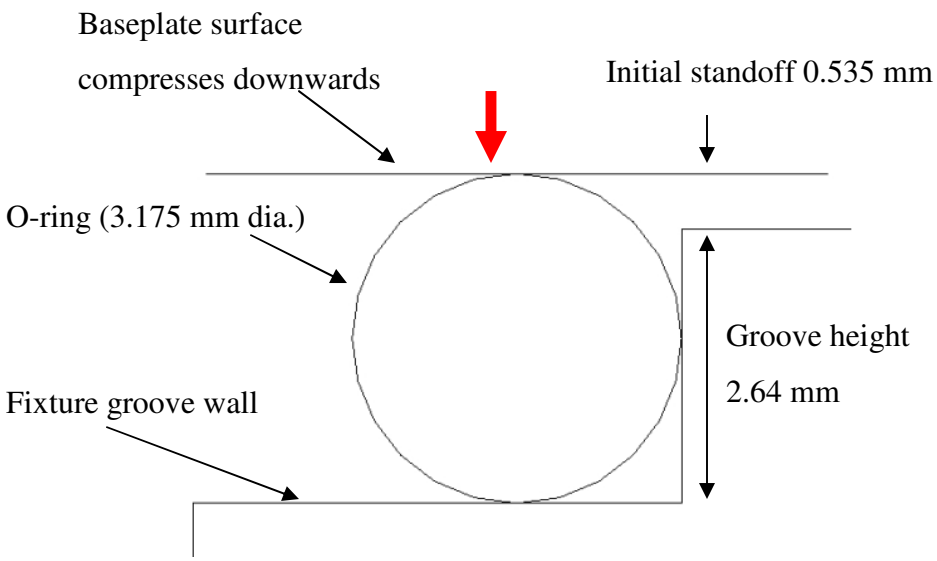

Figure 27. 2D representation of the O-ring and fixture groove.

Figure 28 depicts the results of the 2D analysis using plane strain elements. It shows the evolution of the nominal strain distribution on the O-ring when it is being compressed. In this analysis the baseplate surface travels vertically upwards, compressing the O-ring against the fixture groove wall, which is held stationary. The fixture groove wall and the baseplate surface are meshed with rigid elements. In the 2D analysis, the variations of load and contact area (between the baseplate and the O-ring) with compression are extracted (Figure 29 and Figure 30). As a result, the curves for the plane strain and axis-symmetric models are very close. These curves are used as property inputs for the 3D line gasket elements representing the O-rings in the cooler model. Note that only the portion of load vs. compression curve up to the initial standoff (0.535 mm) is used in calculation as the contact interaction between the baseplate and fixture surface avoids any larger O-ring compression.

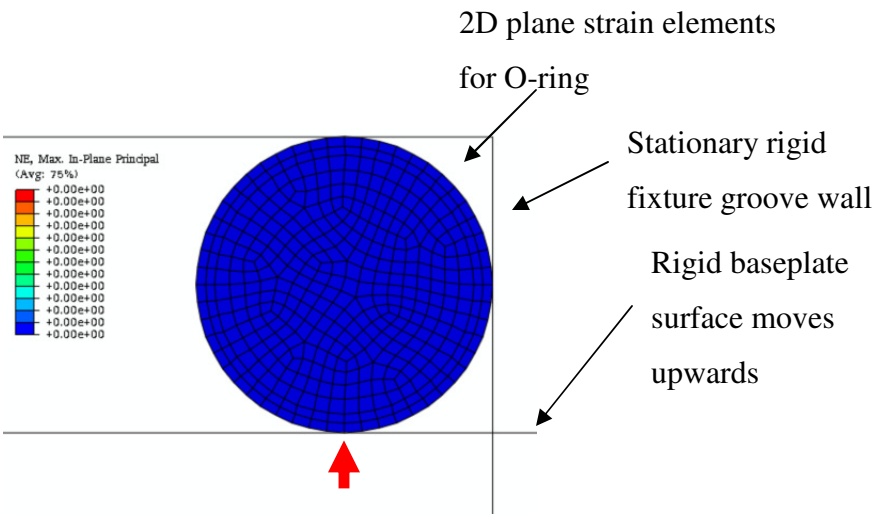

(a) compression = 0 mm

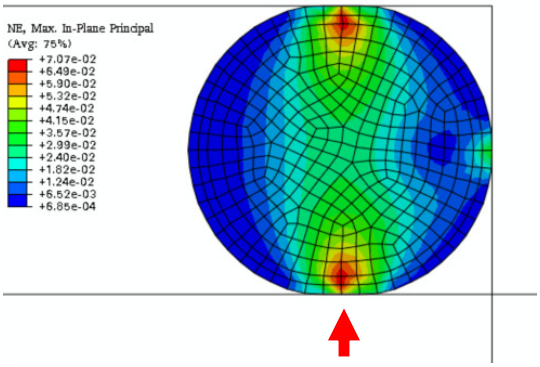

(b) compression = 0.12 mm

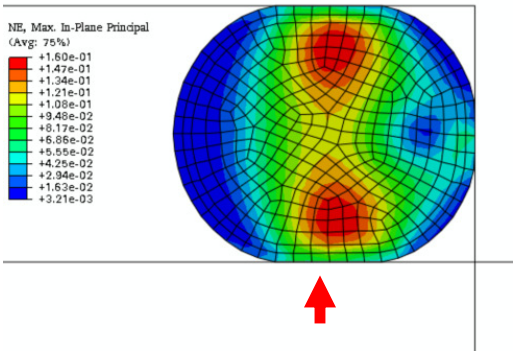

(c) compression = 0.36 mm

Figure 28. Nominal strain evolution on the O-ring when it is under compression (plane strain model).

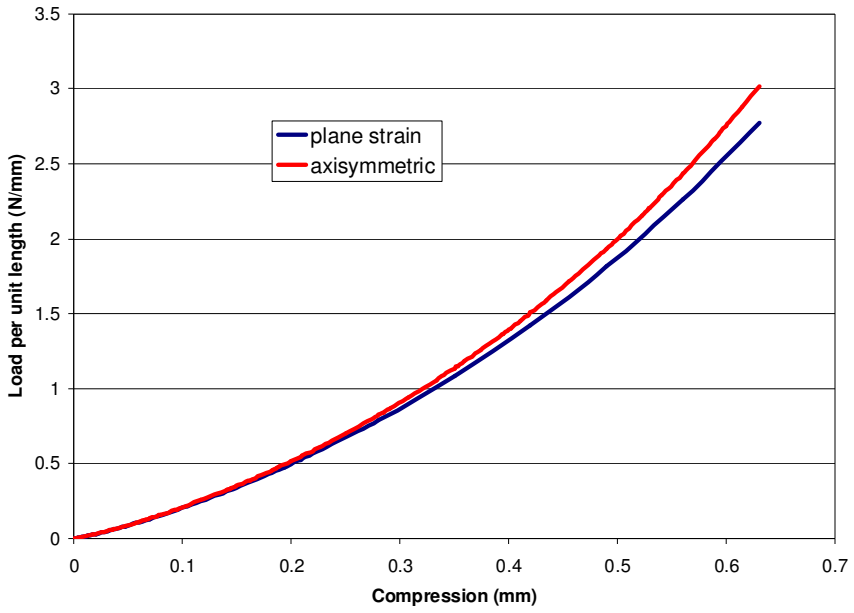

Figure 29. Load- deflection curves for the gasket elements.

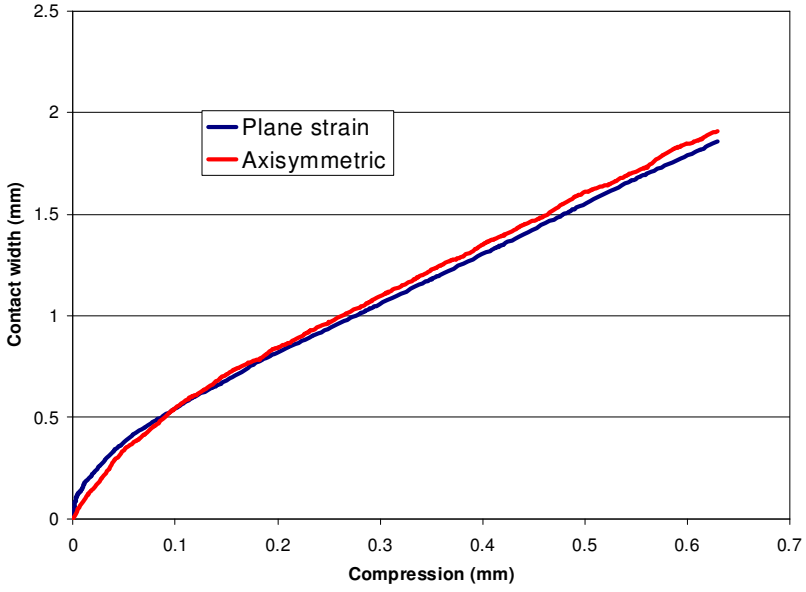

Figure 30. Contact area-compression curves for the gasket elements.

5.3. RESULTS OF NONLINEAR ANALYSIS

All together ten nonlinear models with different maximum pressure loading are run to simulate the experimental PC testing. In order to examine the general behaviour of the cooler model in the nonlinear analysis, only the results for the case with 1-35 bar pressure cycle profile are presented.

After the cooler is bolted-down, high tensile stresses are developed in the critical area of the first coreplate, as shown in the σ_1 plots in Figure 31. The stress state in this area is similar to that observed in the linear model when subjected to pressure loading. This is because the deformed shape of the baseplate caused by the reaction forces from the compressed O-rings is similar to that due to the pressure loading acting in the sealed area. Note that the magnitude of these stresses depends on the size and location of the sealed area, the geometry of the cross-sections of the gasket and fixture groove; and the hardness of the O-rings. In some EOC designs in which harder gaskets are used, the initial bolt-down process will create higher stresses that are detrimental to the durability performance of the oil cooler under subsequent pressure cycles.

Figure 32 to Figure 35 depict the stress and strain states of the cooler in the critical area when it is subjected to the prescribed pressure cycles. At the end of Step 2, when an oil pressure of 35 bar is applied, the stresses in the critical area have increased substantially. The stresses are tensile in nature, as demonstrated by the high magnitude of σ_1, with a maximum value of 141 MPa (Figure 32). The plot of equivalent plastic strain (PEEQ) shows that there is extensive yielding in the area. When the pressure is ramped down to 1 bar at the end of Step 3, the high stresses are reduced in magnitude and their nature are changed from tensile to compressive, with high negative minimum principal stress (σ_3) recorded (-98 MPa min., Figure 33). These stress cycles repeat when the pressure cycle proceeds in Step 4 and 5 (Figure 34 and Figure 35).

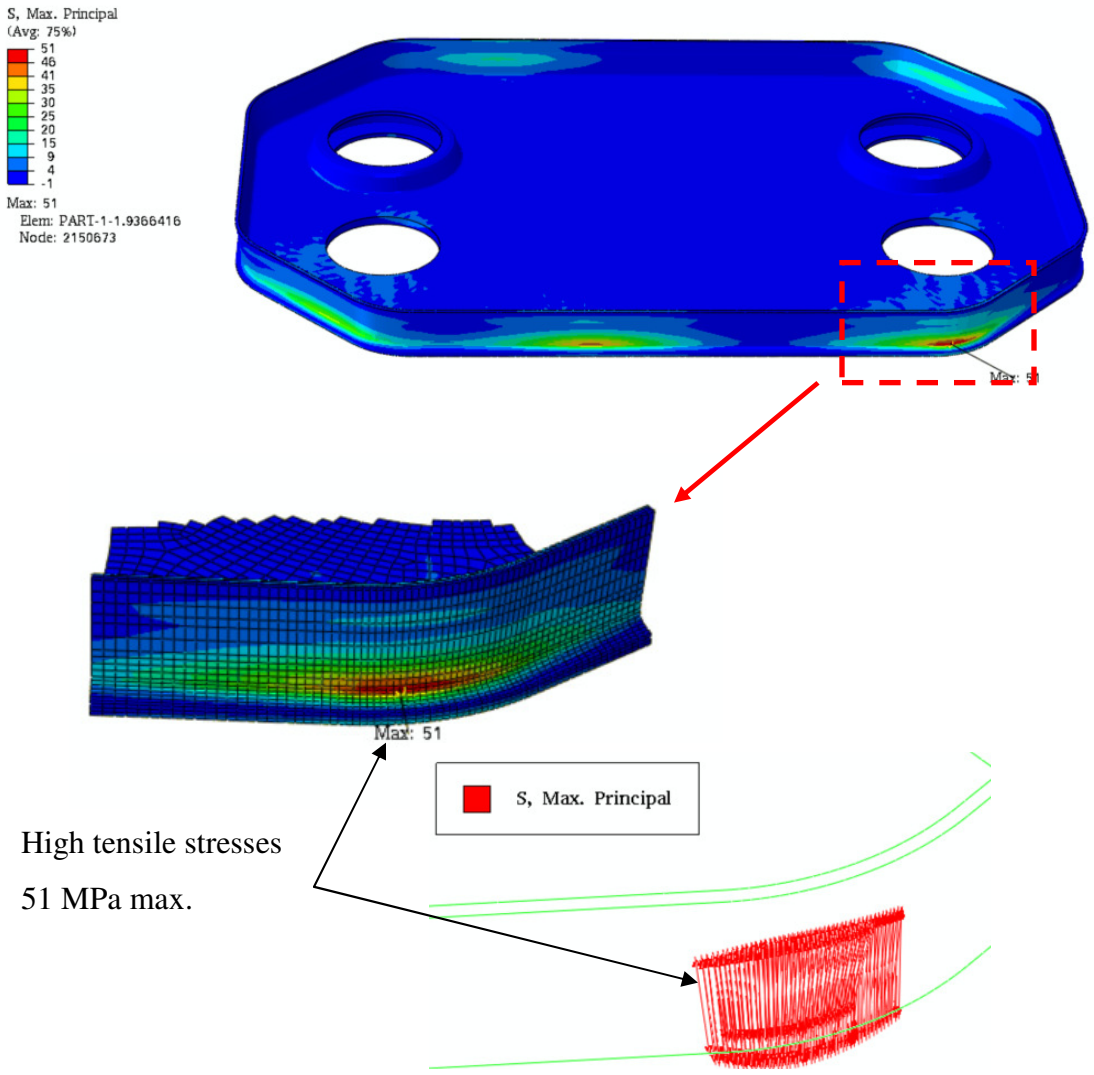

Figure 31. High tensile principal stresses developed in the critical area after the bolt-down step: contours and vector plots.

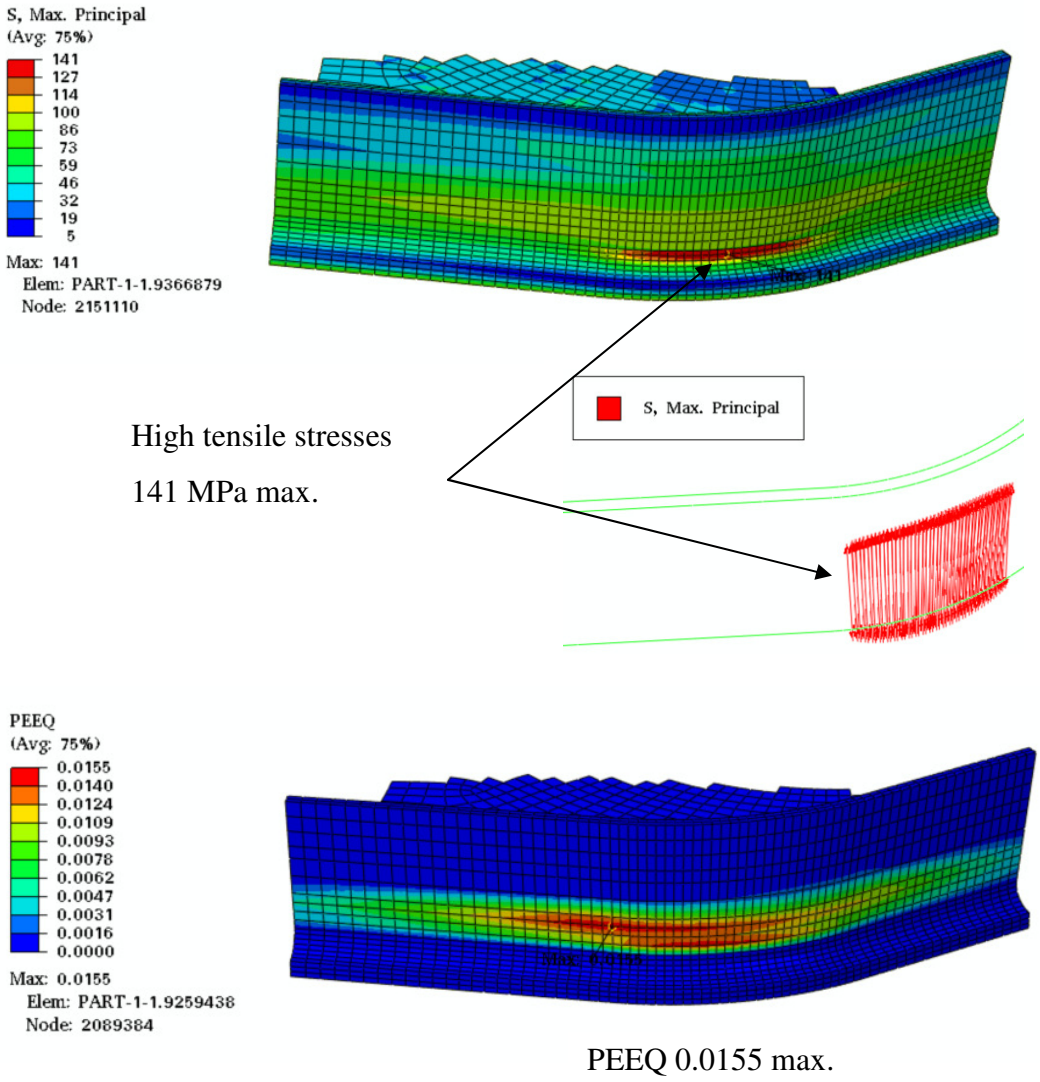

Figure 32. Plots of σ_1 and PEEQ in the critical area at the end of Step 2: 35 bar pressure.

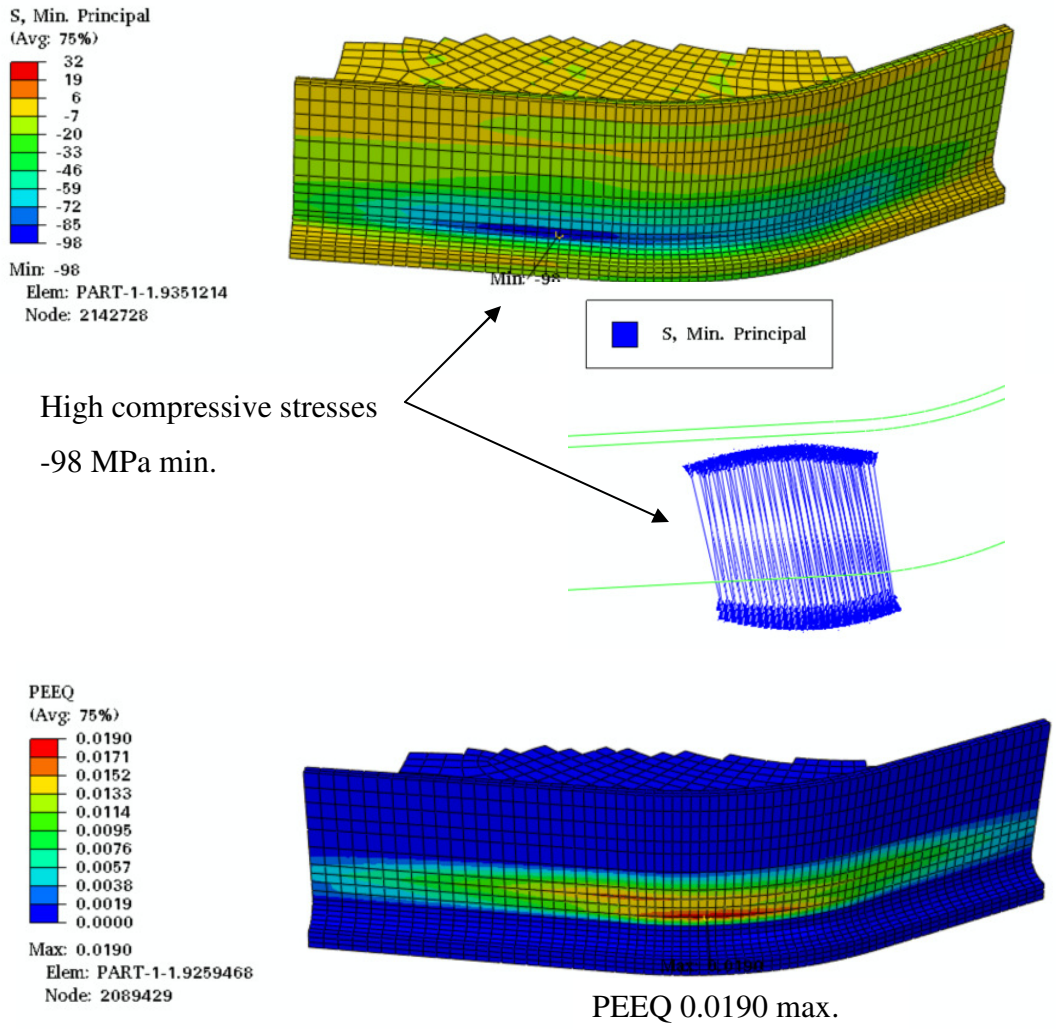

Figure 33. Plots of σ_3 and PEEQ in the critical area at the end of Step 3: 1 bar pressure.

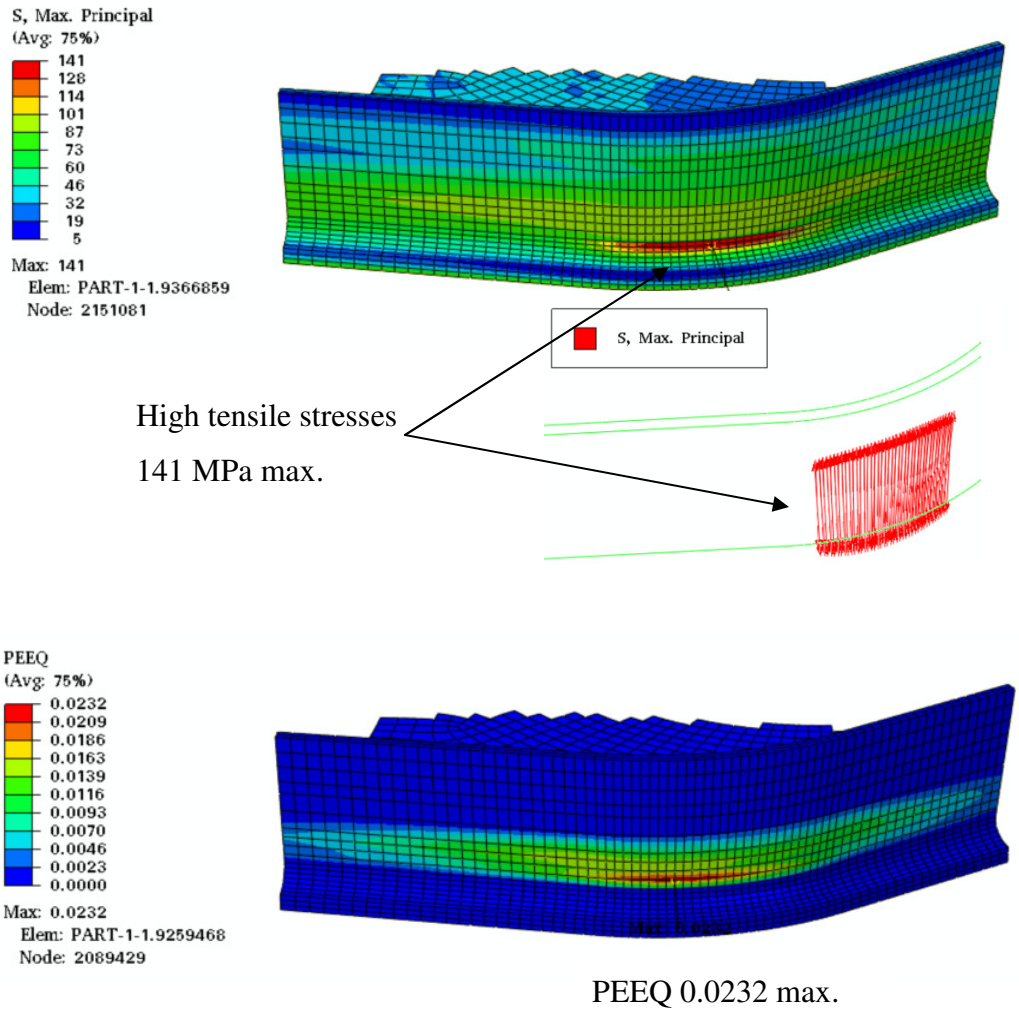

Figure 34. Plots of σ_1 and PEEQ in the critical area at the end of Step 4: 35 bar pressure.

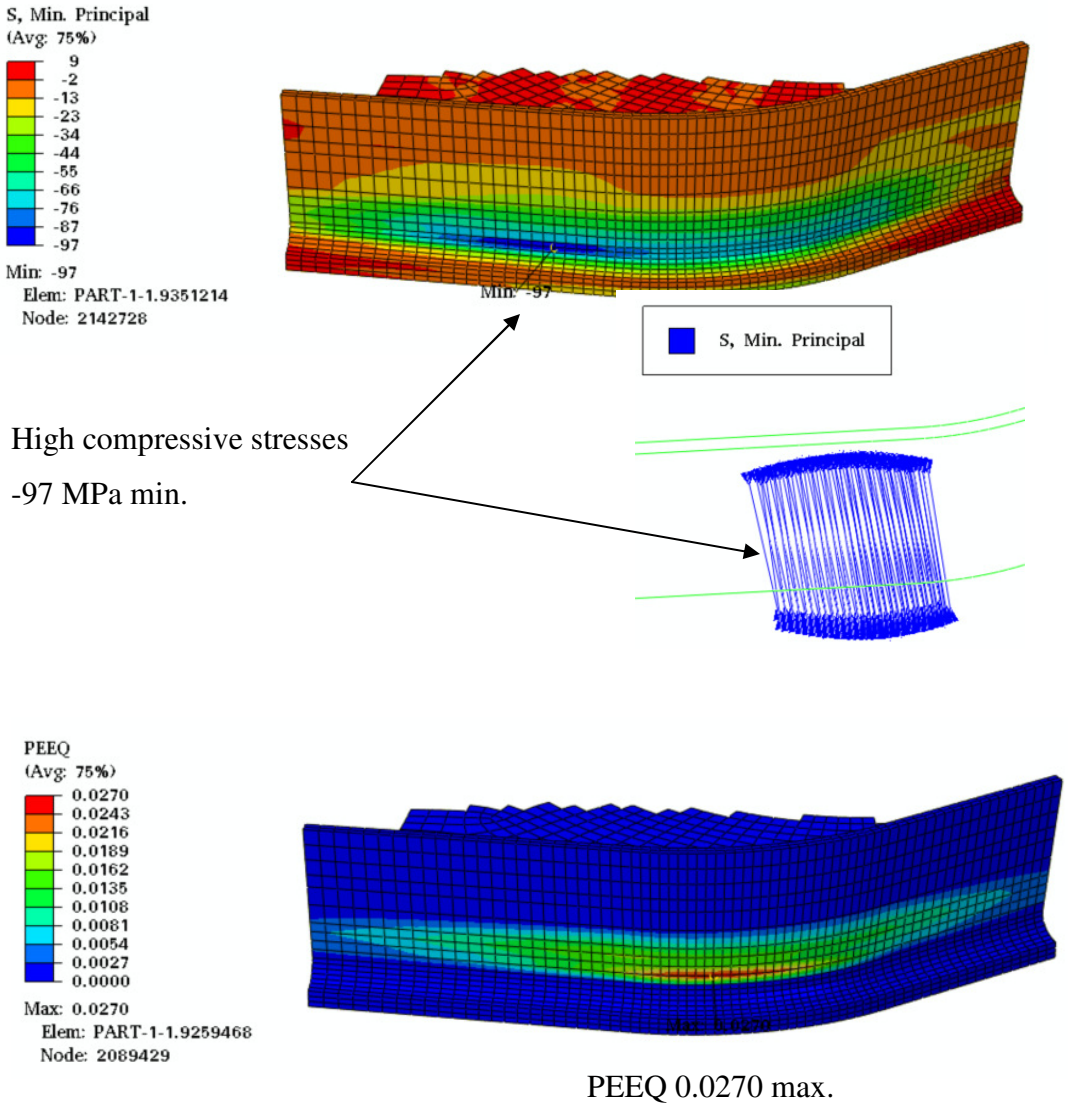

Figure 35. Plots of σ_3 and PEEQ in the critical area at the end of Step 5: 1 bar pressure.

Table 2 summarizes the maximum stress and strain developed in the critical area when the cooler is subjected to the prescribed loading steps.

Load step	Loading condition	Max. stress or strain in the critical area		
		Mises stress (MPa)	σ_1 or σ_3 (MPa)	PEEQ
1	Bolted-down	43	$\sigma_1 = 51$	0
2	35 bar pressure	125	$\sigma_1 = 141$	0.0155
3	1 bar pressure	84	$\sigma_3 = -98$	0.0190
4	35 bar pressure	126	$\sigma_1 = 141$	0.0232
5	1 bar pressure	84	$\sigma_3 = -97$	0.0270

Table 2. Maximum stress and strain developed in the critical area during pressure cycles.

5.4. STRESS-STRAIN EVOLUTION DURING PRESSURE CYCLES

In order to investigate the stress-strain evolution in the critical area during the pressure cycles, the history of the stress and strain tensors at an integration point (IP) of a representative element (IP #7 of element 9259460) are recorded. Figure 36 shows the location of this element and the direction of the direct (true) strains LE11, LE22 and LE33 which are along the global X, Y and Z axes respectively. Note that the direction of LE33 is close to the direction of the high principal stresses, σ_1 and σ_3, mentioned in the previous paragraph. As such, LE33 and direct stress S33 can be used as representative strain and stress components to investigate the evolution of hysteresis loops during pressure cycles.

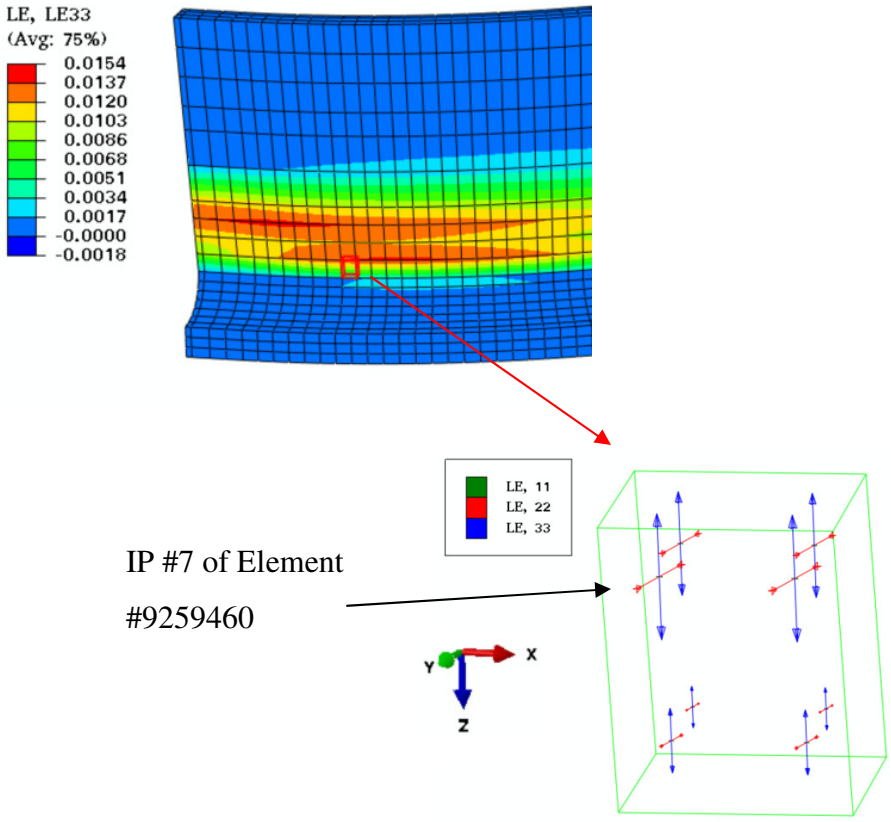

Figure 36. Location of element 9259460 and the direction of direct strain components LE11, LE22 and LE33. Note that LE11 is very small when compared with LE22 and LE33. The contour plot shows LE33 distribution at the end of Step 2 (35 bar pressure).

Figure 37 depicts the variation of direct strain components with load steps. It can be seen that for the whole process, LE33 is tensile, LE22 is compressive and LE11 is almost zero. The plot shows that when undergoing pressure cycles, LE33 and LE22 fluctuate cyclically about non-zero mean strains.

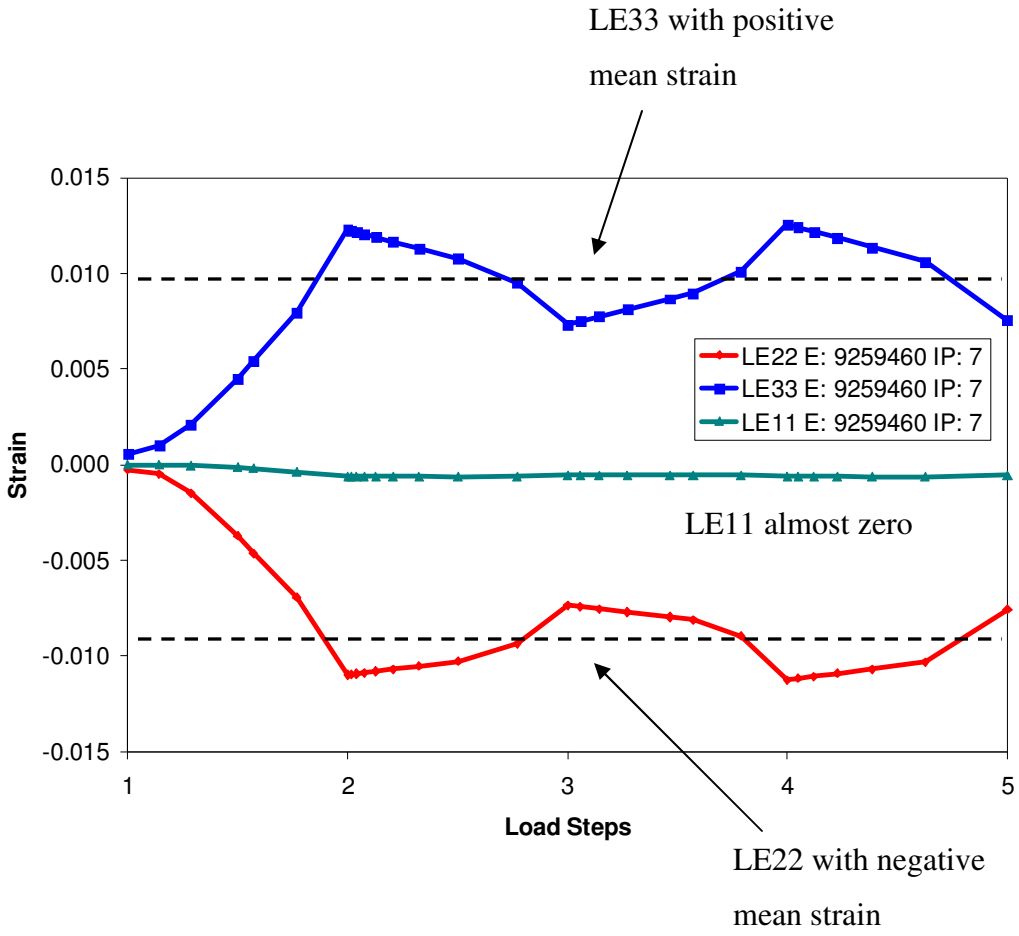

Figure 37. Variation of direct strain components LE11, LE22 and LE33 with load steps.

Figure 38 depicts the variation of direct stress S33 with direct strain LE33. It shows the occurrence of hysteresis loops when the cooler is subjected to pressure cycles. Although the hysteresis loops are not stabilized in the first two pressure cycles, their strain amplitudes and mean stress values are virtually identical. The strain amplitude and the mean stress of a hysteresis loop are important factors governing the fatigue damage incurred by each pressure cycle.

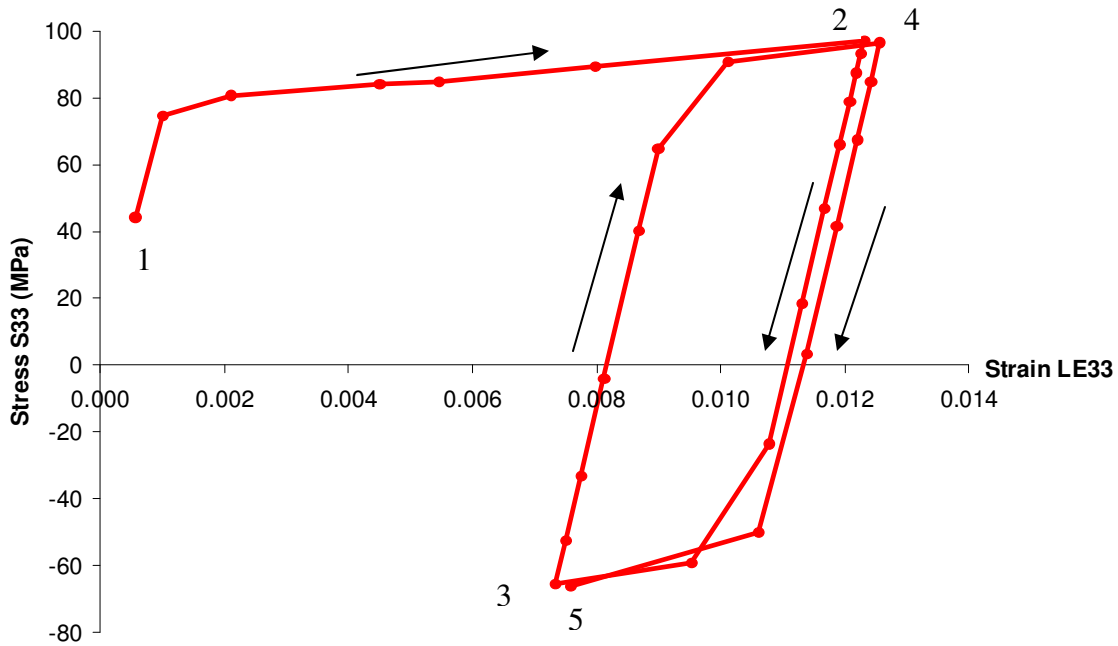

Figure 38. Hysteresis loops formed during pressure cycles with load step numbers.

6. FATIGUE ANALYSIS THEORY

6.1. EQUATIONS FOR UNIAXIAL STRAIN LIFE FATIGUE ANALYSIS

Fatigue calculation to predict the life to crack initiation on the cooler model is performed using fe-safe software, from Safe Technology Ltd [6]. The theories used in performing fatigue analysis of the EOC are discussed thoroughly in the Theory Manual [7]. The EOC fatigue analysis uses strain-life method to evaluate the fatigue life under loading cycles. The calculation requires material properties including the cyclic stress-strain and strain-life curves. The equation for the cyclic stress-strain ($\sigma - \varepsilon$) curve is expressed as:

$$\varepsilon = \frac{\sigma}{E} + \left(\frac{\sigma}{K'} \right)^{\frac{1}{n'}} \qquad (2)$$

where E, K' and n' are the elastic modulus, cyclic strain hardening coefficient and cyclic strain hardening exponent of the material respectively.

The equation for the hysteresis loop stress–strain curve (Ramberg–Osgood equation) that relates stress and strain range ($\Delta\sigma, \Delta\varepsilon$) is given by:

$$\Delta\varepsilon = \frac{\Delta\sigma}{E} + 2\left(\frac{\Delta\sigma}{2K'} \right)^{\frac{1}{n'}} \qquad (3)$$

Typical cyclic stress-strain curve and hysteresis loop for metals are depicted in Figure 39.

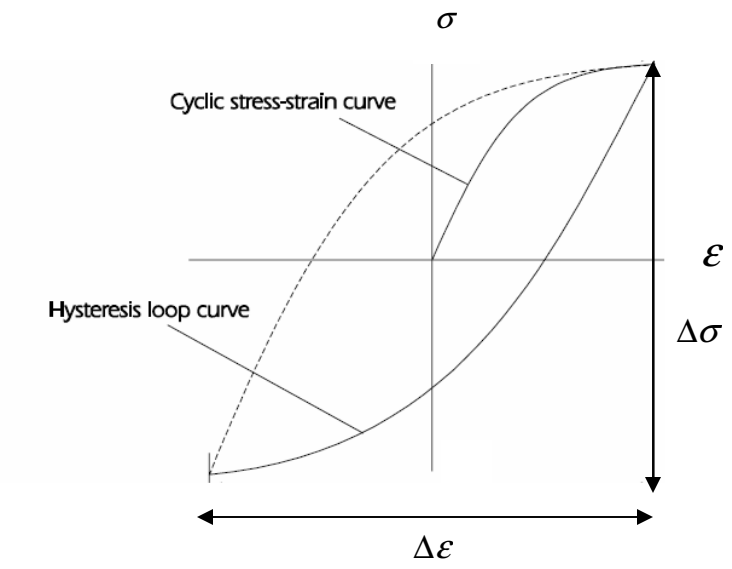

Figure 39. Typical cyclic stress-strain curve and hysteresis loop.

The classical Coffin–Manson description of strain-life relationship for uniaxial stress-strain is expressed as:

$$\frac{\Delta\varepsilon}{2}=\frac{\Delta\varepsilon_e}{2}+\frac{\Delta\varepsilon_p}{2}=\frac{\sigma_f^{'}}{E}(2N_f)^b+\varepsilon_f^{'}(2N_f)^c \tag{4}$$

As depicted in Figure 40, the total strain amplitude $\Delta\varepsilon/2$ is the sum of the elastic strain amplitude $\Delta\varepsilon_e/2$ and plastic strain amplitude $\Delta\varepsilon_p/2$. The above equation relates $\Delta\varepsilon$ to fatigue life N_f (in number of cycles) with the following five material parameters:

E	the elastic modulus
b	the fatigue strength exponent (Basquin's exponent)
$\sigma_f^{'}$	the fatigue strength coefficient
c	the fatigue ductility exponent (Coffin – Mansion exponent)
$\varepsilon_f^{'}$	the fatigue ductility coefficient

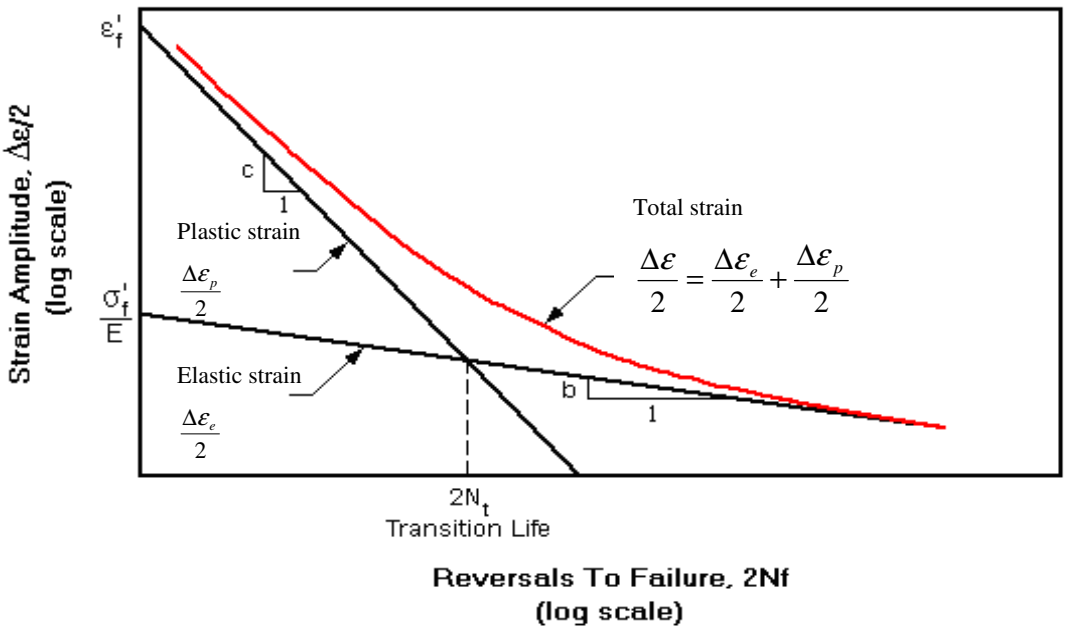

Figure 40. Strain life curve (in red) with elastic and plastic strain amplitude vs. reversals to failure.

Equations (2) to (4) altogether contain seven material parameters: E, K', n', b, σ_f', c and ε_f' that are required for fatigue life calculation. Assuming that Ramberg–Osgood's elastic and plastic strain ranges perfectly correlate with the corresponding Coffin–Manson's ranges, only four of the last six parameters are independent. From the above equations one can derive the following relationships:

$$n' = \frac{b}{c} \tag{5}$$

$$K' = \frac{\sigma_f'}{(\varepsilon_f')^{n'}} \tag{6}$$

The above two equations can be used to determine K' and n' from strain-life parameters when the cyclic stress-strain material properties are not available.

6.2. BROWN-MILLER COMBINED STRAIN CRITERION FOR MUTI-AXIAL FATIGUE ANALYSIS

The aforementioned strain-life equation is only applicable to uniaxial stress-strain condition. For the EOCs that have failed in experimental PC testing, cracks initiate on the surface of the coreplate, in which the stress state is plane stress. However, there is an out-of-plane strain component on the surface, so the strain distribution is tri-axial. As such, multi-axial fatigue theories are used in fatigue life calculation. In strain-life fatigue analysis, there are many multi-axial fatigue theories proposed to meet the need of different material types. Basically they use different criteria to modify the uniaxial strain-life equation. Not all of them give reliable fatigue life prediction for ductile metals. Among them, fe-safe recommends using Brown-Miller combined strain criterion to predict crack initiation of ductile metals [8]. This algorithm is generally agreed to give more realistic life estimates for ductile metals, and tends to be non-conservative for brittle metals.

The Brown-Miller combined strain criterion proposes that the maximum fatigue damage occurs on a plane which experiences the maximum shear strain amplitude, and that the damage is a function of both shear strain and the normal strain on this plane. Kandil, Brown and Miller [9] proposed the following equation, which is a variant of the original Brown-Miller equation:

$$\frac{\Delta\gamma_{\max}}{2}+\frac{\Delta\varepsilon_N}{2}=1.65\frac{\sigma_f^{'}}{E}(2N_f)^b+1.75\varepsilon_f^{'}(2N_f)^c \qquad (7)$$

where $\frac{\Delta\gamma_{\max}}{2}$ and $\frac{\Delta\varepsilon_N}{2}$ are the maximum shear strain and normal strain amplitudes on the plane of maximum shear strain.

In fatigue analysis, it is well known that strain cycles with tensile mean stress cause more fatigue damage than those with zero mean. Based on the observation made on ferrous and non-ferrous metals, Morrow [10] found that the mean stress effect is more significant at long lives, in which elastic conditions predominate. By including the Morrow mean stress correction to the elastic line, the Brown-Miller equation is further modified to the following expression:

$$\frac{\Delta\gamma_{\max}}{2}+\frac{\Delta\varepsilon_N}{2}=1.65\frac{(\sigma_f^{'}-\sigma_{n,m})}{E}(2N_f)^b+1.75\varepsilon_f^{'}(2N_f)^c \qquad (8)$$

where $\sigma_{n,m}$ is the mean normal stress on the plane of maximum shear strain.

6.3. CRITICAL PLANE METHOD

When a component is subject to cyclic loads, the principal strains will fluctuate not only in magnitude, but may also change in orientation during loading history. In such case there is no obvious direction for crack initiation. In performing its fatigue life calculation, fe-safe uses the so-called critical plane method to search for the plane with most damage [11]. For ductile metals under the action of shear strains, fatigue crack initiates on basic planes of maximum shear strain at either 45^o or 90^o to the component surface, as shown in Figure 41. However, the orientation of these basic planes is not unique as they can be any plane rotating about the normal axis of the surface. The critical plane method calculates the damage on these subsidiary planes that are located by rotating each of the basic planes through 180^o at an interval of 10^o increment.

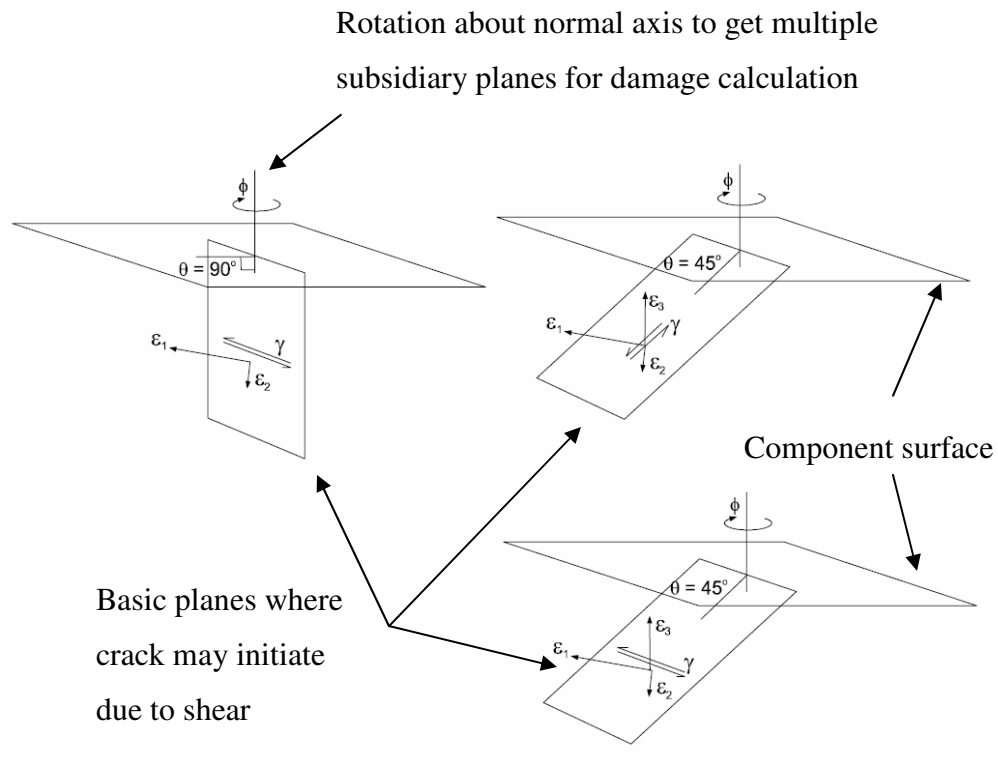

Figure 41. A sketch showing the search procedure for critical plane determination for shear-based crack initiation in ductile metals.

6.4. PLASTICITY CORRECTION OF LINEAR ELASTIC FEA STRESS AND STRAIN DATA

As linear FEA does not account for post-yield material behaviours, plasticity correction is required to convert elastic stress-strain data into elastic-plastic stress-strain data in fatigue analysis. By equating the strain energy for an elastic-plastic material and an infinitely elastic material, Neuber [12] proposed an equation relating the true stress-strain ranges, $\Delta\sigma$ and $\Delta\varepsilon$, to the elastic stress-strain ranges, ΔS and Δe as follows:

$$\Delta\sigma\,\Delta\varepsilon = \Delta S\,\Delta e \qquad (9)$$

Figure 42 explains graphically how the Neuber's plasticity correction rule is applied to uniaxial stress-strain condition. The equation $\Delta\sigma\,\Delta\varepsilon$ = constant is a hyperbola (Neuber hyperbola) linking the point with elastic stress S on the elastic line and the true stress-strain point on the cyclic stress-strain curve.

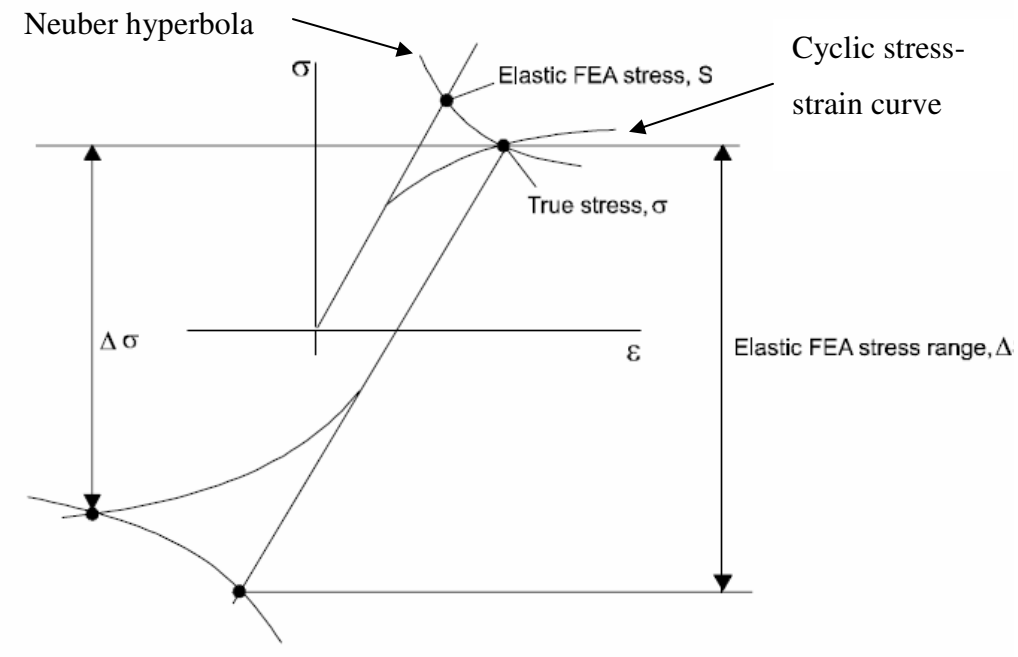

Figure 42. Neuber's rule for uniaxial stress-strain condition.

The equation is modified when applied to biaxial stress state on the surface of a component. The elastically calculated principal stresses and strains (S_1, S_2, e_1 and e_2), and the elastic-plastic principal stresses and strains (σ_1, σ_2, ε_1 and ε_2) are related by the equation (see Figure 43):

$$\sigma_1\varepsilon_1 + \sigma_2\,\varepsilon_2 = S_1\,e_1 + S_2\,e_2 \qquad (10)$$

Note that on the surface of the coreplate, the principal stress S_3 is zero.

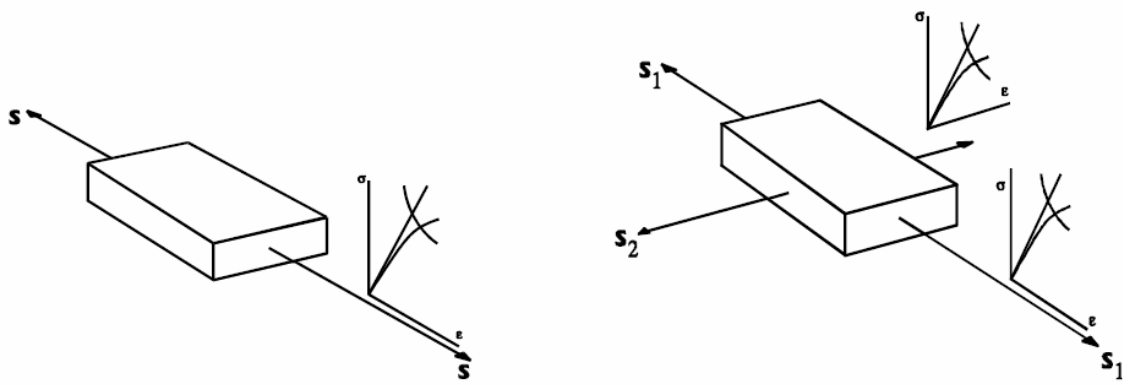

Figure 43. Uniaxial (left) and biaxial (right) Neuber's rule.

6.5. RAINFLOW CYCLE COUNTING ALGORITHM

Rainflow cycle counting algorithm is used in the analysis of fatigue data in order to reduce a spectrum of varying strain, into a set of simple strain reversals. It was first developed by Endo et al. in 1968 [13], who described the process in terms of rain falling off a Japanese pagoda roof. fe_safe uses a similar but more widely utilized cycle counting method published by Socie and Downing [14]. The example shown in Figure 44 is used to illustrate the procedures of the algorithm. The upper picture shows an example of a strain history (data points A-I) plotted vertically. The stress-strain evolution curve is plotted directly below the strain history. In this example, four cycles are identified: one large overall cycle (A-D-I), one intermediate cycle (B-C-B), and two smaller cycles (E-F-E and G-H-G). Each cycle has its own strain range and mean stress which are used in calculating fatigue damage.

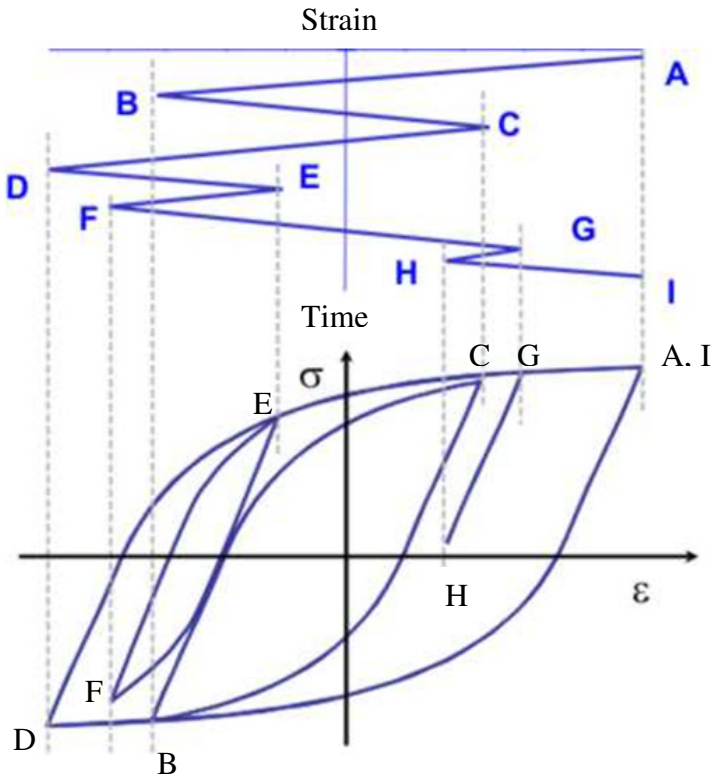

Figure 44. An example of strain history (above) and its corresponding stress-strain hysteresis loops (below).

Figure 45 explains the procedures used in rainflow cycle counting algorithm to sort out the hidden stress-strain cycles from the given strain history illustrated in Figure 44. The procedures are:

1) Reduce the strain time history to a sequence of strain peaks and troughs.

2) Turn the strain history clockwise 90^{o} to form a pagoda roof.

3) A rainflow is started at each peak and trough.

4) When a rainflow path started at a trough comes to a tip of the roof, the flow stops if the opposite trough is more negative than the one the flow started from. Similarly,

when a rainflow path started at a peak comes to a tip of the roof, the flow stops if the opposite peak is more positive than the one the flow started from.

5) If the rain flowing down a roof intercepts the flow from an earlier path, the present path is stopped.

6) The rainflow count applied to the process in Figure 45 results in:

- Half cycles of peak generated strain ranges: A-D, C-C_1, E-F and G-H;
- Half cycles of trough generated strain ranges: B-C, D-I, F-F_1 and H-H_1.

7) Combining the half cycles generated by peaks and troughs into full cycles: A-D-I, B-C-B, E-F-E and G-H-G.

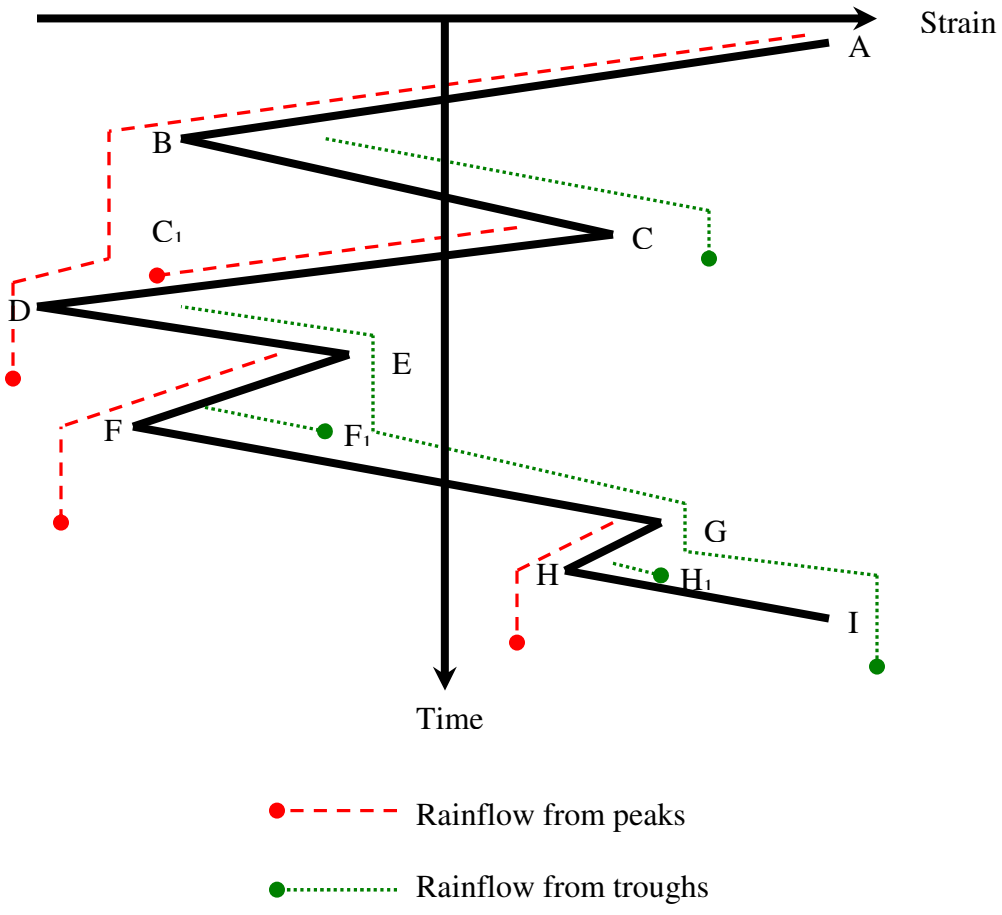

Figure 45. Rainflow counting process of a given strain history.

7. APPROXIMATE FATIGUE MATERIAL MODELS

In the current study, the EOC undergoing PC testing fails at the coreplate, which is made of 3534 aluminum brazing sheet. Since fatigue testing is not viable in the present work, there is no cyclic testing data available for this material. Also, this material is not a common structural aluminum alloy used in automotive or aerospace industry; no published data can be obtained in handbooks or other references. Therefore, an approximate material model is used in the present work. A review of various approximate material models is presented first.

7.1. LITERATURE REVIEW ON EXISTING APPROXIMATE MATERIAL MODELS FOR UNIAXIAL STRAIN-LIFE EQUATION

Many estimates of uniaxial strain–life parameters (b, c, $\sigma_f^{'}$ and $\varepsilon_f^{'}$) from simple testing have been proposed in the literature, mainly for steel and aluminum alloys. The most commonly used method consists of estimating the parameters from properties derived from a monotonic tensile test. These tensile test properties include elastic modulus (E), tensile strength (S_U), reduction in area at fracture (RA), true fracture strain ($\varepsilon_f = 1/(1-RA)$) and true fracture strength (σ_f).

In 1965 Manson proposed the so-called Universal Slopes Method [15], in which the slopes for the elastic and plastic lines of the strain–life curve, b and c, were assumed the same for all metals (b = -0.12 and c = -0.6). In 1977, Mitchell et al.[16] proposed that not only $\sigma_f^{'}$, but also b is a function of S_U; and $\varepsilon_f^{'}$ is equal to ε_f. They proposed the Manson's slope c to be -0.6 for ductile metals and -0.5 for high strength metals. This method was proposed for steel only. In 1988, Muralidharan and Manson [17] revisited the Universal Slopes Method by introducing the ratio S_U/E to estimate both coefficients

$\sigma_f^{'}$ and $\varepsilon_f^{'}$. Based on optimization using experimental data of 47 materials including steel, aluminum and titanium, they found that the coefficient of the plastic line is strongly influenced by the ratio S_U/E, with the ductility term becoming less important when compared with the original Universal Slopes Method. Also, both exponents were changed to b = -0.09 and c = -0.56. This is referred to as the Modified Universal Slopes Method (Mslope model) in the literature. It is 'universal' in the sense that the same exponents are applied to steel and aluminum alloys. In 1990, Baumel and Seeger [18] proposed that the strain–life estimates should be separated according to different alloy families. They observed that both b and c are significantly lower in aluminum and titanium alloys than in steels. In their model, $\sigma_f^{'}$ depends on S_U, and $\varepsilon_f^{'}$ is 0.35 for aluminum alloys. They were the first to ignore the monotonic measure of material ductility in estimating $\varepsilon_f^{'}$. This model, known as Uniform Material Model or Seeger's approximate material model (Seeger model), uses only S_U and E in estimation, and does not need other properties like RA. It is simple and widely used in commercial fatigue software packages such as fe-safe. This model also proposes estimates for the cyclic stress–strain curve parameters $n^{'}$ and $K^{'}$. All other models do not have any estimates for these parameters and they need to be calculated using the earlier equations (5) and (6). In 1993, Ong [19] revisited Manson's four-point correlation method and proposed a few modifications to better fit the experimental data of 49 steels from SAE J1099 technical report on fatigue properties. In this model, b and c are assumed to be functions of S_U and ε_f, while $\varepsilon_f^{'}$ equals to ε_f. In 1995, Park and Song [20] evaluated all existing methods proposed using published data on 138 materials (16 Al, 6 Ti and 116 steels). They found that life predictions using Mslope model are slightly conservative at short lives and non-conservative at long lives. However, they concluded that Mslope model still gives the best performance in life prediction. They also suggested when ε_f is not available, Seeger model can be used as an alternative giving satisfactory results. In 1999, Roessle and Fatemi [21] studied measured properties of 20 steels, together with published data for 49 steels, and arrived at basically the same conclusions as Park and Song. They found

that the Mslope and Seeger models provide satisfactory predictions to estimating strain–life curve. Furthermore, they found no strong correlation between $\sigma_f^{'}$ and σ_f. They also found that using ε_f to estimate $\varepsilon_f^{'}$ can result in significant error. Finally, they proposed a model using hardness and E only. The method was evaluated for steels with hardness in the range between 150 and 700 HB and was shown to provide good approximation of the strain–life curve. In 2002, Meggiolaro and Castro [22] conducted an extensive evaluation of existing approximate models based on published properties of 820 alloys (724 steels, 81 Al and 15 Ti). They found that constant estimates for the ratio $\sigma_f^{'}$ / S_U are in better agreement with studied data and the correlation between $\sigma_f^{'}$ and σ_f is not good and should not be used. Also, it was concluded that $\varepsilon_f^{'}$ does not correlate well with monotonic tensile test properties. In particular, $\varepsilon_f^{'}$ should not be estimated from ε_f. A new model called the Median Method was proposed based on the assumption that better life predictions are obtained simply from constant estimates of the parameters b, c, $\varepsilon_f^{'}$ and the ratio $\sigma_f^{'}/S_U$. These parameters were calculated for each alloy group using the median value obtained from a statistical analysis of the published material data. For aluminum, the constant estimates for $\sigma_f^{'}/S_U$, $\varepsilon_f^{'}$, b and c were obtained as 1.9, 0.28, -0.11 and -0.66 respectively. It was concluded that the Median Method, together with Rosessle–Fatemi, Seeger and Mslope models give good prediction for steels. In 2003, Park and Song [23] proposed a new model for aluminum alloys called the Modified Mitchell's model (Mod_Mitchell model). Based on the same optimization method used in the derivation of the original Mitchell's strain–life equation parameters, they obtained new estimates for the parameters, using experimental data of 16 aluminum alloys. Based on these experimental data, they compared the new method with other existing methods. They concluded that the original Mitchell's method, Seeger model and Mod_Mitchell model give reasonably good life predictions. Among them, the Mod_Mitchell model provided the best results.

The estimates for the strain-life equation parameters of the above approximate models are summarized in Table 3. The following can be concluded from these research works on the prediction of strain–life parameters for aluminum alloys. Firstly, among all these models, the Mslope, Seeger and Mod_Mitchell models have the best performance in life prediction. However, these models cannot give good prediction over the whole life range, from short to long lives. Secondly, the parameter $\varepsilon_f^{'}$ cannot be expressed as a function of ε_f alone. Finally, most of these models derived the parameters using material test data as inputs for optimization. Mslope model used the data from aluminum and non-aluminum alloys altogether to get universal values for b and c. Mod_Mitchell model used wrought and cast aluminum alloys altogether. It is expected that the prediction will be better if the experimental data used are limited to the alloys that have similar material behaviors to the one being approximated.

In the current study, the Mslope, Seeger and Mod_Mitchell models are used as the approximate fatigue material models for the aluminum brazing sheet. Furthermore, the Mslope model is re-assessed and a revised form of it for aluminum alloys is proposed. The fatigue life predictions of the EOC in PC testing using these four material models are carried out and compared with experimental data, over the entire range of testing.

Author	Year	Applicability to materials	Strain-life parameter estimates			
			σ_f'	ε_f'	b	c
Manson	1965	Steels & Al	$1.9S_U$	$0.76\varepsilon_f^{0.6}$	-0.12	-0.6
Mitchell	1977	Steels	$S_U + 345$ (MPa)	ε_f	$\frac{1}{6}\log\frac{0.5S_U}{S_U+345}$	-0.6 for "ductile" -0.5 for "strong"
Muralidharan-Manson	1988	Steels & Al	$0.623E(\frac{S_U}{E})^{0.832}$	$0.0196(\frac{S_U}{E})^{-0.53}\varepsilon_f^{0.155}$	-0.09	-0.56
Baumel-Seeger	1990	Steels	$1.5S_U$	0.59 if $\frac{S_U}{E} < 0.003$ $0.812\text{-}74\frac{S_U}{E}$ otherwise	-0.087	-0.58
		Al	$1.67S_U$	0.35	-0.095	-0.69
Ong	1993	Steels	$S_U(1+\varepsilon_f)$	ε_f	$\frac{1}{6}\log\frac{(S_U/E)^{0.81}}{6.25\sigma_f/E}$	$\frac{1}{4}\log\frac{0.0074-\sigma_f'(10^4)^b/E}{2.074\varepsilon_f}$
Meggillaro-Castro	2002	Steels	$1.5S_U$	0.45	-0.09	-0.59
		Al	$1.9S_U$	0.28	-0.11	-0.66
Park-Song	2003	Al	$S_U + 335$ (MPa)	ε_f	$\frac{1}{6}\log\frac{0.446S_U}{S_U+335}$	-0.664

Table 3. Approximate material models for estimation of strain-life equation parameters.

7.2. RE-ASSESSMENT OF MSLOPE MODEL FOR ALUMINUM ALLOYS

Several researches have indicated that the Mslope model provides excellent prediction of fatigue life when compared with other proposed models. In 1988 Muralidharan and Manson developed the Mslope model by revisiting the original Universal Slopes equation and introducing a new form of strain–life equation:

$$\Delta\varepsilon = A_1 \varepsilon_f^{\alpha_1} (\frac{S_U}{E})^{\beta_1} (N_f)^{\gamma_1} + A_2 (\frac{S_U}{E})^{\beta_2} \varepsilon_f^{\alpha_2} (N_f)^{\gamma_2} \qquad (11)$$

The constants in equation (11), $A_1, A_2, \alpha_1, \alpha_2, \beta_1, \beta_2, \gamma_1 and\ \gamma_2$, were determined by optimization with least squares approach using experimental fatigue test data of 47 alloys including steel, aluminum and titanium. They came up with the following strain-life equation, expressed in the following standard form:

$$\frac{\Delta\varepsilon}{2} = 0.623(\frac{S_U}{E})^{0.832} (2N_f)^{-0.09} + 0.0196(\frac{S_U}{E})^{-0.53} \varepsilon_f^{0.155} (2N_f)^{-0.56} \qquad (12)$$

They found that the influence of ductility on the elastic line is negligible and the plastic line is strongly affected by the ratio of S_U/E.

In fatigue analysis of the current EOC model that involves failures on aluminum brazing sheet, the Mslope model of Muralidharan and Manson needed to be improved. The brazing sheet is made of non-heat treatable 3534 aluminum, a modified form of 3003 aluminum with improved strength. An attempt is made in the present work to get better estimates for the constants in equation (11) for this alloy as the work of Muralidharan and Mansion was based on a collection of alloys including steels, aluminum and titanium. It is desirable if the test data for similar non-heat treatable aluminum alloys, like 1000, 3000 and 5000 series aluminum, are used in optimization. After an extensive material search on handbooks and references, the fatigue data of 51 aluminum alloys are collected. However, among them, only 18 are wrought aluminum and with full material data including the required monotonic tensile test properties [24, 25, 26]. Their material test

data are listed in Appendix A5. They include 1000 (3), 2000 (8), 5000 (3), 6000 (3) and 7000 (1) series alloys. Among them, only 6 are non-heat treatable alloys. In order to have broader input data for optimization calculation, data from all 18 materials are included.

Based on these test data, the following revised form of equation (12) of Muralidharan and Manson was obtained for aluminum alloys:

$$\frac{\Delta\varepsilon}{2} = 2.766\left(\frac{S_U}{E}\right)^{1.086}(2N_f)^{-0.101} + 0.0537\left(\frac{S_U}{E}\right)^{-0.409}\varepsilon_f^{\,0.456}(2N_f)^{-0.639} \qquad (13)$$

The approximate material model for aluminum using equation (13) is being referred to as the Mslope_Al model in the present study.

7.3. EVALUATION OF LIFE PREDICTION PERFORMANCE OF APPROXIMATE FATIGUE MATERIAL MODELS BASED ON TENSILE AND FATIGUE TEST DATA OF ALUMINUM ALLOYS

The parameters of the strain–life equation based on the Mslope, Seeger, Mod_Mitchell models, and the newly revised Mslope_Al model for aluminum alloys are summarized in Table 4. Before applying these approximate material models to predict fatigue life of EOC undergoing pressure cycle testing, the performance of them in life predictions based on test data of the aforementioned 18 aluminum alloys are first evaluated. Figure 46 to Figure 49 compare the correlation between the predicted life and the experimental life of these aluminum alloys. The predicted life is calculated by applying the approximate models to derive the strain-life parameters from tensile test data. The experimental life is calculated based on the strain-life test data. The 3 and 10 times scatter bands are added to highlight the level of correlation. Firstly, it can be seen that for all these approximate models, most of the data points lies within 10 times scatter band, except for a few points belonging to three 6000 series alloys. This indicates that these approximate models give very conservative life prediction at long lives for 6000 series aluminum alloys. Secondly,

the percentage of data points lying within 3 times scatter band is compared. The comparison in Table 5 concludes that among these models, Mslope_Al yields the best correlation by having the largest percentage of data points lying within 3 times scatter band.

Models	$\sigma_f^{'}$	$\varepsilon_f^{'}$	b	c
Mslope	$0.623(\frac{S_U}{E})^{0.832}E$	$0.0196(\frac{S_U}{E})^{-0.53}\varepsilon_f{}^{0.155}$	-0.09	-0.56
Seeger	$1.67\,S_U$	0.35	-0.095	-0.69
Mod_Mitchell	S_U +335 (MPa)	ε_f	$-\frac{1}{6}\log(\frac{S_U+335}{0.446S_U})$	-0.664
Mslope_Al	$2.766(\frac{S_U}{E})^{1.086}E$	$0.0537(\frac{S_U}{E})^{-0.409}\varepsilon_f{}^{0.456}$	-0.101	-0.639

Table 4. Four approximate models for strain – life equation.

Models	Percentage of data points lying within 3 times scatter band
Mslope	77
Seeger	70
Mod_Mitchell	75
Mslope_Al	87

Table 5. Comparison of life prediction performance of different approximate models using test data of 18 Al alloys.

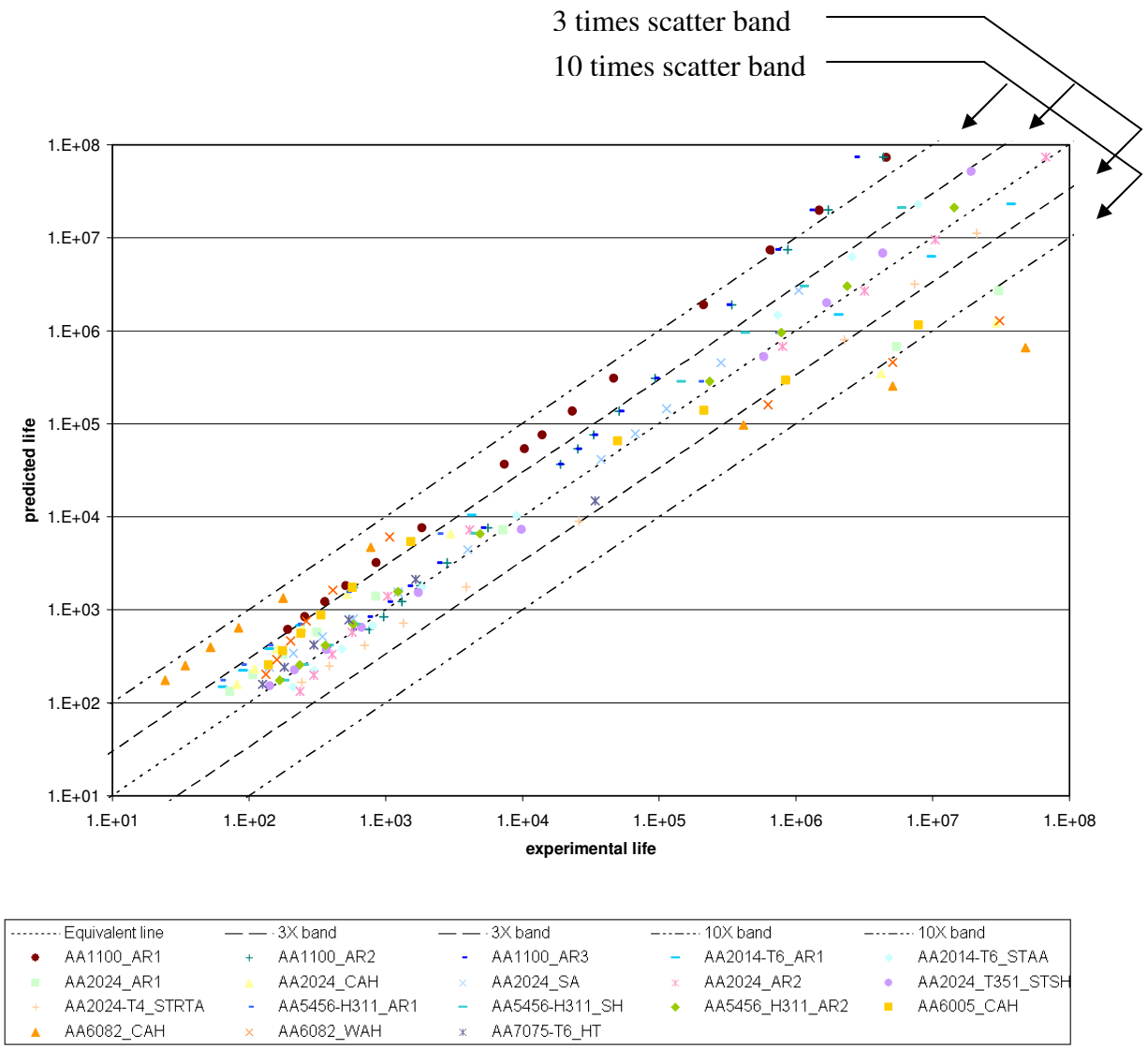

Figure 46. Life prediction correlation of the Mslope model using test data of 18 aluminum alloys.

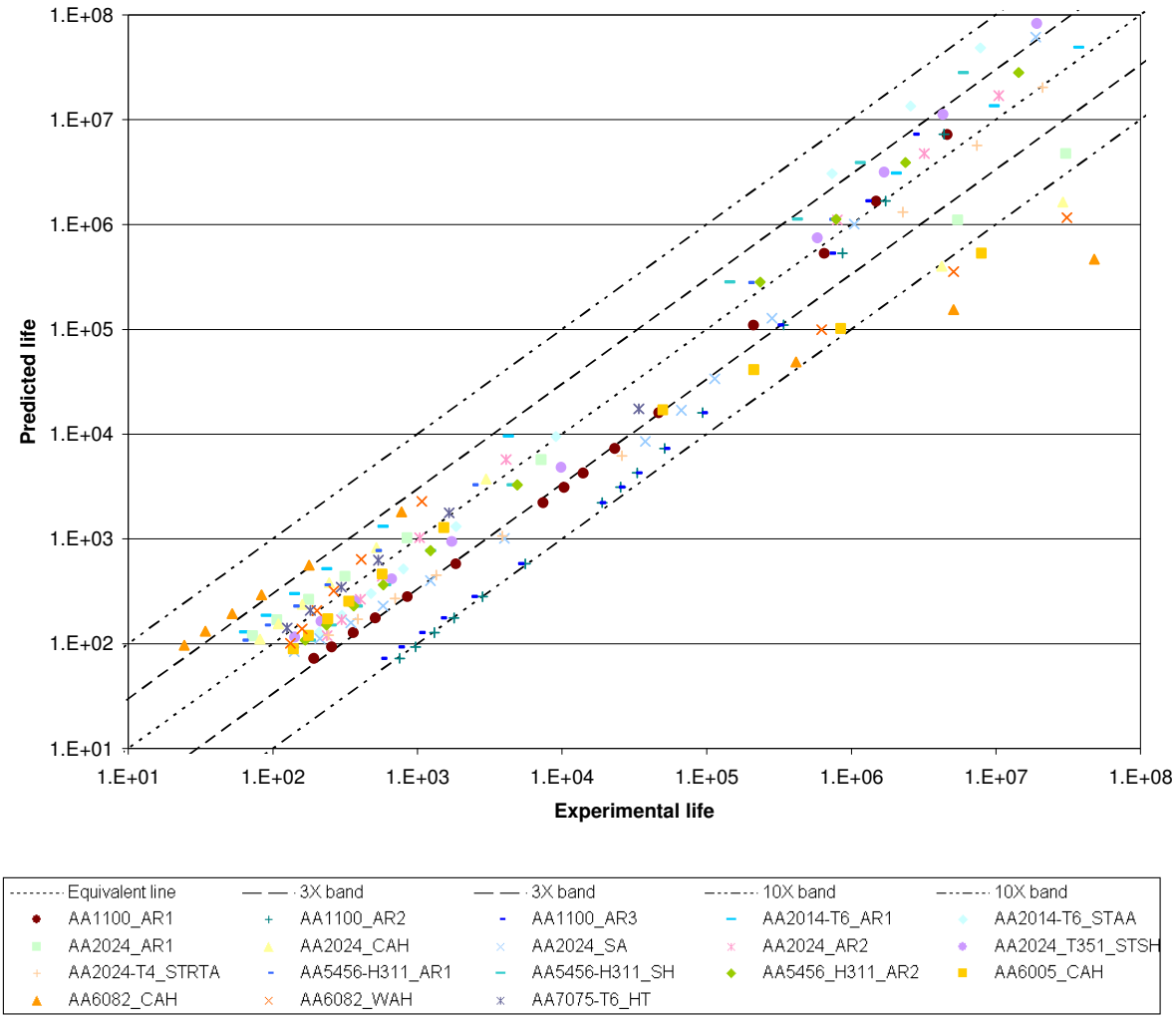

Figure 47. Life prediction correlation of the Seeger model using test data of 18 aluminum alloys.

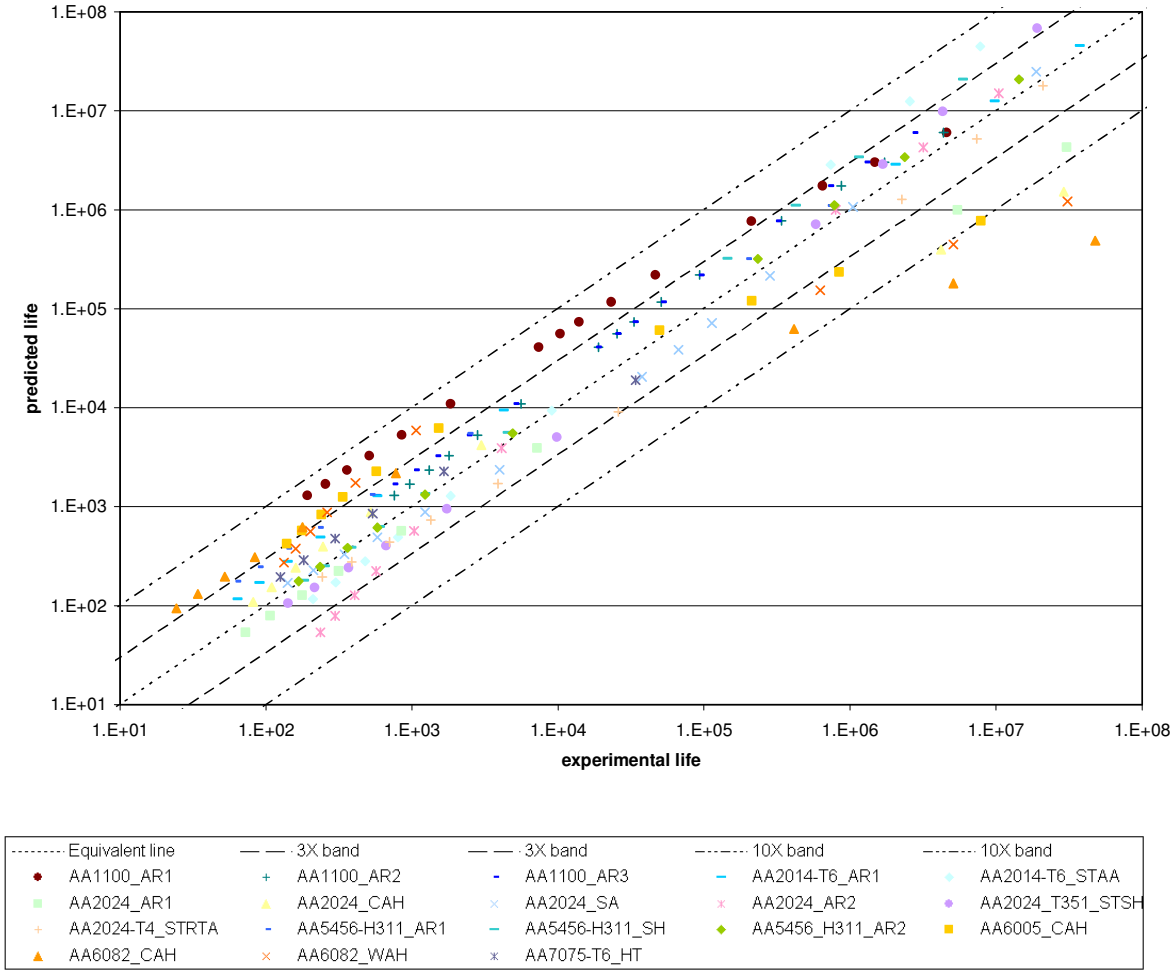

Figure 48. Life prediction correlation of the Mod_Mitchell model using 18 aluminum alloys.

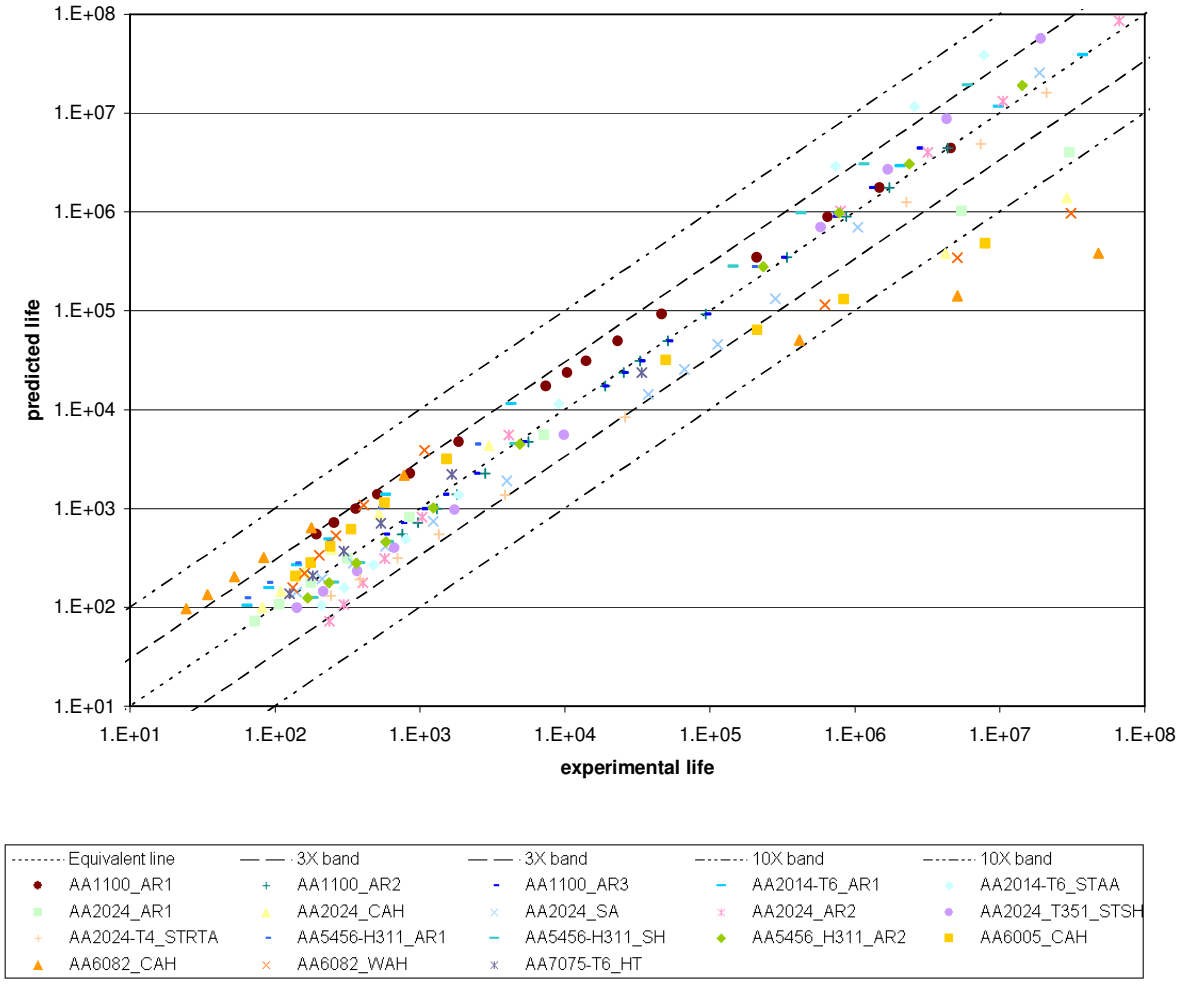

Figure 49. Life prediction correlation of the Mslope_Al model using test data of 18 aluminum alloys.

7.4. APPROXIMATE FATIGUE MATERIAL PROPERTIES FOR COREPLATE MATERIAL

Tensile test of post-braze 3534 aluminum coreplate material yields the following properties:

$$E = 69\text{GPa},\ S_U = 138\text{MPa},\ \varepsilon_f = 1.61.$$

From these data, the estimates for the strain-life and cyclic stress-strain parameters for different approximate material models are calculated and compared in Table 6. The strain-life curves are shown in Figure 50. Note that only the Seeger model gives estimates for the cyclic stress–strain curve parameters. For other models, the values are determined by equations (5) and (6).

Models	Strain – life parameters				Cyclic stress – strain parameters	
	σ_f'	ε_f'	b	c	n'	K'
Mslope	244.1	0.569	-0.09	-0.56	0.161	267.3
Seeger	230.5	0.35	-0.095	-0.69	0.110	222.2
Mod_Mitchell	473	1.61	-0.148	-0.664	0.222	425.5
Mslope_Al	224.3	0.850	-0.101	-0.639	0.158	230.1

Table 6. Estimates for parameters of fatigue properties for coreplate material.

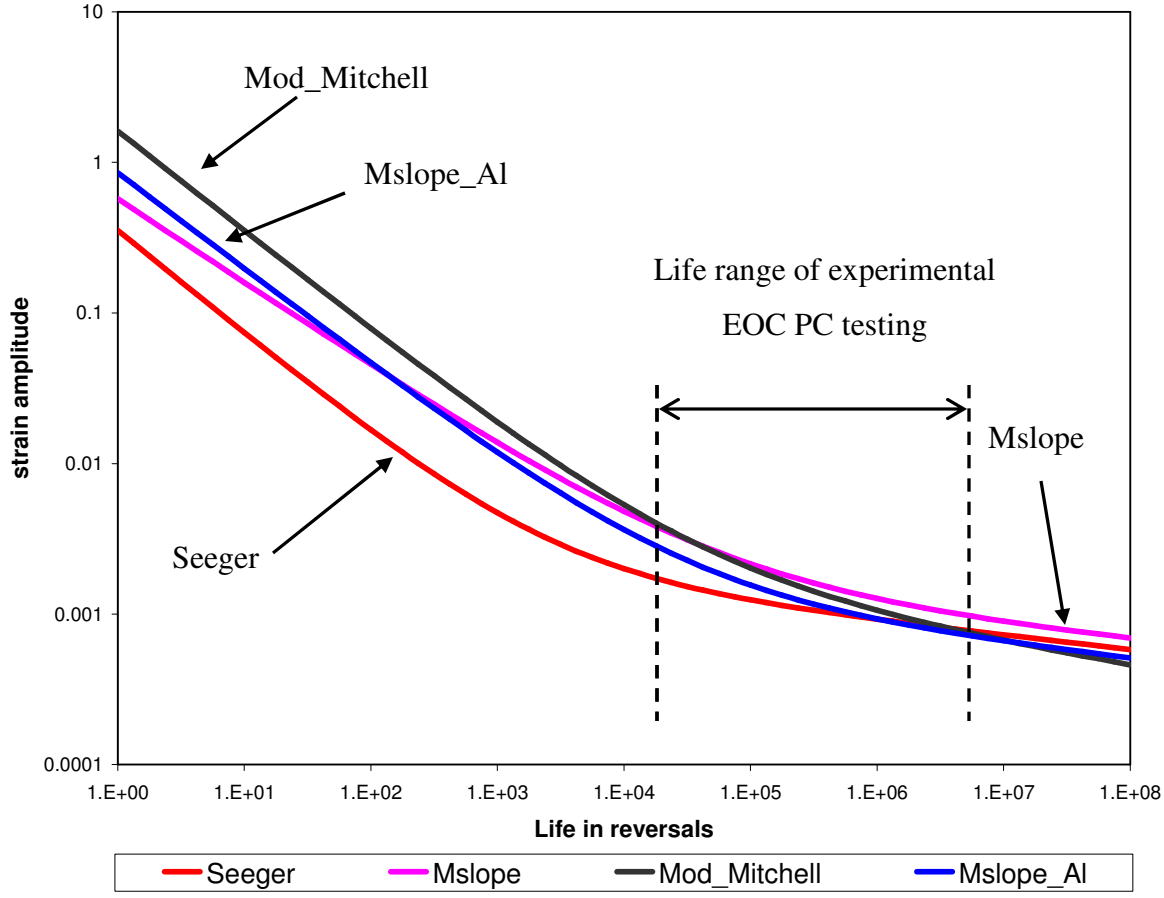

Figure 50. Strain-life curves for different approximate models for coreplate material.

In the present study, the life range of all oil coolers in the experimental PC testing is about 7 k to 3.5 M cycles (14 k to 7 M reversals). For this life range, the Seeger model will give shortest life prediction for low cycle failures and Mslope model will give longest life prediction for high cycle failures.

7.5. INFLUENCE OF STRAIN-LIFE PARAMETERS ON LIFE PREDICTION – A PARAMETER SENSITIVITY STUDY

The accuracy of fatigue life prediction using approximate material model depends heavily upon good estimation of strain-life parameters $\sigma_f^{'}$, $\varepsilon_f^{'}$, b, and c. Any deviation in the estimation of each parameter affects the predicted fatigue life. A sensitivity study is performed to investigate the influence of each parameter individually on the accuracy of life prediction. Firstly, a baseline strain-life curve of the coreplate material is established. The Seeger model is chosen arbitrarily and its numerical estimates for the parameters (Table 6) are used to establish the baseline strain-life curve of the coreplate material. Secondly, modified strain-life curves are derived by altering the numerical value of one parameter of the baseline curve at a time, with either 30% increase or reduction in value. The life prediction based on the baseline curve and the modified curves are correlated to investigate the influence of each parameter on the accuracy of life prediction, and the results are depicted in Figure 51 to Figure 54.

Some conclusions can be made from these correlation curves in the life range pertaining to experimental PC testing. Firstly, the change of fatigue ductility coefficient, $\varepsilon_f^{'}$, has little influence on life prediction, especially at long lives. Secondly, the deviation of fatigue ductility exponent, c, has a substantial impact on life predictions, especially in low cycle failures of the EOC. Finally, both fatigue strength coefficient, $\sigma_f^{'}$, and fatigue strength exponent, b, have large impact on life prediction for high cycle failures. The sensitivity study indicates that in life prediction of EOC PC testing using an approximate fatigue material model, accurate prediction for high cycle failures is more difficult than that for low cycle failures.

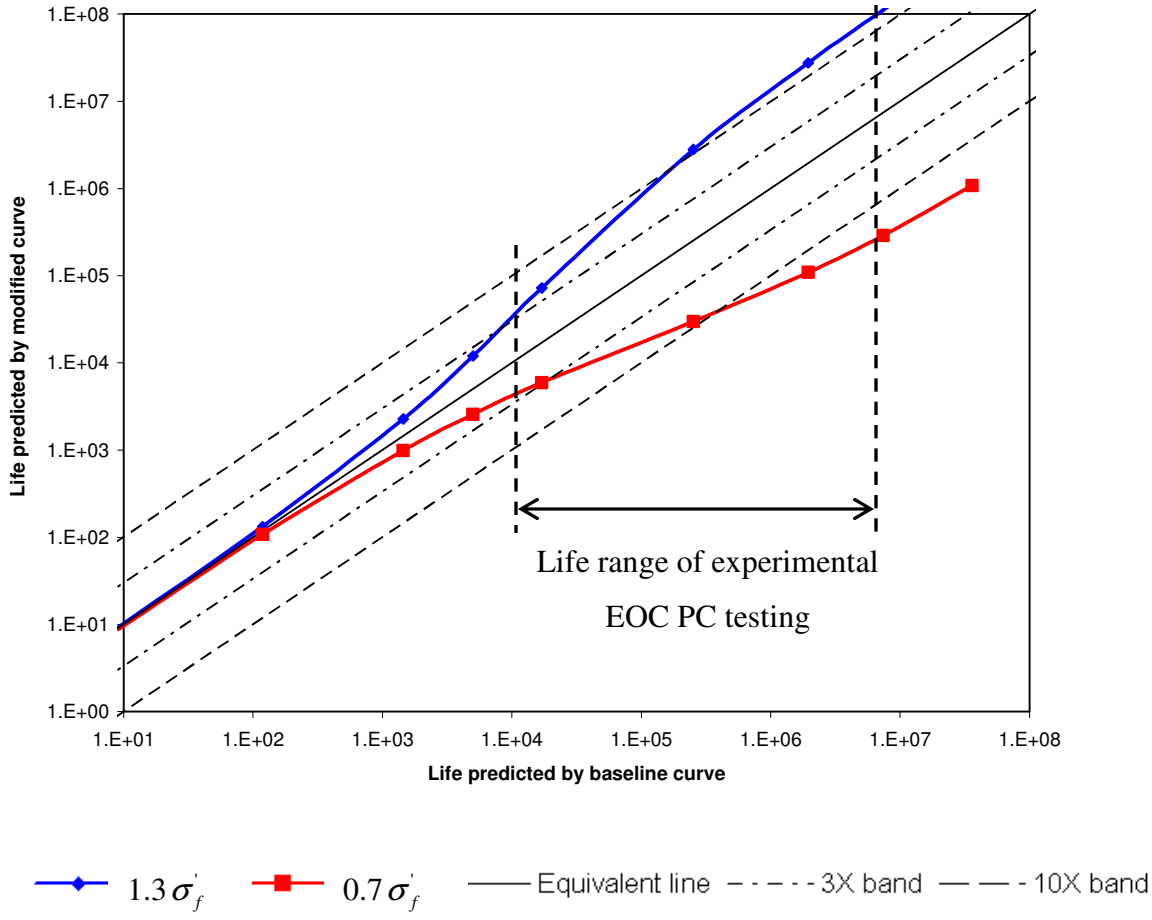

Figure 51. Influence of $\sigma_f^{'}$ on life prediction (life in reversals).

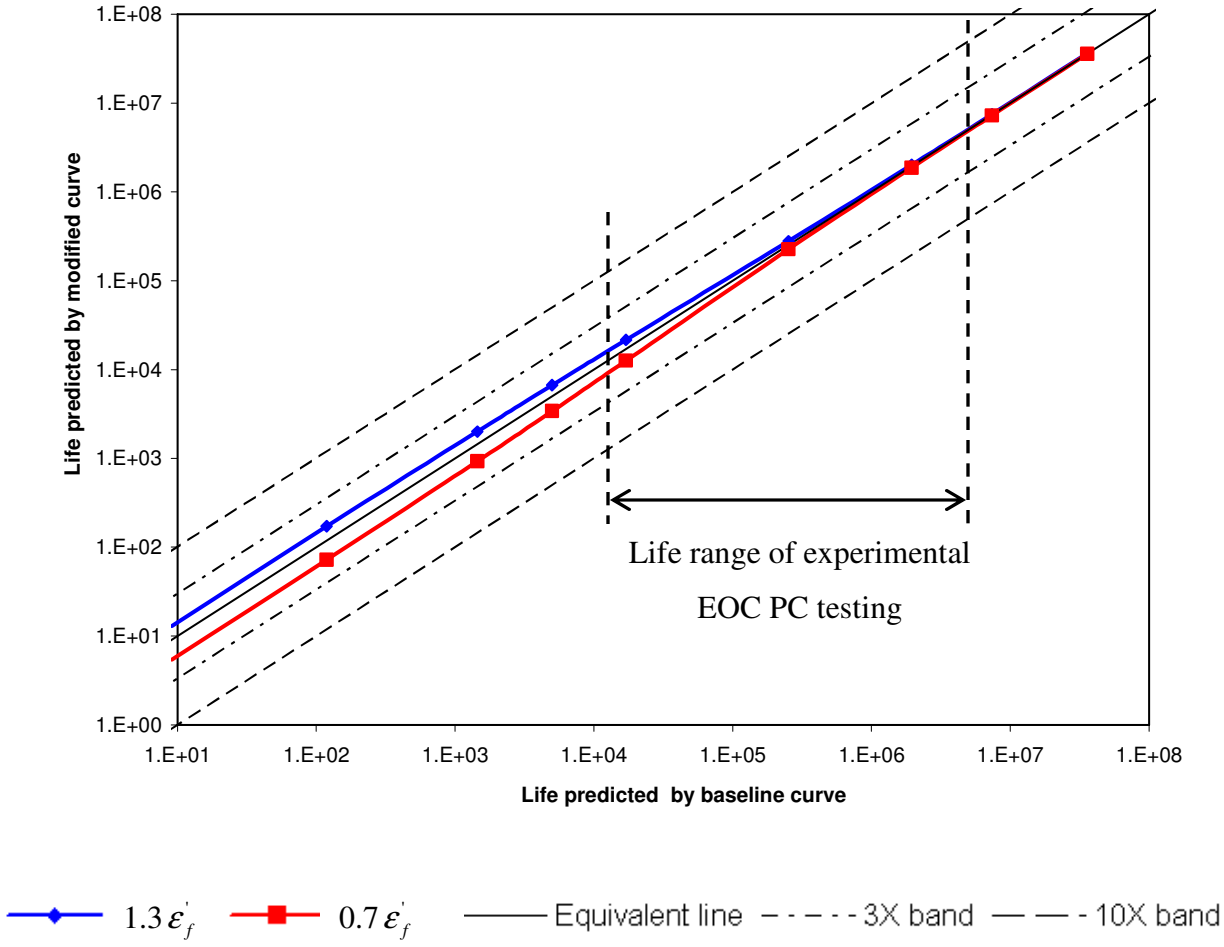

Figure 52. Influence of $\varepsilon_f^{'}$ on life prediction (life in reversals).

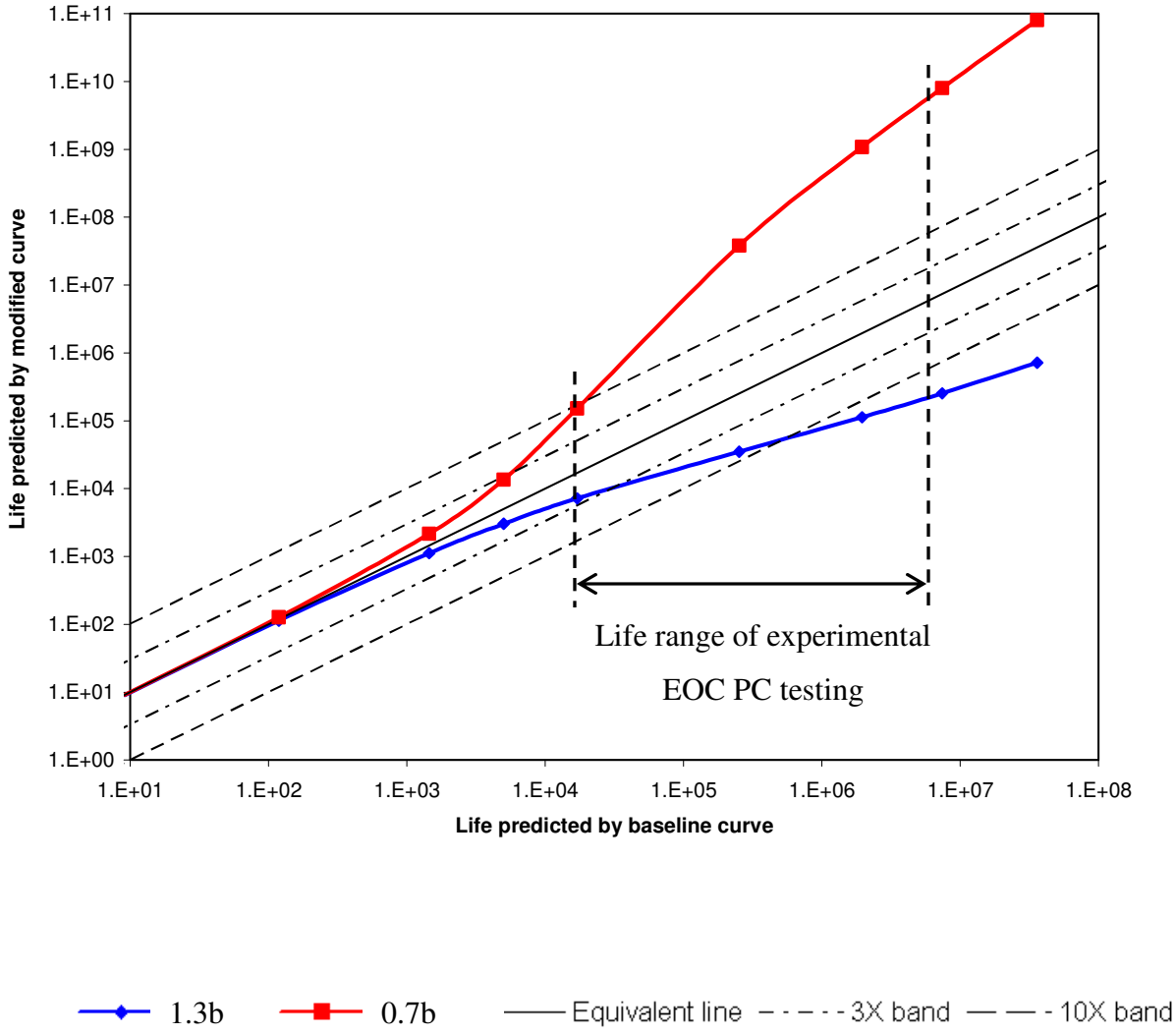

Figure 53. Influence of b on life prediction (life in reversals).

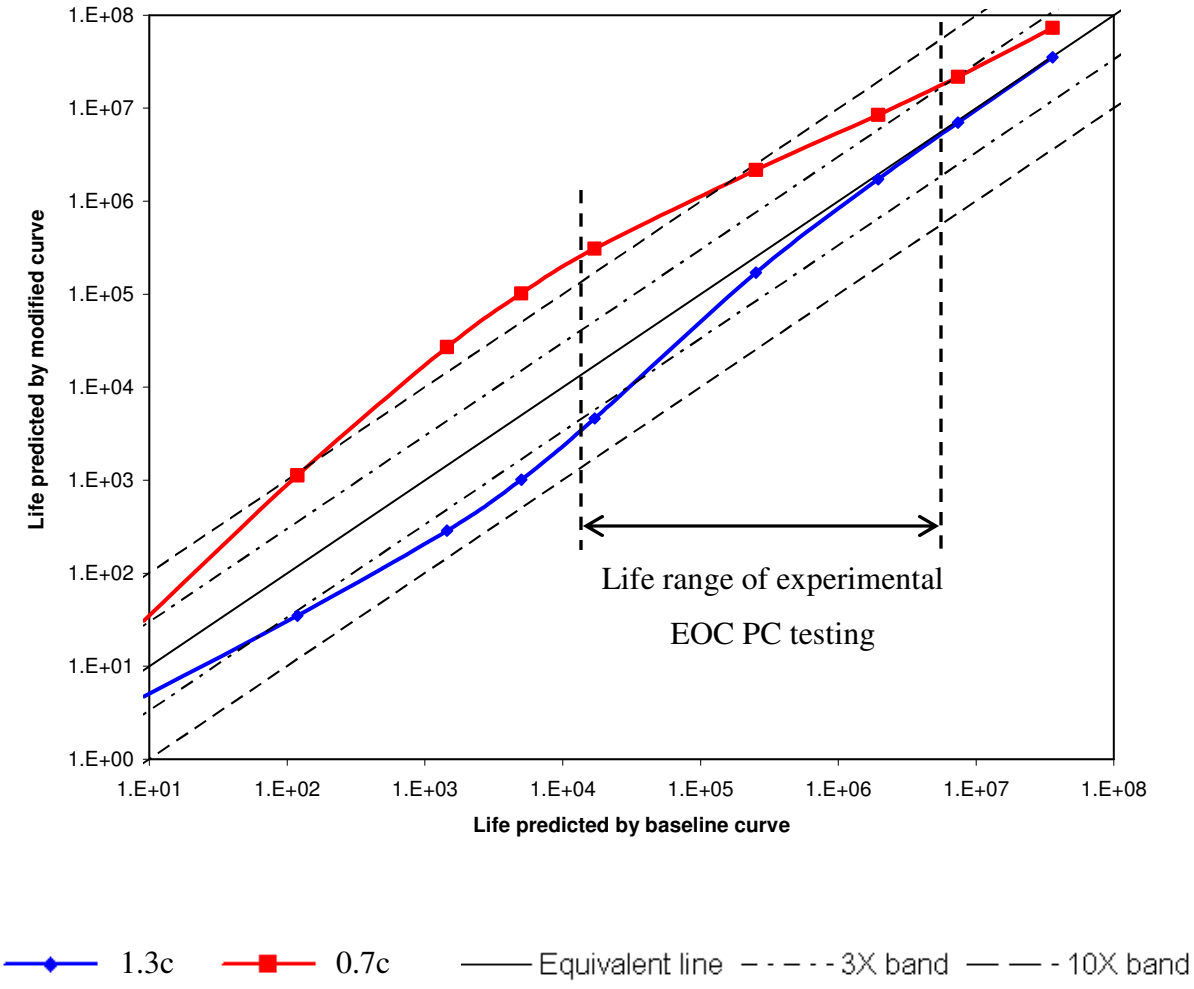

Figure 54. Influence of c on life prediction (life in reversals).

8. LIFE PREDICTION OF EOC FAILURES USING FEA RESULTS

8.1. OVERVIEW OF DIFFERENT SIMULATION APPROACHES OF USING FEA RESULTS IN FATIGUE ANALYSIS

Fatigue analysis can be performed using linear or nonlinear FEA results. In the past, most of the fatigue predictions based on simulation were conducted using linear results, especially in cases in which the structure is subjected to load cycles of long time history. In spite of great advancement in computer hardware capability in recent years, using nonlinear results, from an FEA with a large number of steps defined by the loading history, to perform fatigue life calculation is still computationally prohibitive. However, as the PC testing of the EOC in the current study uses simple repetitive load cycles, it is viable to perform nonlinear FEA to get stress and strain datasets for subsequent fatigue life calculation. The performances of two simulation approaches are investigated as described below.

1) The fatigue life calculation is based on linear elastic FEA stress results:

This is the simplest approach in which a linear FEA with an arbitrary pressure loading is performed to provide elastic stress results for fatigue analysis. In fatigue analysis, these elastic stress results are scaled according to the loading defined by a specified pressure cycle profile. Mean stress effect and plasticity corrections are included in the calculation.

2) The fatigue life calculation is based on nonlinear FEA stress and strain results:

Firstly, a multiple-step nonlinear analysis is performed. The analysis steps include the bolt-down of the cooler and the subsequent application of pressure cycles. The stress and

strain (both elastic and plastic strains) datasets are used in fatigue life calculation and no plasticity correction is needed.

8.2. LIFE PREDICTION BASED ON LINEAR FEA RESULTS

This is the simplest simulation approach in which a linear FEA is performed with the EOC model fully clamped at the bolt-hole areas and subject to a pressure loading of 20 bar. It uses a simplified mounting configuration that does not include the effect of the initial bolt-down of the cooler to the fixture. No O-ring interaction and fixture contact interaction are included in the analysis. The subsequent fatigue analysis uses Brown-Miller material algorithm and Neuber's plasticity correction to calculate the fatigue life for each node. The critical plane search method is used to locate the plane with most damage. For each node, the analysis process is summarized as follows:

- The stress tensors are scaled according to the loading history defined by the pressure cycle profile and the time history of each of the six components of the stress tensor are calculated.
- The time histories of the in-plane principal stresses are calculated.
- The time histories of the three principal strains are calculated from the stresses.
- Multi-axial Neuber's plasticity correction is used to convert the elastic stress-strain histories into elastic-plastic stress-strain histories.
- The basic planes of maximum shear strain are defined using planes perpendicular to and at 45^{o} to the surface.
- For each of the three basic planes, 18 subsidiary planes spaced at 10^{o} increments are formed by rotation about the axis normal to the surface.
- For each subsidiary plane, the time histories of the damage parameters are cycle counted. For Brown-Miller material algorithm, the damage parameters are shear

and normal strain. Individual fatigue cycles are identified using the Rainflow cycle counting algorithm.

- For each subsidiary plane, the time history of normal stress is calculated and cycle counted. For each cycle, the mean normal stress is calculated and used in the Morrow mean stress calculation.
- For each subsidiary plane, the fatigue damage for each cycle is calculated and the total damage is summed using Miner's Rule [27]. The plane with the shortest life is defined as the most critical plane of crack initiation.

The stress results of the linear FEA are used as inputs for fatigue calculation. The pressure cycle profiles used in experimental PC testing are used to define the loading cycles. Life prediction calculation in the critical area of the coreplate is performed using the approximate material models including the Mslope, Seeger, Mod_Mitchell and Mslope_Al. Figure 55(a) is a typical plot showing the distribution of the predicted life (Loglife, in log scale) in the critical area. This Loglife plot depicts the predicted life to crack initiation at the surface nodes when the cooler is subject to 1–20bar pressure cycles. In this case, the Mslope approximate material model is used in fatigue calculation. The stress plot in Figure 55(b) is copied from Figure 22, and used as a reference to show the stress distribution obtained from the corresponding linear FEA.

In this case (Mslope, 1-20 bar PC), the minimum Loglife is 6.196 that represents a predicted life of 1.57 million cycles. This occurs at the base of the coreplate, in the area above the braze fillet. In the experimental test, the failures of three EOCs occur at 0.29, 0.35 and 0.46 million cycles. The predicted location of failure is consistent with that observed in testing but the life predictions are non-conservative, with over-estimated life results.

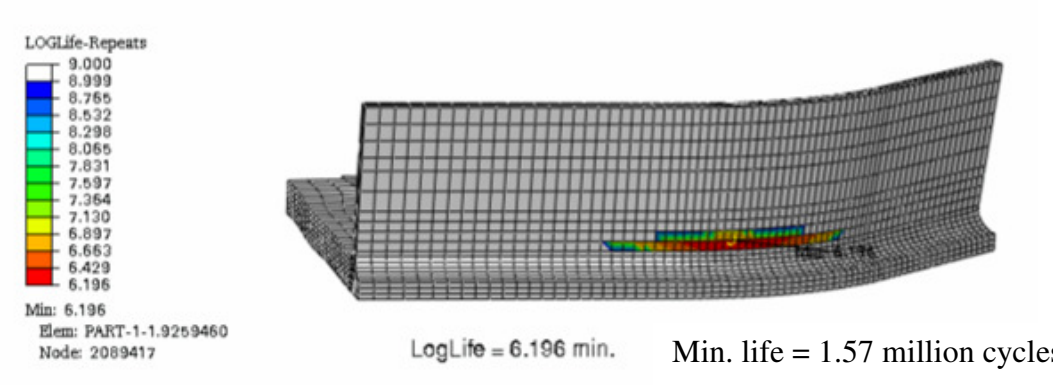

(a)

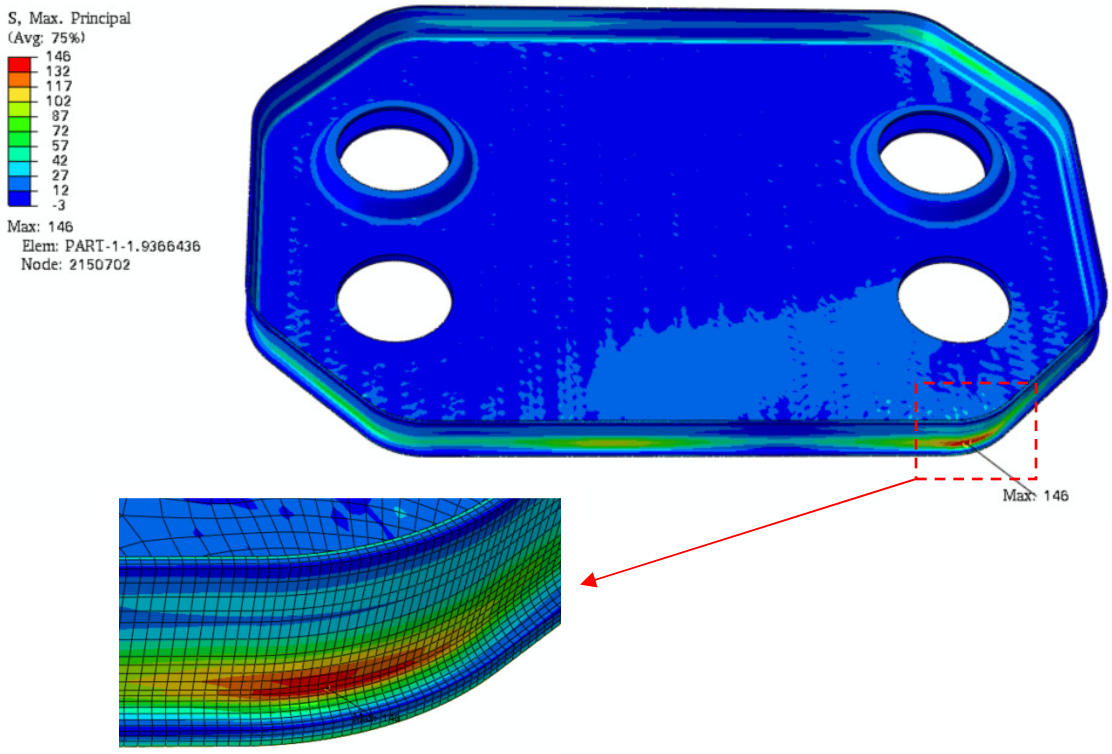

(b)

Figure 55. (a) Fatigue life plot (in log scale) and (b) stress plot (MPa) in linear analysis for 1-20 bar pressure cycles. The life prediction calculation uses the Mslope model.

Fatigue life predictions based on linear FEA results are carried out for each approximate material model as well as for each pressure cycle test profile. Figure 56 compares the performance of life predictions using the Mslope, Seeger, Mod_Mitchell and Mslope_Al models, based on linear FE results. The Mslope model gives non-conservative predictions for the whole life range and yields erroneous estimations at long lives. Mod_Mitchell is a better model, but it gives non-conservative predictions for the whole life range, too. Most of the data points fall within 3 times scatter band except for those at short lives. The Seeger model gives good predictions at both short and long lives. If the elastic modulus and tensile strength are the only tensile properties available for the coreplate material, using linear simulation together with the Seeger model in fatigue life calculation is a simple and fast approach, which is good for durability performance comparison purposes. Finally, The Mslope_Al model gives the best predictions. All data points are lying within the 3 times scatter band. In conclusion, if a simple linear FE analysis is performed, the subsequent fatigue analysis using the Mslope_Al model can give accurate fatigue life prediction for both high cycle and low cycle fatigue failures. On the other hand, The Mslope model is unreliable; in particular, it will give erroneous predictions for high cycle failures.

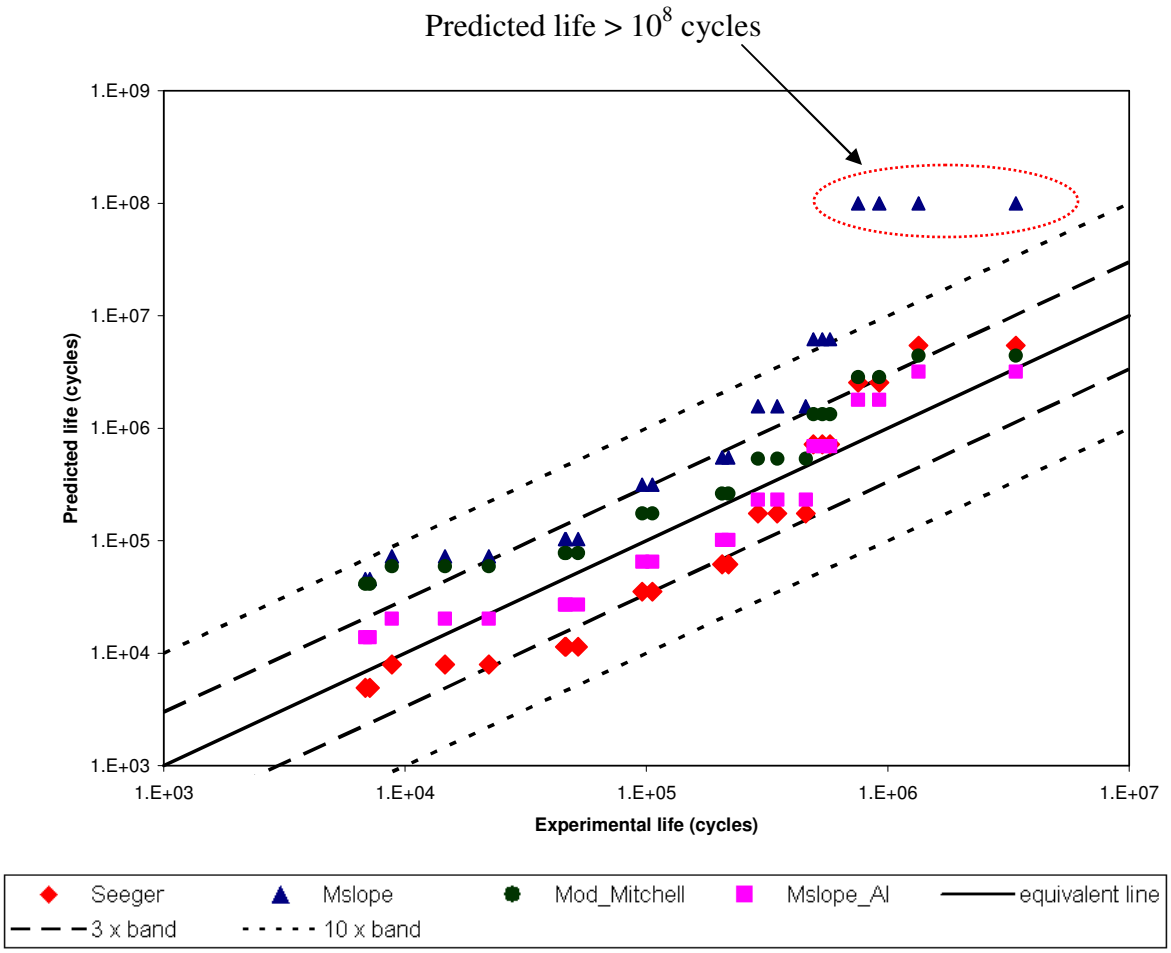

Figure 56. Life prediction correlation based on linear FEA results.

8.3. LIFE PREDICTION BASED ON NON-LINEAR FEA RESULTS

In this simulation approach, a nonlinear FEA is performed to obtain stress and strain data for fatigue life calculation. The modeling procedure and results of the nonlinear analysis have been discussed earlier in Section 5. It is a multi-step elastic-plastic analysis including initial bolt-down of cooler and subsequent application of pressure cycles. In fatigue analysis, fe-safe uses a similar procedure as that using linear FEA results (Section 8.2) to calculate the fatigue life for each node lying on the surface in the critical area. The only exception is when using results from an elastic-plastic FEA, stress and strain datasets are input in pairs. The time histories of the stress and strain tensors are calculated and there is no need to perform plasticity correction.

Figure 57 shows the life prediction results for the 1-35 bar pressure cycle case. The Mslope is used as the approximate material model.

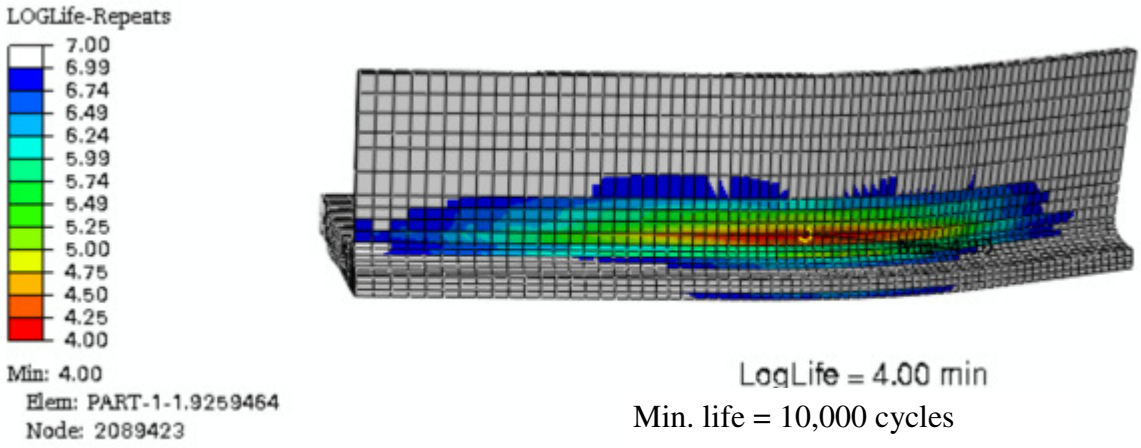

Figure 57. Life prediction based on nonlinear FEA results in the case of 1-35 bar pressure cycles. The Mslope model is used as the material model.

Figure 58 compares the performance of life predictions using the Seeger, Mslope, Mod_Mitchell and Mslope_Al models, based on nonlinear FEA results. The Mslope model gives good predictions at short lives but becomes very non-conservative at long lives. On the contrary, the Seeger model gives good predictions at long lives but is conservative at short lives. Both the Mod_Mitchell and Mslope_Al models give good predictions for the whole life range, with data points lying within the 3 times scatter band.

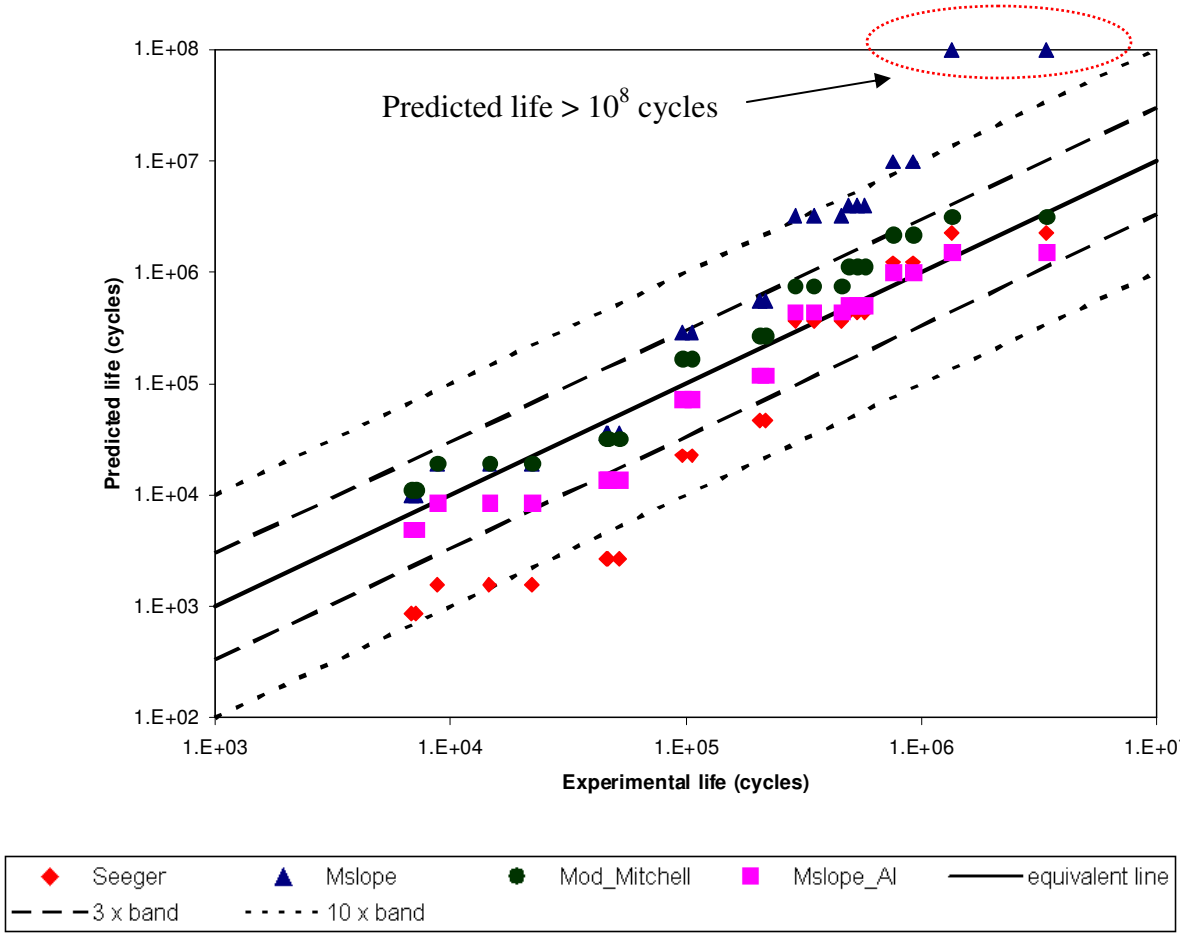

Figure 58. Life prediction correlation based on nonlinear FE results.

8.4. SUMMARY OF DIFFERENT APPROACHES FOR LIFE PREDICTION OF EOC PRESSURE CYCLE FAILURES

For each approximate model, the performances of using linear and nonlinear FE results in fatigue life prediction are compared in Figure 59 to Figure 62.

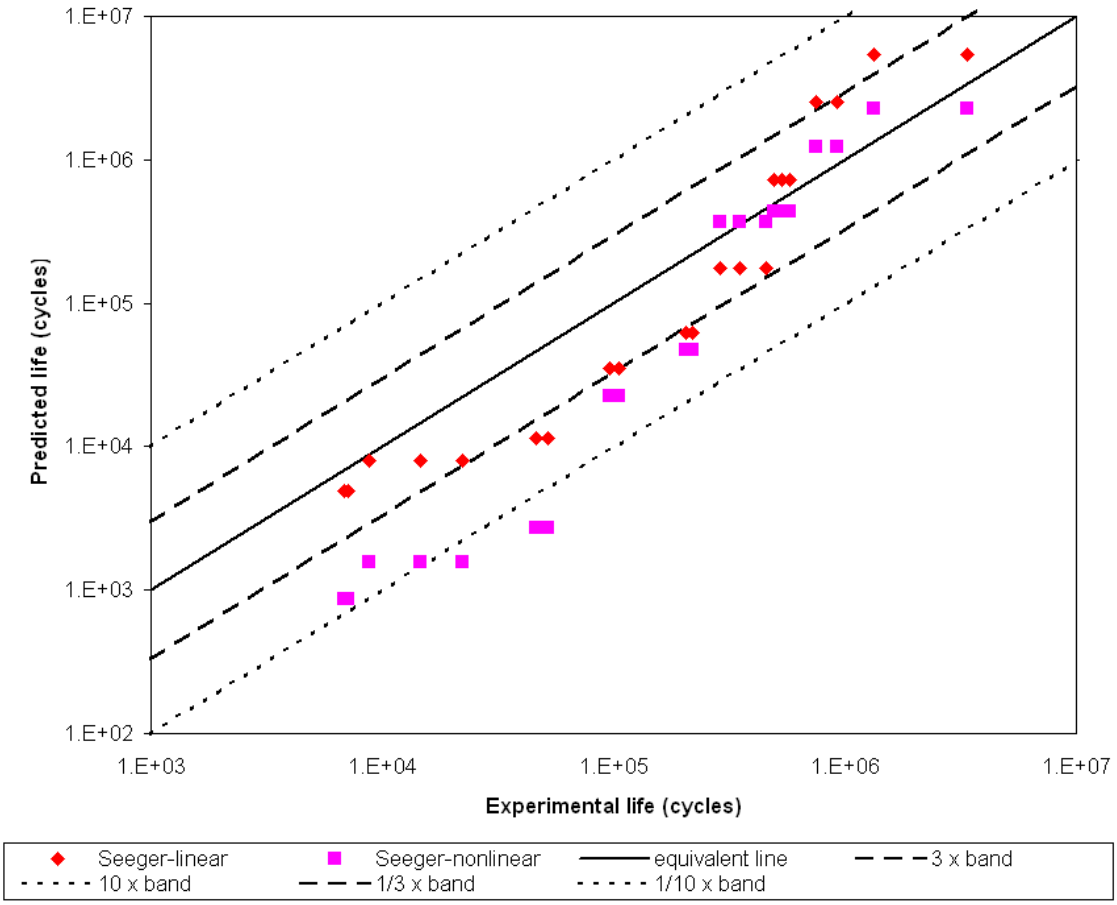

Figure 59. Life prediction correlation for different approaches using the Seeger model.

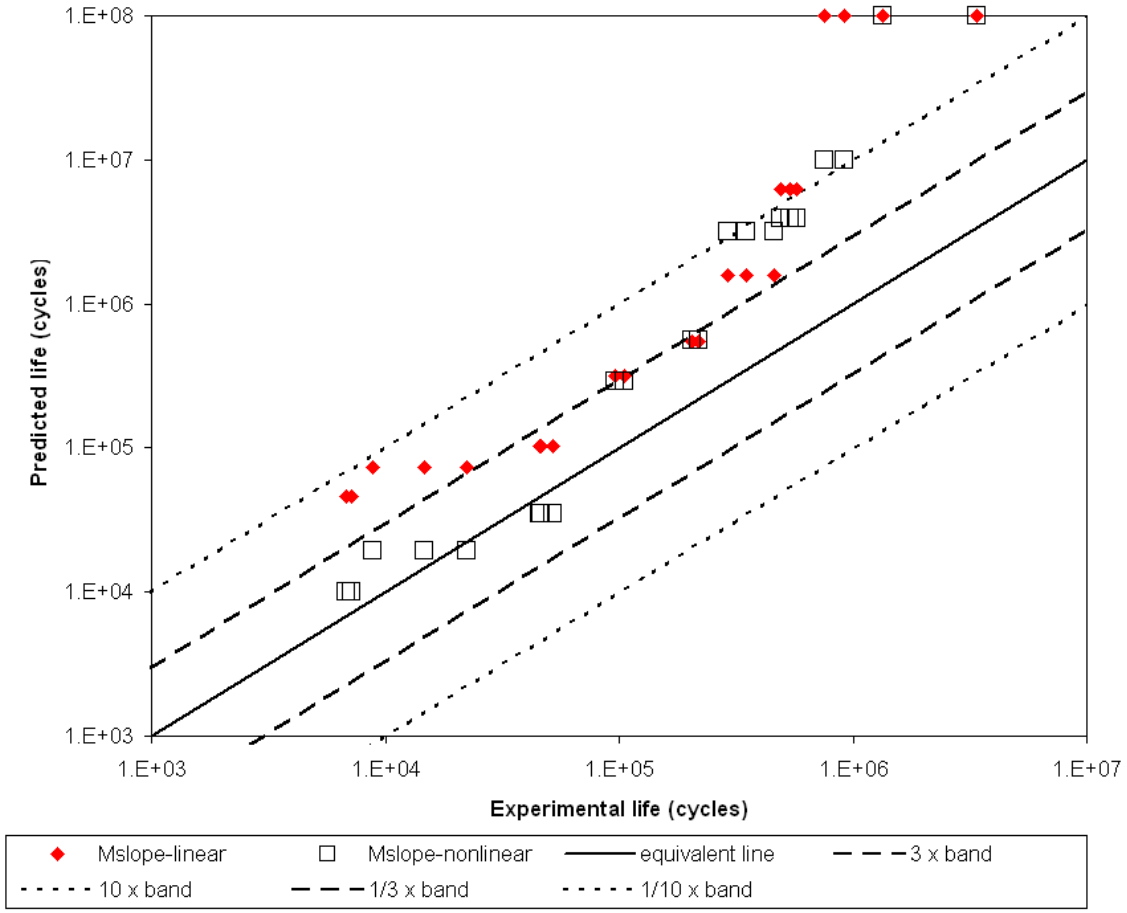

Figure 60. Life prediction correlation for different approaches using the Mslope model.

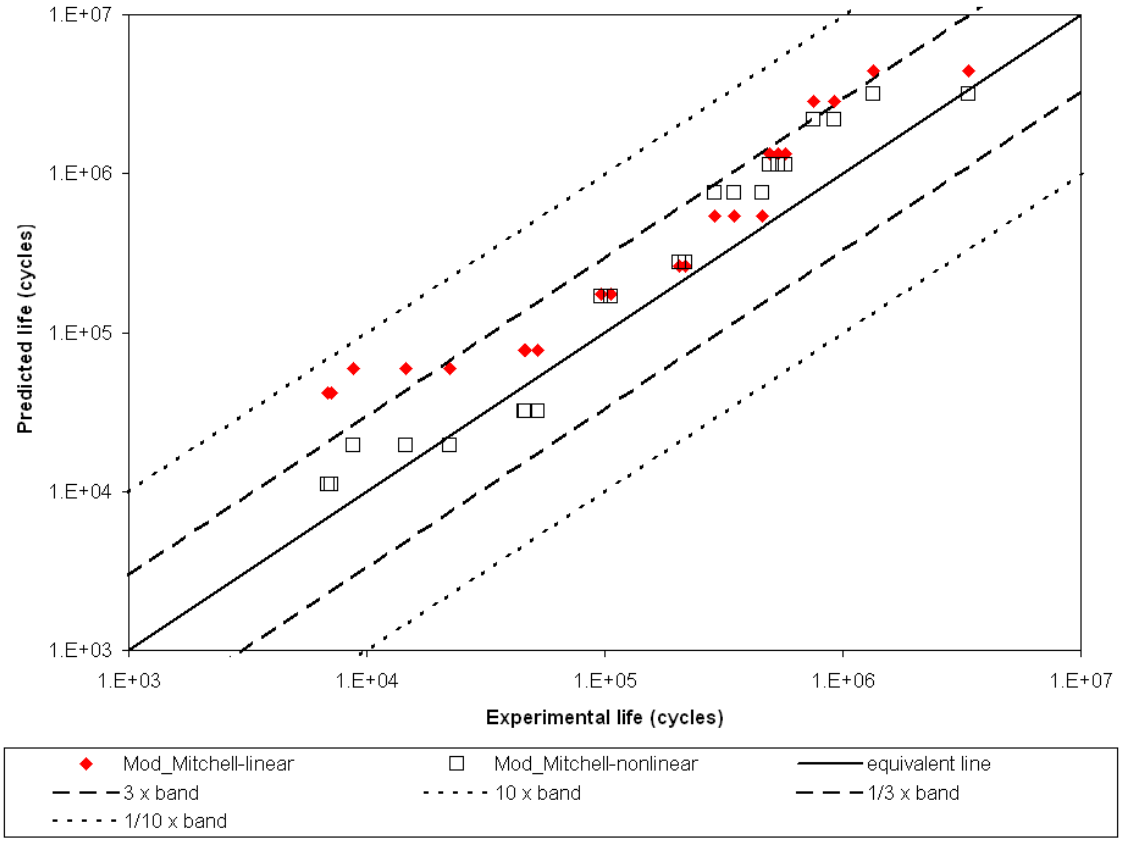

Figure 61. Life prediction correlation for different approaches using the Mod_Mitchell model.

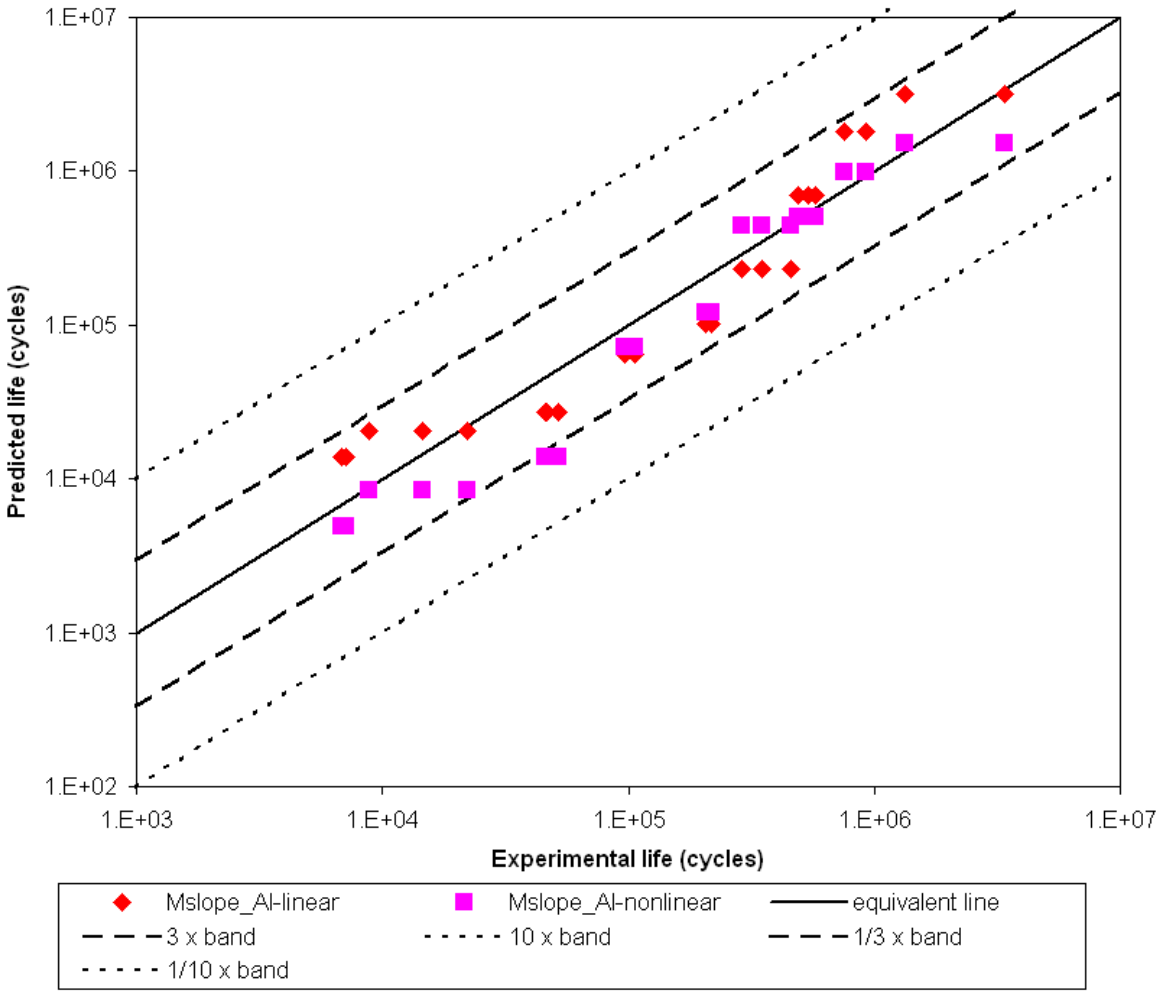

Figure 62. Life prediction correlation for different approaches using the Mslope_Al model.

The Seeger model generally gives conservative predictions at short lives and non-conservative predictions at long lives. For the approach using results from a simple linear FEA, this model gives good predictions at either short lives or long lives, but gives conservative predictions at middle lives. The performance in prediction of short lives is worse when nonlinear FEA results are used. Note that among all models, the Seeger model is the simplest one that only requires elastic modulus and tensile strength of the material. In conclusion, in the scenario in which only minimal tensile properties of the

coreplate material are available, using linear simulation together with the Seeger model in fatigue life calculation is a simple and fast approach, which is useful for EOC durability performance comparison purposes.

The Mslope model generally gives non-conservative predictions, and the life estimates for long lives are erroneous. This model is not suggested to be used in the linear FEA simulation approach. For the approach using nonlinear FEA, this model gives accurate predictions only at short lives. As such, the Mslope model is not recommended to be used in EOC PC testing life prediction.

The Mod_Mitchell model used in the approach with linear FEA results gives non-conservative predictions at short lives. However, it gives good life predictions when fatigue calculation is based on nonlinear FEA results. It is recommended that this model can be used in predicting EOC fatigue life using nonlinear FEA data.

The Mslope_Al model gives good life prediction for simulations using either linear or nonlinear FEA results. In general, using nonlinear results gives better prediction, especially at short lives below 10,000 cycles and at long lives above 1 million cycles. However, this nonlinear approach requires the modeling of the bolt-down step that needs more inputs like the properties of the O-rings or gaskets. Furthermore, if the cooler model is very large, it will be computationally prohibitive due to computer hardware limitations. In such a case, a simple and quick linear analysis using a simplified clamping configuration still gives life estimates with an acceptable level of accuracy. On the other hand, due to the advance in computer hardware technology, performing multiple-step nonlinear analysis on large FE models becomes viable. In conclusion, life prediction using nonlinear FE results together with the Mslope_Al approximate material model is preferred and recommended as the best approach.

9. INVESTIGATION OF DIFFERENT STRAIN-LIFE EQUATIONS WITH MEAN STRESS CORRECTION

9.1 AN OVERVIEW OF MEAN STRESS CORRECTION METHODS

Dowling [28] did a thorough investigation of the mean stress effects in fatigue analysis in both stress-life and strain-life approaches. For the strain-life approach, he compared the performance of different mean stress correction equations including Morrow, Smith-Watson-Topper (SWT) and Walker. He correlated the strain-life curves predicted by these equations, with the strain-life test data of three steels, four aluminum alloys and one titanium alloy. He concluded that the Walker equation gives the best correlation for these metals provided that the governing material parameter in the equation, γ, is known. The parameter γ is obtained by fitting the equation to test data, which are not always available. Apart from this, he found that the SWT equation gives good results for all metals studied. He recommended SWT as the preferred choice for mean stress correction, if the Walker equation is not applicable. For the Morrow equation, he found that the results are good for steel but not for aluminum alloys. He attributed this to the term $\sigma_f^{'}$ used in the Morrow equation. He explained that in the original Morrow stress-life equation with mean stress correction, this term should be true fracture strength σ_f, instead of fatigue strength coefficient $\sigma_f^{'}$. Morrow equation is more commonly expressed in terms of $\sigma_f^{'}$ because σ_f is usually not available. From the steels and aluminum alloys he studied, the values of σ_f and $\sigma_f^{'}$ were very close for steel, but had a large difference for aluminum. He used this to explain why the Morrow mean stress correction equation is only good for steels but not aluminum alloys. However, his conclusion is only based on the investigation on four types of heat-treatable aluminum alloys: 2014-T6, 2024-T3, 2024-T4 and 7075-T6. In the current study, an attempt is

made to investigate the performance of using the SWT mean stress correction method in the life prediction of fatigue failures that occur on the coreplate of the EOC.

9.2 STRAIN-LIFE EQUATIONS AND MEAN STRESS CORRECTIONS IMPLEMENTED IN FE-SAFE

In the fatigue analysis of EOC failures carried out so far, the Brown-Miller combined strain strain-life criterion with Morrow mean stress correction is used for life calculation. Equation (8) is rewritten below:

$$\frac{\Delta\gamma_{\max}}{2}+\frac{\Delta\varepsilon_N}{2}=1.65\frac{(\sigma_f^{'}-\sigma_{n,m})}{E}(2N_f)^b+1.75\varepsilon_f^{'}(2N_f)^c \qquad (8)$$

The Brown-Miller strain-life criterion is recommended for ductile metal like aluminum. However, for this strain-life criterion, the Morrow equation is the only mean stress correction method available in fe-safe. Thus, in order to investigate the performance of the SWT mean stress correction method, other strain-life criteria have to be considered. In fe-safe, several bi-axial strain-life algorithms are available including Brown-Miller, principal strain and maximum shear strain. Furthermore, the Morrow, Walker and SWT mean stress correction methods are implemented in some of these strain-life equations. In the present study, the equations using Morrow and SWT mean stress corrections are investigated, but not for Walker as the parameter γ of the coreplate material is not available. Table 7 lists the four strain-life equations investigated. Note that the SWT mean stress correction is only available for the principal strain strain-life criterion.

Equation	Strain-life criterion	Mean stress correction method
BM-Morrow	Brown-Miller	Morrow
PS-SWT	Max. principal strain	SWT
PS-Morrow		Morrow
MS-Morrow	Max. shear strain	

Table 7. Different strain-life and mean stress correction equations investigated.

The principal strain criterion proposes that fatigue cracks initiate on the planes which experience the largest amplitude of maximum principal strain. The principal strain strain-life equation is expressed as:

$$\frac{\Delta\varepsilon_1}{2} = \frac{\sigma_f^{'}}{E}(2N_f)^b + \varepsilon_f^{'}(2N_f)^c \qquad (14)$$

where $\Delta\varepsilon_1$ is the maximum principal strain range. The principal strain criterion is only recommended for the analysis of brittle materials like cast irons and high strength steels. It usually gives non-conservative predictions for ductile metals like aluminum.

The equation for principal strain strain-life criterion with Morrow mean stress correction (PS-Morrow) is expressed as:

$$\frac{\Delta\varepsilon_1}{2} = \frac{(\sigma_f^{'} - \sigma_m)}{E}(2N_f)^b + \varepsilon_f^{'}(2N_f)^c \qquad (15)$$

where σ_m is the mean normal stress on the plane of maximum principal strain.

The equation for principal strain strain-life criterion with SWT mean stress correction (PS-SWT) is expressed as:

$$\frac{\Delta\varepsilon_1}{2}\sigma_{1,\max} = \frac{(\sigma_f')^2}{E}(2N_f)^{2b} + \varepsilon_f'\sigma_f'(2N_f)^{b+c} \qquad (16)$$

where $\sigma_{1,\max}$ is the maximum normal stress on the plane of maximum principal strain.

The maximum shear strain criterion is based on the observation that fatigue cracks usually initiate on shear planes. It proposes that cracks will initiate on planes which experience the maximum shear strain amplitude. The maximum shear strain-life equation is expressed as:

$$\frac{\Delta\gamma_{\max}}{2} = 1.3\frac{\sigma_f'}{E}(2N_f)^b + 1.5\varepsilon_f'(2N_f)^c \qquad (17)$$

where $\Delta\gamma_{\max}$ is the maximum shear strain range. This criterion gives conservative life estimates for ductile metals, but gives non-conservative life estimates for brittle metals.

The equation for maximum shear strain with Morrow mean stress correction (MS-Morrow) is expressed as:

$$\frac{\Delta\gamma_{\max}}{2} = 1.3\frac{(\sigma_f' - \sigma_{n,m})}{E}(2N_f)^b + 1.5\varepsilon_f'(2N_f)^c \qquad (18)$$

where $\sigma_{n,m}$ is the mean normal stress on the plane of maximum shear strain.

9.3 APPLICATION OF DIFFERENT STRAIN-LIFE EQUATIONS AND MEAN STRESS CORRECTIONS TO EOC LIFE PREDICTION

The previous work has concluded that using the Mslope_Al approximate material model gives the best correlation in life predictions of EOC failures, in both linear and nonlinear simulation approaches. An attempt is made to further investigate the performance in life prediction using other strain-life equations with different mean stress corrections. The equations in Table 7 are used in the fatigue life calculation using both linear and nonlinear results, with Mslope_Al as the approximate material model.

Figure 63 compares the life prediction correlations of different strain-life equations based on linear FEA results. Obviously, PS-SWT yields the worst correlation by giving conservative results. It indicates that the SWT mean stress correction method is worse than that of Morrow in predicting the EOC failures. On the other hand, the predictions made by BM-Morrow, PS-Morrow and MS-Morrow are very close, with all data points lying within the three times scatter band.

Figure 64 compares the life prediction correlations of different strain-life equations based on nonlinear FEA results. Once again, PS-SWT has the worst performance by giving conservative predictions, especially at long lives. The predictions made by BM-Morrow, PS-Morrow and MS-Morrow have no significant difference.

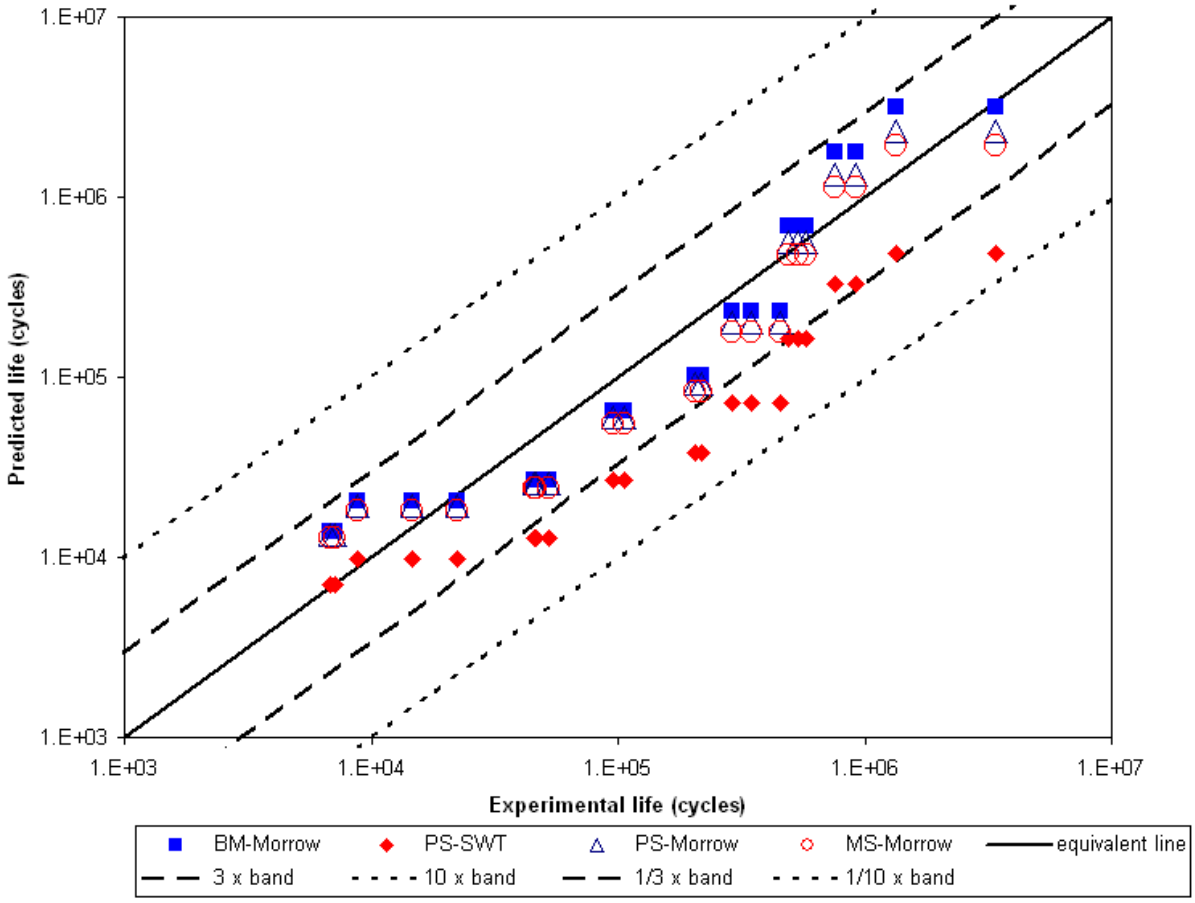

Figure 63. Life prediction correlation using different strain-life equations based on linear FEA results (Mslope_Al material model).

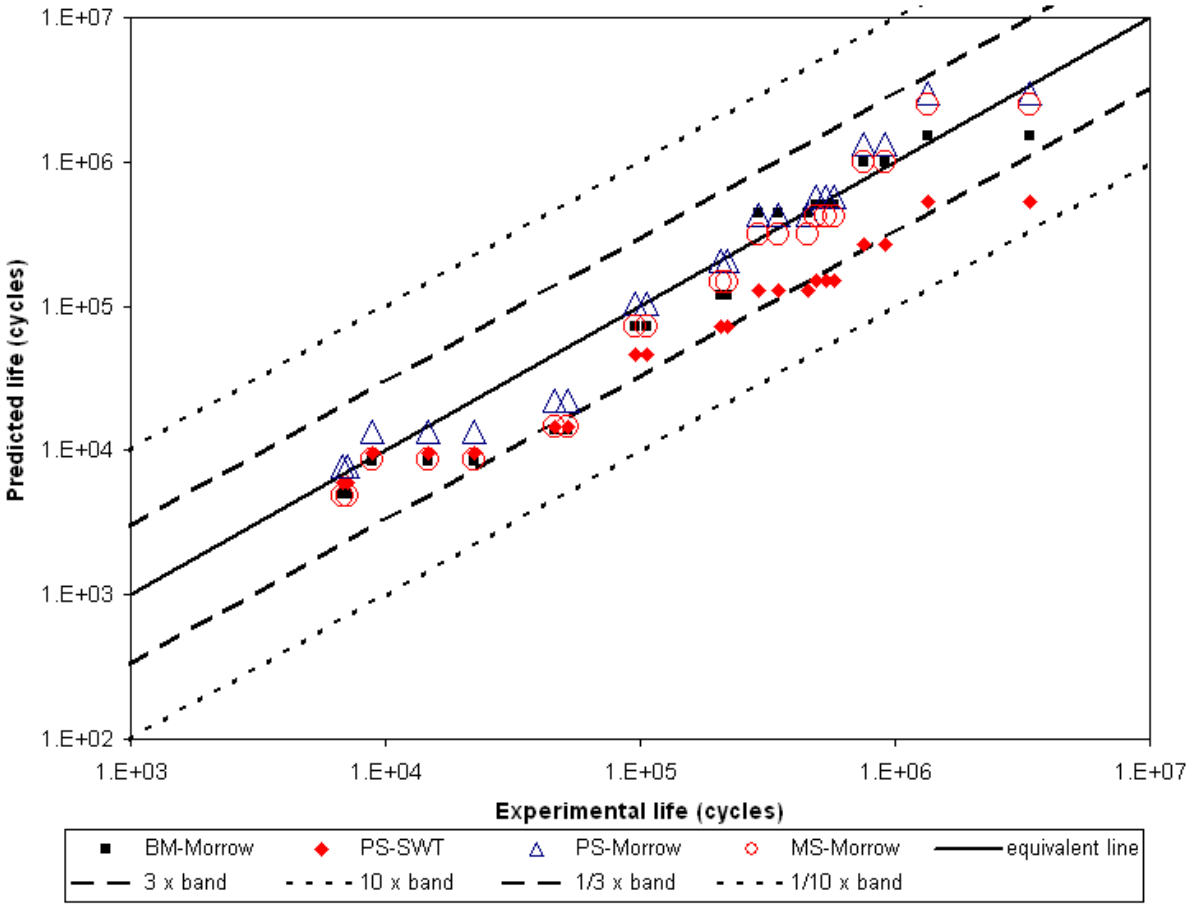

Figure 64. Life prediction correlation using different strain-life equations based on nonlinear FEA results (Mslope_Al material model).

10. CONCLUSIONS & RECOMMENDATIONS

10.1. CONCLUSIONS

In the product development stage of a new EOC design, computer simulation is widely used to predict its fatigue life pertaining to pressure cycle failures. This technology reduces the amount of prototype testing required and helps cut the lead time to product launch. The viability of using simulation to evaluate the durability performance of a new cooler design depends upon the accuracy of fatigue life prediction of pressure cycle failures.

The objective of the research is to develop a practical simulation methodology to accurately predict the fatigue life of EOC undergoing PC testing. The study focuses on answering two key questions of the simulation process. First, it investigates the effect of using linear and nonlinear FEA to provide stress or strain results for subsequent fatigue life prediction. Second, due to lack of fatigue material properties for the aluminum coreplates, in which failures have occurred, there is a need to use approximate material models in fatigue life calculation. These approximate models relate the strain-life parameters to monotonic tensile test properties. The study has attempted to find out the material model that gives good correlation in life prediction. The life prediction correlation based on three existing models from literature that appear to have good performance for aluminum alloys: the Seeger, Mslope and Mod_Mitchell models, and a revised model, the Mslope_Al, are evaluated.

Fatigue analysis based on the results of a simple linear analysis together with the Seeger model gives good predictions at both short and long lives. If the elastic modulus and tensile strength are the only tensile properties available for the coreplate material, it is suggested that using linear simulation together with the Seeger model in fatigue life

calculation is a simple and fast approach, which is useful for durability performance comparison purposes. On the other hand, the Mslope model is not recommended to be used in EOC life prediction because it gives inaccurate predictions especially for high cycle failures. The Mod_Mitchell model gives good life predictions when fatigue calculation is based on nonlinear FEA results. It is recommended that this model can be used in predicting EOC fatigue life using nonlinear FEA data.

The Mslope_Al model, which is a re-assessment of the Mslope model using the fatigue data of 16 wrought aluminum alloys, gives good life prediction for simulations using either linear or nonlinear approaches. In general, using nonlinear results gives better prediction, especially at short lives and long lives. However, this nonlinear approach not only requires more inputs like the properties of the gaskets, but also will be computationally prohibitive for large cooler models. In such a case, a simple and quick linear analysis still gives life estimates with an acceptable level of confidence. In conclusion, using nonlinear FE results together with the Mslope_Al approximate material model is recommended to be the best approach for life prediction of EOC pressure cycle failures.

In the first part of the study, all fatigue life calculations are carried out using the Brown-Miller combined strain strain-life criterion with Morrow mean stress correction. Further work has been done to evaluate the life prediction performance using other strain-life criteria, together with either Morrow or SWT mean stress correction. It is found that SWT mean stress correction method is worse than that of Morrow in EOC fatigue life prediction in both linear and nonlinear approaches. Using the principal strain criterion with SWT mean stress correction gives conservative life prediction in both approaches. On the other hand, there are no significant differences in life prediction correlations using the principal strain, the Brown-Miller and the maximum shear strain strain-life criteria, with Morrow mean stress correction. As such, the Brown-Miller combined strain

criterion with Morrow mean stress correction is still the recommended strain-life model used in fatigue life calculation.

10.2. RECOMMENDATIONS FOR FUTURE WORK

In the present study, the life prediction correlations of four approximate models: Seeger, Mslope, Mod_Mitchell and Mslope_Al, have been compared in two different ways. The first one focuses on the material strain-life curve correlation. In this method, the fatigue data and tensile properties of 16 wrought aluminum alloys are used for strain-life curve correlation. The second method compares the performance pertaining to the failure of an EOC under pressure cycles. In this method, the experimental data from EOC testing are used for life prediction correlation. Both methods have shown that Mslope_Al is the best model. However, the best way to verify that Mslope_Al is a good model is to compare the predicted strain-life curve with that from fatigue testing of the coreplate material. It is recommended to conduct fatigue testing on the coreplate material. Of course, fatigue testing is expensive and time consuming. Furthermore, performing a fully reversed strain controlled test on a thin specimen requires additional accessories to prevent buckling. A feasibility study on performing a fully reversed test on the coreplate brazing sheet has been carried out at the University of Waterloo [29]. The study has shown that the test can be performed successfully on a multiple-layer specimen with thin sheets glued together, with the application of anti-buckling shims. Another suggestion to prevent buckling is to conduct a test with positive strain only. This method needs post-test data analysis to convert the test data into a strain-life curve with zero mean strain. It is planned to carry out the testing on post-braze coreplate sheet using either methods.

When using the Mslope_Al model, the life prediction correlation results show that there is no substantial performance difference in the linear and nonlinear simulation approaches, even though the nonlinear approach is marginally better. This nullifies the effort to run nonlinear analysis which is supposed to give better prediction. This may be

due to the sealing configuration of the EOC used in the study. This EOC uses two small O-rings for sealing. The O-rings are sitting in the open grooves on the test fixture. As the O-rings are not fully confined, they are allowed to expand inwards when under compression. Some EOCs have a different sealing configuration. Their gaskets are placed into casting grooves that limit their sideway expansion. In such cases, due to the incompressibility nature of the rubber material, large upward reaction force on the baseplate will be created during the bolt-down process. Life prediction using linear FEA does not account for the mean stress effect due to the tensile stresses developed in the critical failure spot during the bolt-down process. In the EOC studied, this effect is small as the stresses are low (see Figure 31). For an EOC with confined gaskets, these stresses are high and fatigue life will be over-predicted if their contribution to mean stress calculation is ignored. Thus, for this kind of EOC, it is suspected that there will be a larger difference in life predictions using linear and nonlinear approaches. To verify this conjecture, it is suggested to continue the work on an EOC that uses gaskets that give large resistance to compression. These can be gaskets that are confined, gaskets made of harder rubber or gaskets with a larger sealing perimeter.

APPENDICES

A1. ASSEMBLY DRAWING OF THE EOC

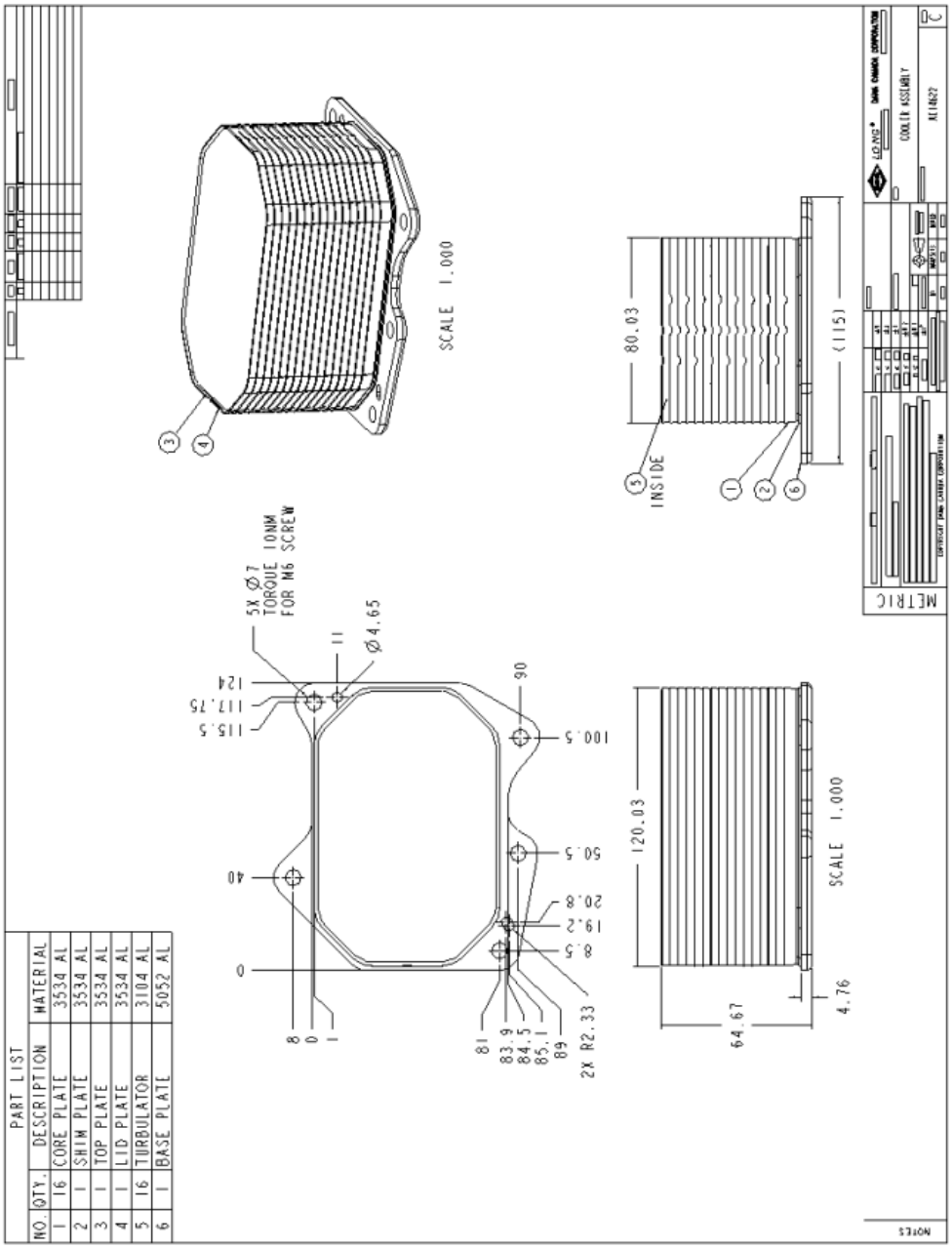

A2. DRAWING OF THE FIXTURE USED IN PC TESTING

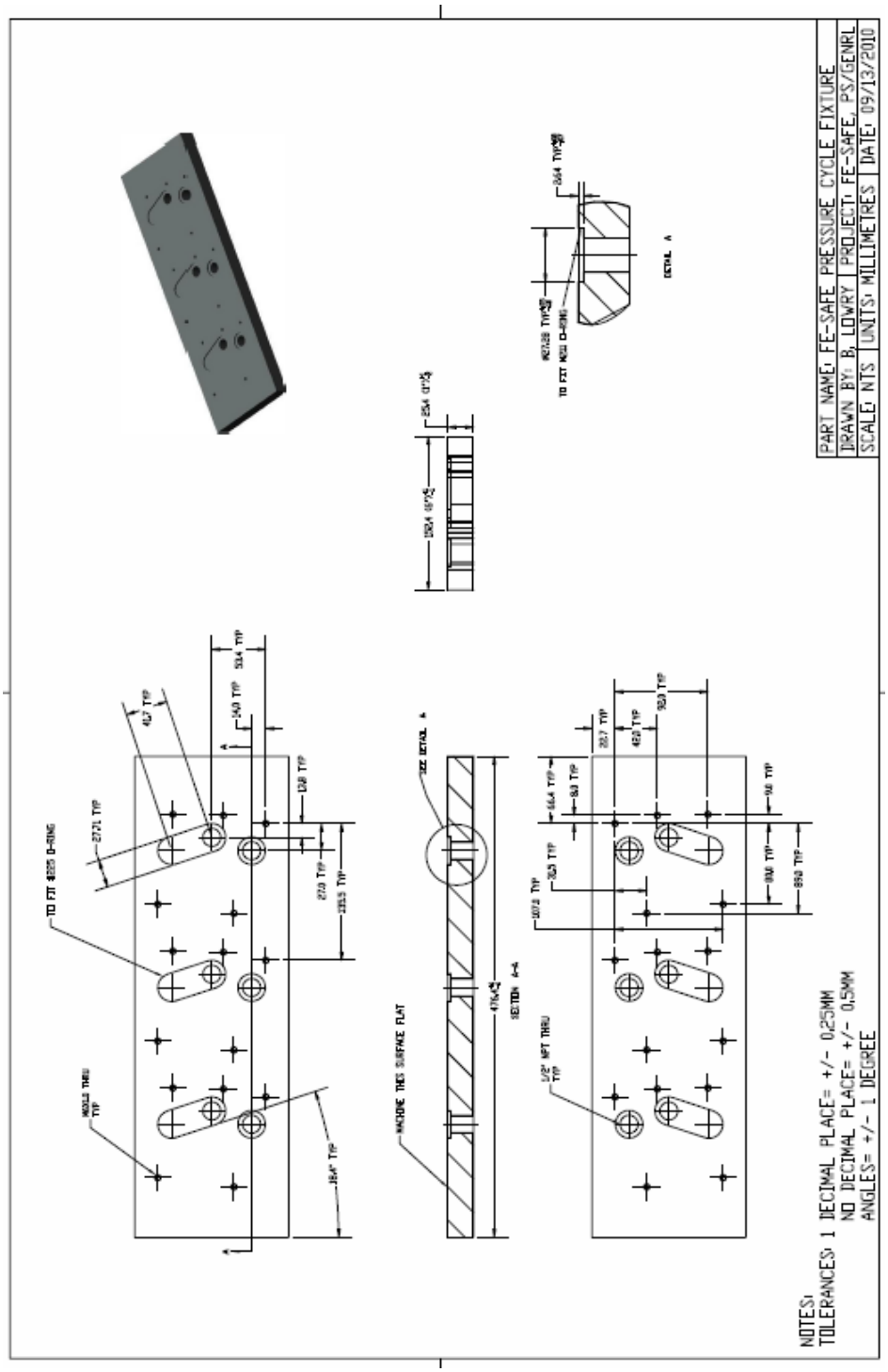

A3. MICRO-INDENTATION TESTING OF BRAZE FILLET MATERIAL

Spherical indentation testing has been proposed as an alternative to conventional uniaxial tensile testing for determining the stress-strain response of strain hardening materials. An attempt has been made to investigate the applicability of the method to obtain material inputs of the braze fillet material for FEA calculation. The micro-indentation testing of a braze fillet sample of the EOC, including post-testing data analysis, is performed by the Department of Mechanical & Material Engineering of University of Western Ontario. The testing method, the background theory and the related equations used to derive the stress-strain curve from indentation load-depth curve are discussed thoroughly in the papers by Oviasuyi [30] and Weiler [31]. The testing is performed with a computer controlled micro-indentation hardness tester with a spherical indenter of 45μm diameter. Figure 65 depicts the image of the spherical indentations made on the fillet section surface.

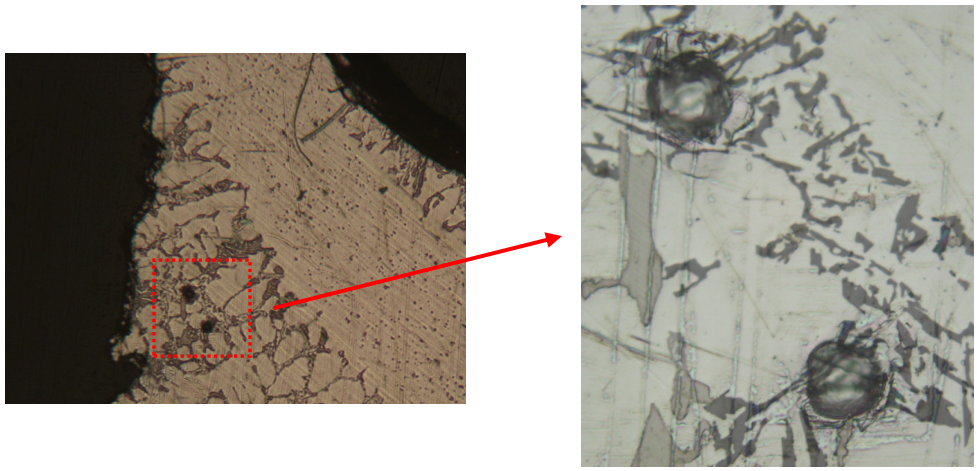

Figure 65. Micro-indentation spots on the braze fillet surface.

For each indentation location, a load-depth curve is obtained, which consists of a series of loading and unloading curves at different load values (Figure 66).

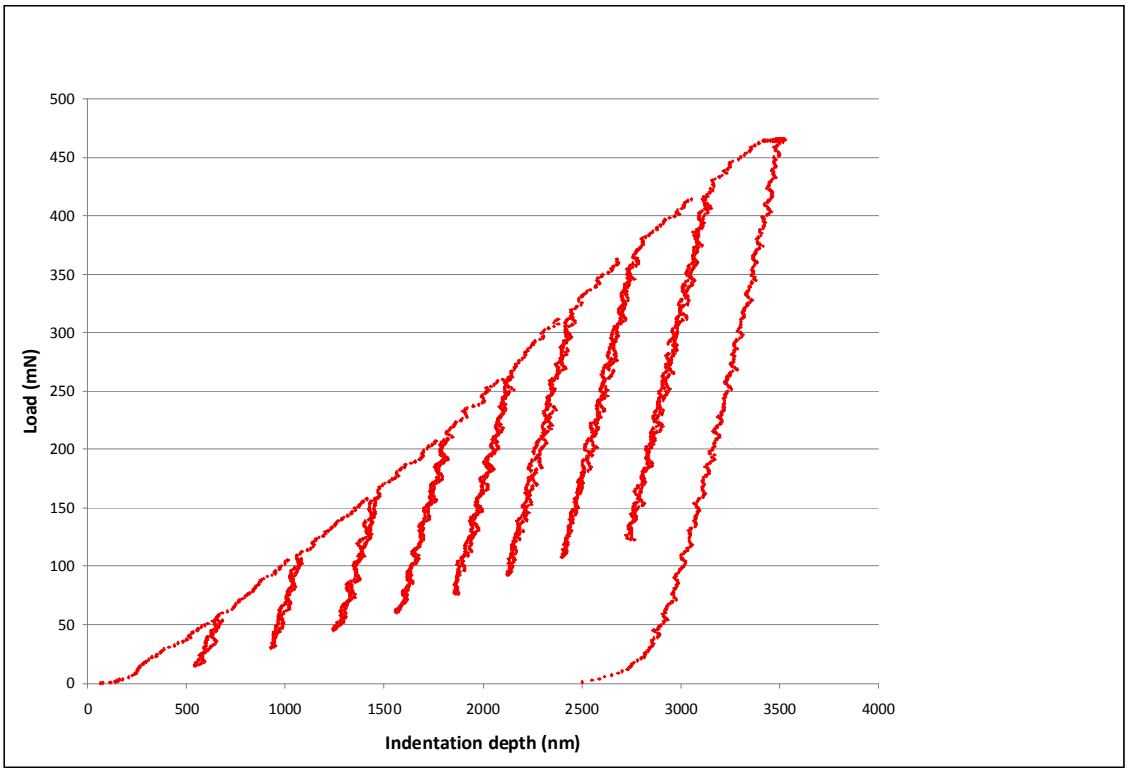

Figure 66. A typical load-depth curve obtained in the micro-indentation testing.

From the load-depth curve, the average flow stress and average strain at each load point are calculated. Totally, three curves are obtained from indentation results at three locations of the braze fillet. The curves are compared with that for A380 cast Al in Figure 67. The indentation curves only cover the strain range of 0.04 to 0.1. Two of the curves have good correlation with A380 cast Al curve in the strain range tested.

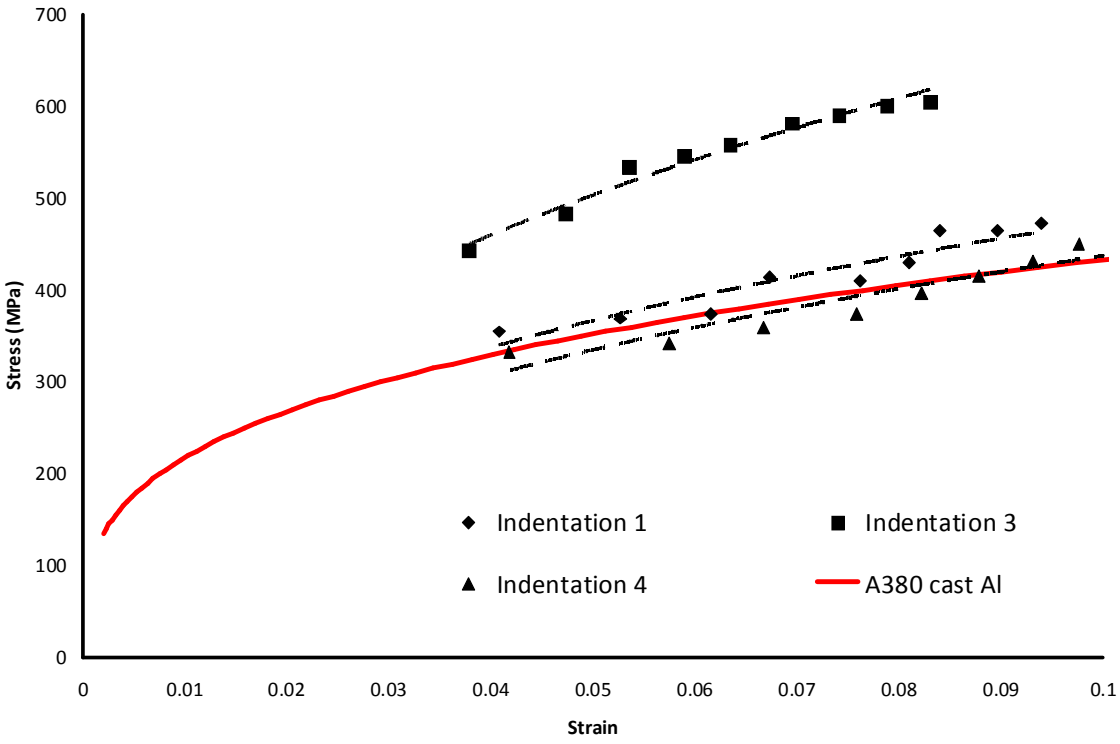

Figure 67. Flow stress-strain curves derived from indentation test results at three spots and the curve for A380 cast Al [4].

A4. HYPERELASTIC MODEL FOR O-RINGS

The O-rings are made of FKM rubber (Viton fluoroelastomer) with durometer hardness A75. FKM rubber is an elastomer with very little compressibility compared to shear flexibility. The material properties are represented by Yeoh hyperelastic material model, which is one of the models that use strain energy function to define the behaviours of rubber materials. In Abaqus, Yeoh strain energy function is expressed in the form [32]:

$$U = C_{10}(\overline{I}_1 - 3) + C_{20}(\overline{I}_1 - 3)^2 + C_{30}(\overline{I}_1 - 3)^3 + \frac{1}{D_1}(J^{el} - 1)^2 + \frac{1}{D_2}(J^{el} - 1)^4 + \frac{1}{D_3}(J^{el} - 1)^6 \quad (19)$$

where U is the strain energy per unit reference volume; C_{i0} and D_i are temperature dependent material parameters; $\overline{I}_1$ is the first deviatoric strain invariant defined as:

$$\overline{I}_1 = \overline{\lambda}_1^2 + \overline{\lambda}_2^2 + \overline{\lambda}_3^2,$$

where the deviatoric stretches $\overline{\lambda}_i = J^{-\frac{1}{3}}\lambda_i$; J is the total volume ratio; J^{el} is the elastic volume ratio; and λ_i are the principal stretches. The initial shear modulus and bulk modulus are given by:

$$\mu_0 = 2C_{10},\ K_0 = \frac{2}{D_1}.$$

J^{el} relates to J and the thermal volume ratio, J^{th} by:

$$J^{el} = \frac{J}{J^{th}}.$$

J^{th} is given by:

$$J^{th} = (1 + \varepsilon^{th})^3,$$

where ε^{th} is the linear thermal expansion strain that is obtained from the temperature and the isotropic thermal expansion coefficient.

The Yeoh model parameters for the O-ring material used in the current study are provided by the Sealing Group of Power Technologies Group, Dana Corporation. The Sealing Group has conducted lab testing to characterize the rubber material used. The following summarizes the procedures used to characterize the O-ring material:

1) Tests are performed on the specimens: uniaxial tensile test, biaxial tensile test, planar tensile test and volumetric compression test.
2) The stress-strain data from these tests are calibrated by Abaqus to obtain the hyperelastic model parameters [32].

After calibration, the following Yeoh model parameters for the O-ring material at room temperature are obtained:

$$C_{10} = 0.8690$$

$$C_{20} = 0.00159$$

$$C_{30} = 0.00134$$

$$D_1 = 0.000758$$

$$D_2 = 0.00000899$$

$$D_3 = -0.00000246$$

Figure 68 compares the uniaxial stress-strain curve of the O-ring material based on the calibrated Yeoh model, with that from the uniaxial tensile test. It shows a good correlation between the curves.

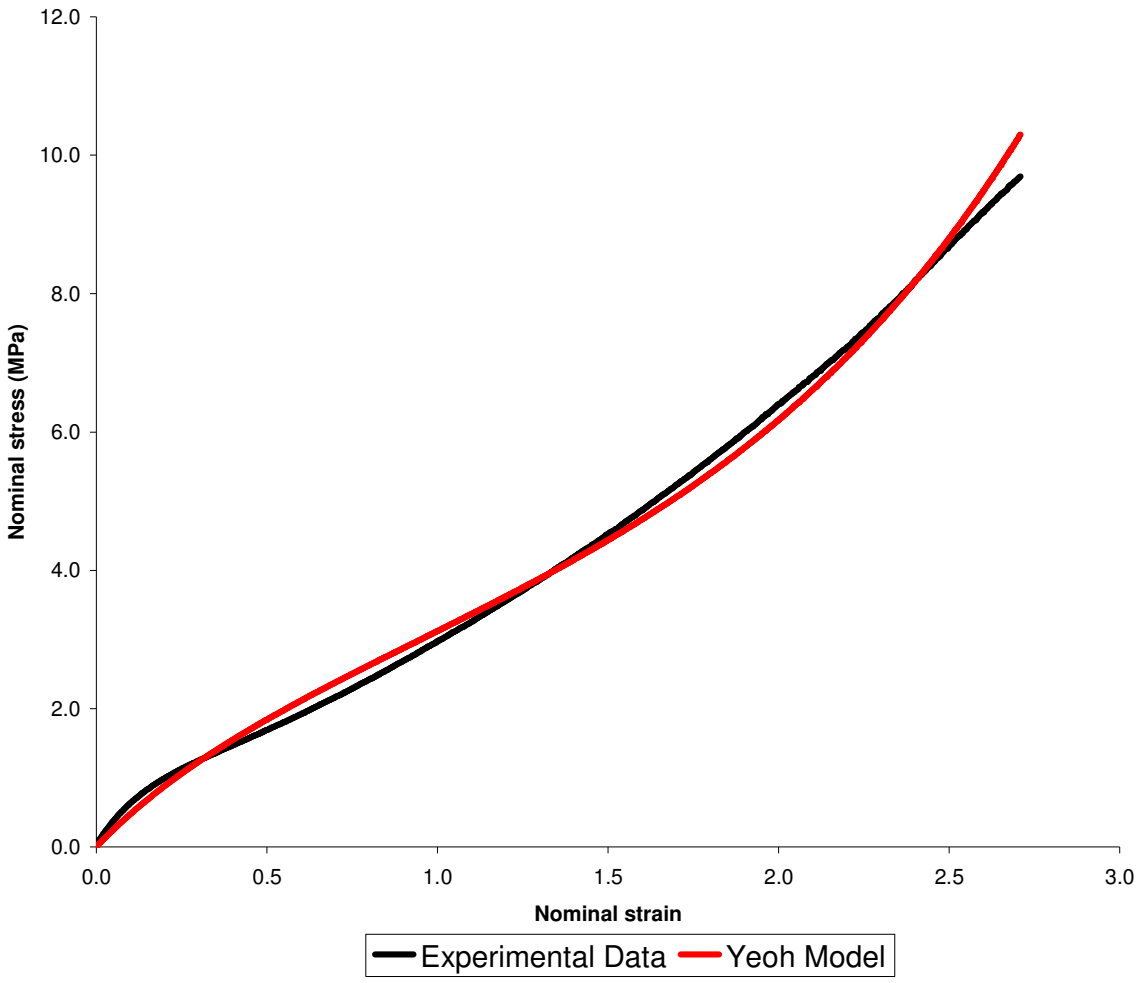

Figure 68. Comparison between the uniaxial tensile stress-strain curves from calibrated Yeoh model and experimental testing, for the O-ring material.

A5. MATERIAL TEST DATA OF 16 AL ALLOYS USED IN DEVELOPING THE MSLOPE_AL MODEL.

	Label	Material	Heat treatment
1	AA1100_AR1	AA1100	As Received
2	AA1100_AR2	AA1100	As Received
3	AA1100_AR3	AA1100	As Received
4	AA2014-T6_AR1	AA2014-T6	As Received
5	AA2014-T6_STAA	AA2014-T6	Solution treated & artificially aged
6	AA2024_AR1	AA2024	As Received
7	AA2024_CAH	AA2024	Cold aged & hardened
8	AA2024_SA	AA2024	Soft annealed
9	AA2024_AR2	AA2024	As Received
10	AA2024-T351_STSH	AA2024-T351	Solution treated & strain hardened
11	AA2024-T4_STRA	AA2024-T4	Solution treated & room temp aged
12	AA5456-H311_AR1	AA5456-H311	As Received
13	AA5456-H311_SH	AA5456-H311	Strain hardened
14	AA5456-H311_AR2	AA5456-H311	As Received
15	AA6005_CAH	AA6005	Cold aged & hardened
16	AA6082_CAH	AA6082	Cold aged & hardened
17	AA6082_WAH	AA6082	Warm aged & hardened
18	AA7075-T6_HT	AA7075-T6	Heat treated

	Label	Monotonic tensile test properties				Strain-life equation parameters			
		E (MPa)	UTS (MPa)	RA	ε_f	$\sigma_f^{'}$ (MPa)	$\varepsilon_f^{'}$	b	c
1	AA1100_AR1	69050	110	87.6	2.090	159	0.467	-0.092	-0.613
2	AA1100_AR2	69000	110	88.0	2.090	193	1.800	-0.106	-0.690
3	AA1100_AR3	69000	110	87.6	2.090	170	0.981	-0.107	-0.624
4	AA2014-T6_AR1	69050	511	25.0	0.288	776	0.269	-0.091	-0.742
5	AA2014-T6_STAA	69000	510	25.0	0.288	848	0.420	-0.106	-0.650
6	AA2024_AR1	73300	490	16.0	0.174	782	0.197	-0.082	-0.644
7	AA2024_CAH	74100	446	24.0	0.301	687	0.514	-0.074	-0.830
8	AA2024_SA	74600	245	38.0	0.478	314	0.162	-0.091	-0.452
9	AA2024_AR2	73300	490	16.0	0.174	891	4.206	-0.103	-1.056
10	AA2024-T351_STSH	73000	469	25.0	0.288	1103	0.220	-0.124	-0.590
11	AA2024-T4_STRA	70000	476	35.0	0.431	1014	0.210	-0.110	-0.520
12	AA5456-H311_AR1	69050	400	34.6	0.425	702	0.200	-0.102	-0.655
13	AA5456-H311_SH	69000	400	35.0	0.431	724	0.460	-0.110	-0.670
14	AA5456-H311_AR2	69000	400	34.6	0.425	701	0.400	-0.102	-0.655
15	AA6005_CAH	66700	260	58.0	0.868	481	1.095	-0.084	-0.867
16	AA6082_CAH	74500	348	25.5	0.294	445	0.116	-0.054	-0.641
17	AA6082_WAH	74550	383	45.4	0.605	554	5.375	-0.068	-1.208
18	AA7075-T6_HT	71120	580	33.0	0.400	886	0.446	-0.076	-0.759

REFERENCES

1 Abaqus Analysis User's Manual Version 6.11, Dassault Systemes Simulia Corp., Providence, RI, USA.

2 Private communication, "Elevated Temperature Mechanical Properties for 3003, 3534 and 5052 Aluminum Alloys", Report No. ICD07-188, Innoval Technology Ltd, UK, 2007.

3 Private communication, "Tensile Testing Data for 3104 aluminum", Novelis Global Technology Center, USA, 2008.

4 Private communication, "A380 Cast Aluminum Material Properties Development Revision B", Dana Automotive System Group, Dana Corporation, USA, 2009.

5 Shigley, J.E., Mischke, C.R. and Budynas, R.G., Mechanical Engineering Design. 7th ed., New York, McGraw-Hill, 2003, chapter 8, pp. 424.

6 fe-safe User Manual Version 6.2, Volume 1: User Guide, Safe Technology Ltd, Sheffield, UK.

7 fe-safe User Manual Version 6.2, Volume 2: Fatigue Theory Reference Manual, Safe Technology Ltd, Sheffield, UK.

8 fe-safe User Manual Version 6.2, Volume 2: Fatigue Theory Reference Manual, chapter 7, section 7.4.7, "Brown-Miller Combined Strain Criterion", Safe Technology Ltd, Sheffield, UK.

9 Kandil, F.A., Brown, M.W. and Miller, K.J. (1982), "Biaxial Low Cycle Fatigue Fracture of 316 Stainless Steel at Elevated Temperatures", book 280, The Metals Society, London.

10 Morrow, J. (1968), "Fatigue Properties of Metals", Fatigue Design Handbook, Society of Automotive Engineers, pp. 21-30.

11 fe-safe User Manual Version 6.2, Volume 2: Fatigue Theory Reference Manual, chapter 7, section 7.5, "Critical Plane Analysis", Safe Technology Ltd, Sheffield, UK.

12 Neuber, H. (1961), "Theory of Stress Concentration for Shear Strained Prismatic Bodies with Arbitrary Non-Linear Stress-Strain Law", Journal of Applied Mechanics, vol. 28, pp. 544-550.

13 Endo, T. and Matsuishi, M. (1974), "Damage Evaluation of Metals for Random or Varying Loading", Proceedings of Symposium on Mechanical Behaviour of Materials, Vol. 1, The Society of Material Science, Kyoto, Japan.

14 Socie, D.F. and Downing S.D. (1982), "Simplified Rainbow Cycle Counting Algorithms", International Journal of Fatigue, Vol. 4, No. 1, pp. 31-40.

15 Manson, S.S. (1965), "Fatigue: A Complex Subject – Some Simple Approximations", Journal of Experimental Mechanics, Society of Stress Analysis, pp. 193-226.

16 Mitchell, M.R., Socie, D.F. and Caulfield, E.M. (1977), "Fundamentals of Modern Fatigue Analysis", Fracture Control Program Report No. 26, University of Illinois, USA, pp. 385-410.

17 Muralidharan, U. and Manson, S.S (1988), "A Modified Universal Slopes Equation for Estimation of Fatigue Characteristics of Metals", Journal of Engineering Material & Technology, Transactions of ASME; vol. 110, pp. 55-58.

18 Baumel, A. Jr. and Seeger, T (1990), "Materials Data for cyclic loading–Supplement 1", Elsevier Science Publishers, Amsterdam.

19 Ong, J.H. (1993), "An Evaluation of Existing Methods for the Prediction of Axial Fatigue Life from Tensile Data", International Journal of Fatigue, vol. 15 (1), pp. 13-19.

20 Park, J.H. and Song, J.H. (1995), "Detailed Evaluation of Methods for Estimation of Fatigue Properties", International Journal of Fatigue, vol.17 (5), pp. 365-373.

21 Roessle, M.L. and Fatemi, A. (2000), "Strain-controlled Fatigue Properties of Steels and Some Simple Approximations", International Journal of Fatigue, vol. 22, pp. 495-511.

22 Meggiolaro, M.A. and Castro, J.T.P. (2004), "Statistical Evaluation of Strain-life Fatigue Crack Initiation Predictions", International Journal of Fatigue, vol. 26, pp. 463-476.

23 Park, J.H. and Song J.H. (2003), "New Estimation Method of Fatigue Properties of Aluminum Alloys". Transactions of ASME, vol. 125, pp. 208-214.

24 Boiler, C. and Seeger, T (1987), "Materials Data for cyclic loading, Part D: Aluminum & Titanium Alloys", Elsevier Science Publishers, Amsterdam.

25 Technical Report on Fatigue Properties SAE J1099 (1975), Society of Automotive Engineers.

26 Smith, R.W., Hirchberg, M.H. and Manson, S.S. (1963), "Fatigue Behaviors of Materials under Strain Cycling in Low & Intermediate Life Range", NASA Technical Note D-1574, NASA, USA.

27 Miner, M.A. (1945), "Cumulative Damage in Fatigue", Journal of Applied Mechanics, Vol. 12, Transactions of ASME, Vol. 67, pp. A159-A164.

28 Dowling, N.E., (2004), "Mean Stress Effects in Stress-Life and Strain-Life Fatigue", Society of Automotive Engineers, F2004/51.

29 Private communication (2012), Jahed, H., "Feasibility Study on Fully Reverse Fatigue Test of Al Clad Sheets", University of Waterloo, Ontario, Canada.

30 Oviasuyi, R., Klassen, R.J (2012), "Deducing the stress-strain response of anisotropic Zr-2.5%Nb pressure tubing by spherical indentation testing", Journal of Nuclear Materials.

31 Weiler, J.P., Wood, J.T., Klassen, R.J., Berkmortel, R., Wang, G. (2005) , "The effect of grain size on the flow stress determined from spherical microindentation of die-cast magnesium AM60B alloy", Journal of Materials Science, 40, pp. 5999 – 6005.

32 Abaqus Analysis User's Manual Version 6.11, Volume III, Section 21.5.1, Dassault Systemes Simulia Corp., Providence, RI, USA.